Aircraft Data Collection System

A Senior Project
presented to
the Faculty of College of Engineering
California Polytechnic State University,
San Luis Obispo

Amy Kronsteiner
Danny Marx
Collin Heller
Nathaniel Garcia
Nicholas Riccobono
Scott Parks
Albert Liu

June 2010

Aircraft Data Collection System

Nathaniel Garcia, Collin Heller, Amy Kronsteiner, Albert Liu, Daniel Marx, Scott Parks, and Nick Riccobono
California Polytechnic State University, San Luis Obispo, California, 93401

This report outlines the design and building process for an interchangeable testing device that collects aircraft performance data. Included is the project objectives, system requirements, management plan, design concept development, design details, manufacturing procedures, and project verification test plans. The device is a wing-mounted Pitot-static system integrated with an Electronic Flight Instrument System (EFIS).

Nomenclature

G	=	g-force
V	=	velocity
H	=	specific depth
D	=	diameter
h	=	specific height
d_1	=	inner diameter
d	=	outer diameter
p_0	=	total pressure
p_1	=	static pressure
ρ	=	density
I	=	input current
T_{Ref}	=	reference temperature
R_{Ref}	=	resistance at the reference temperature
a,b,c	=	coefficients of calibration
T_w	=	temperature of wire
T_f	=	temperature of fluid
A_w	=	wire surface area

I. Introduction

THIS document details the building progress of an aircraft data collection system. The project was presented to the team by an experimental aircraft kit manufacturing company, Van's Aircraft, of Aurora, Oregon. The company needed a portable system that could measure and collect performance data to verify and calibrate existing instruments on their aircraft.

Van's Aircraft wishes to implement this testing device during the flight tests of their newly manufactured aircraft. A calibrated testing device will gather the aircraft's performance data and compare it to the aircraft's existing instruments. The testing device will collect the performance data and record it to be later reviewed on a computer. Being able to view performance curves of an aircraft during climbs, descents, turns, take off and landing will allow customers to see the difference in aircraft models and allow manufacturers to improve aircraft in certain areas of performance. Currently, Van's Aircraft sends pre-manufactured kits to customers and gives baseline performance for certain engine selections and weight metrics. However, customers are open to add different engines or other body modifications and will not know how much better it performs than the unmodified model.

When this project successfully completed, Van's Aircraft will be able to provide accurate performance data about each of their models to their customers and see how small modifications will affect their aircraft. Previously, the method of comparing different aircraft or modified aircraft involved testing two planes simultaneously while carrying out the same maneuvers. With this testing device, the performance curves for each plane can be collected and compared to see where each model performed better.

II. Background

The CAFÉ foundation and NASA have done research on portable barometers, where a measurement device is added to an aircraft that is independent of the plane's existing Pitot-static tube. Several designs for these devices range from trailing cones and trailing bombs to wing mounted systems.

The team considered four options for mounting the aircraft data collection system: behind the aircraft (in a trailing cone or bomb), on the tail, on the landing gear, and on the wing of the aircraft. The optimal mounting location would allow the system to have access to the free stream without any obstructions. The preferred choice, the wing mounted system, will allow accurate readings because it will have plenty of access to undisturbed air, whereas any trailing system would have to be so far behind the plane that it would be impractical for our project due to the complexity of what is contained within the device.

Unlike systems in the past, ours will be completely interchangeable between aircraft and will not depend on the aircraft to supply power. The advantage of this system is that no permanent damage is done to the plane during installation. This allows for easy comparison between a variety of aircraft.

III. Objective and Requirements

Once completed, our system will be able to collect accurate performance data to be extracted for analysis on a computer. This device will be used as a baseline calibration tool for experimental aircraft, knowing that the device yields accurate readings will allow the user to determine the accuracy of the aircraft's instruments and, if any modifications are made, what gains or losses have been added.

The system requirements were developed from Van's Aircraft's specifications. The requirements have been divided into four categories: Data Requirements, Collection and Calculation Requirements, Physical Requirements, and Performance Requirements.

A. Data Requirements

The following requirements outline how the data should be collected and stored.

1) All data shall be collected at a rate of one hertz or better
2) The data shall be accurate to within one percent
3) The data shall be stored in Comma Separated Value (CSV) form
4) The data shall be transferable to a USB removable drive

B. Collection and Calculation Requirements

The following requirements outline what the system should collect and calculate.

1) The system shall calculate true airspeed
2) The system shall collect indicated airspeed
3) The system shall collect pressure altitude
4) The system shall collect outside air temperature
5) The system should calculate ground speed
6) The system should collect acceleration in the vertical direction
7) The system may calculate acceleration in the lateral and longitudinal directions
8) The system may collect pitch, yaw, and roll data

C. Physical Requirements

The following requirements outline the system's dimension and installation requirements.

1) The system shall weigh no more than ten pounds
2) The system shall not exceed 25 square inches by 36 inches
3) Installation of the system shall take no longer than thirty minutes
4) The system should install without permanently altering the aircraft

D. Performance Requirements

The system must operate within the following ranges:

1) The system shall operate within a temperature range of -40°F to 120°F
2) The system shall operate at accelerations up to ten Gs
3) The system shall operate in an altitude range from -500 feet to 18,000 feet
4) The system shall operate at speeds up to 300 miles per hour

IV. Management Plan

The management plan for the project includes all of the schedules and group member responsibilities along with the cost report and budget. Our project is broken into four subsystems; GRT-Sport Electronic Flight Instrument System (EFIS), Eagle Tree Flight Data Recorder (FDR) Pro, Chassis/cuff, and Pitot-tube/boom. Each subsystem is outlined by its primary responsibility and each group member that contributed to its progress. A sample of a Gantt chart outlining the progress and milestones of the Chassis and Cuff subsystem is shown below in Figure 4-1, to see the entire schedule for the winter quarter refer to Appendix G. The cost report outlines all of our expenses throughout this building quarter; a sample of the tables can be seen in Figure 4-4.

A. Subsystems

Original Chassis Team:

Team Member	Major	Projects and Responsibilities
Danny Marx	Aero	• Chassis Concept Design • Chassis Design (CAD) • Parts Manufacturing
Nick Riccobono	Aero	• Chassis Concept Design • Parts Manufacturing • Composite Lay-ups
Nathan Garcia	C.P.E	• Power Supply • Wiring Configuration
Albert Liu	Aero	• Harness System • Composite Lay-ups • Parts Manufacturing

Table 4-1: *Chassis subsystem group member contributions*

Current Chassis Team:

Team Member	Major	Projects and Responsibilities
Collin Heller	Aero	• Chassis Concept Design • Chassis Design (CAD) • Parts Manufacturing
Danny Marx	Aero	• Parts Manufacutring
Amy Kronsteiner	Aero	• Chassis Concept Design • Parts Manufacturing

Table 4-2: *Chassis Redesign subsystem group member contributions*

Pitot-tube/Boom Team:

Team Member	Major	Projects and Responsibilities
Collin Heller	Aero	• Pivot Joint Design (CAD) • Pivot Joint Concept Design • Air Disturbance Analysis • Parts Manufacturing
Amy Kronsteiner	Aero	• Pivot Joint Concept Design • Pitot-tube Integration • Parts Manufacturing

Table 4-3: *Pitot-tube measurement subsystem group contributions*

GRT EFIS Team:

Team Member	Major	Projects and Responsibilities
Nathan Garcia	C.P.E	• Interfacing • Configuration • Calibration
Albert Liu	Aero	• Configuration • Component Integration

Table 4-4: *GRT-Sport subsystem group contributions*

EagleTree EFIS Interface and Calibration/Testing:

Team Member	Major	Projects and Responsibilities
Scott Parks	E.E	• System Integration • Concept Design • Calibration • Parts Manufacturing

Table 4-5: *EagleTree FDR subsystem group contributions*

Testing Verification Team:

Team Member	Major	Projects and Responsibilities
Amy Kronsteiner	Aero	• Testing Verification
Nick Riccobono	Aero	• Testing Verification

Table 4-6: *Testing Verification Plan group contributions*

Cost Report and Scheduling Team:

Team Member	Major	Projects and Responsibilities
Amy Kronsteiner	Aero	• Parts Allocation • Weekly Meetings
Albert Liu	Aero	• Finance and Budget • Cost Report • Bill of Material
Nick Riccobono	Aero	• Parts Allocation • Schedule Design

Table 4-7: *Cost Report and Scheduling group contributions*

B. Sample Schedule

Below is a sample of the Gantt chart that was followed during the building quarter. The full Gantt chart can be seen in Appendix G.

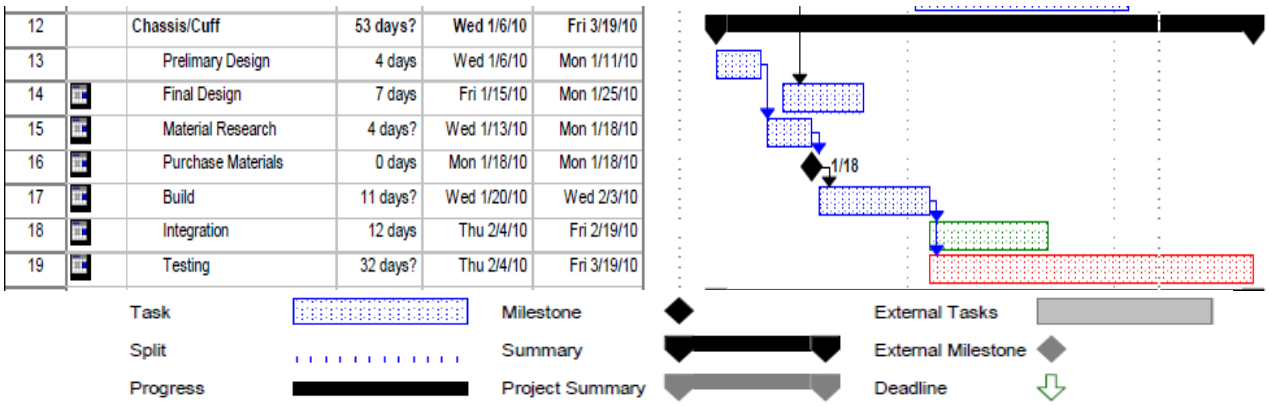

12		Chassis/Cuff	53 days?	Wed 1/6/10	Fri 3/19/10
13		Prelimary Design	4 days	Wed 1/6/10	Mon 1/11/10
14		Final Design	7 days	Fri 1/15/10	Mon 1/25/10
15		Material Research	4 days?	Wed 1/13/10	Mon 1/18/10
16		Purchase Materials	0 days	Mon 1/18/10	Mon 1/18/10
17		Build	11 days?	Wed 1/20/10	Wed 2/3/10
18		Integration	12 days	Thu 2/4/10	Fri 2/19/10
19		Testing	32 days?	Thu 2/4/10	Fri 3/19/10

Figure 4-1: *Chassis and Cuff Schedule Sample and Legend. Tasks labeled as blue, green or red corresponds to completed task, in progress and incomplete respectively.*

C. Cost Report

Given a total budget of $5000, we have spent $4,148.53 to design and build two prototype systems; the GRT-Sport EFIS (Figure 4-2) and the EagleTree FDR (Figure 4-3).

The cost breakdown of the GRT-Sport prototype system, as seen in Figure 4-2, was broken up into four categories: System Cost, Old Frame Cost, New Frame Cost, and Other Cost. For the EFIS system, 87% of the cost came from System Cost, 6% from Old Frame Cost, 2% from New Frame Cost, and 5% from Other Cost. The total cost for our EFIS system came out to be $3,729.32.

The cost breakdown for the EagleTree FDR prototype system as seen in Figure 4-3, was broken up into the same three categories: System Cost, Frame (Body) Cost, and Other Cost. Final cost came to $927.68, where 56% of the cost came from System Cost, 24% from Body Cost, and 20% from other costs.

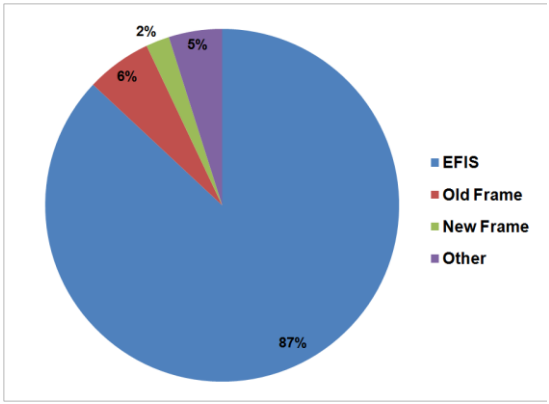

Figure 4-2: *GRT-Sport EFIS Cost Breakdown*

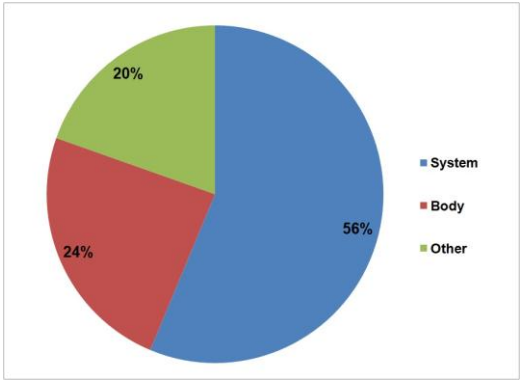

Figure 4-3: *EagleTree FDR Cost Breakdown*

After redesigning our frame, we were able to determine that it only cost an additional $80 for our new frame. We were able to keep the cost low by recycling parts from our old frame. The Body Cost and Other Cost were the main concern. The Body Cost totaled to be $303.64, which included both the new frame and old frame. Our Body design is interchangeable with both our EFIS system and Flight Recorder system, so the Body Cost will remain constant. Also, almost all of the components that we purchased for our Body design came from McMaster-Carr Supply Company. The Other Cost totaled to be $181.83. The Other Cost included any disposable material used in the construction of our system. Some of these items included sandpaper, epoxy, and

respirators. Most of the items categorized as Other Cost were purchased from Aircraft Spruce and Specialty Company.

V. Design Concept Development

The concept development to each subsystem involved trade studies to find the most ideal materials, pre-manufactured goods and overall integration to the aircraft. Consideration was taken when designing each system to ensure compatibility between hardware and software.

A. GRT-Sport EFIS system

Computer System Design Decisions

For the purpose of aircraft performance data collection, a computer system is needed to read and store data for extraction by the user from instrumentation including a Pitot-static tube, Outside Air Temperature (OAT) probe, and a GPS system. We devised two possible solutions to incorporate into our design: designing and building a computer system tailored to the project specifications, or integrating a third-party Electronic Flight Instrument System (EFIS) that would meet the project requirements.

Figure 5-1: *EFIS LCD display*

Electronic Flight Instrument System (EFIS)

There are a variety of different EFIS modules on the market and, through the use of a trade study, we were able to select a clear winner to use for our purposes. We selected the GRT Sport, a Sport model made by Grand Rapids Technologies. While the GRT Sport scored decent in all categories, it was a stand out when it came to its data storage and GPS capabilities. Most EFIS modules had the capability to internally record data, stream output data or even save it to a removable memory card. The GRT Sport is actually able to record its data directly to a removable flash drive. This feature not only satisfied the requirement of saving the flight data, but made it easily transferable to a computer as well.

The implementation of the GPS system was greatly simplified with the GRT Sport as well. Some EFIS modules had ports to connect an external GPS receiver chosen at the user's discretion to retrieve the GPS data. The GRT Sport simplified this task by integrating a GPS receiver into the EFIS. This meant that to have GPS capabilities the user must simply plug in the supplied GPS antenna.

Functional Solution*:* By purchasing an EFIS, we would eliminate the time required to research, design, assemble, test, and develop a computer system that interfaces with instrumentation and computes and stores data on

Revision History
Rev A – First version

Connector A Description
Mating Connector: 37-pin Female D-sub (Instrument has 37-pin Male D-sub)

Pin	Function	Wire Color	Pin	Function	Wire Color
1⇨	Primary Power Input	RED	20	Tone (Future use)	
2▽	Secondary Power Input	RED/BLU	21▽	Clock Power 12V @ <1 ma	RED/WHT
3⇨	GND	BLK	22	AP1 (Future use)	
4⇨	MAG_GND	BLK	23	AP2 (Future use)	
5⇨	MAG_X	WHT/GRN	24	AP3 (Future use)	
6⇨	MAG_Y	WHT/BRN	25	AP4 (Future use)	
7⇨	MAG_Z	WHT	26	TORQUE (Future use)	
8⇨	MAG_CNTRL	WHT/BLU	27	NAVAID (Future use)	
9⇨	MAG_PWR	WHT/RED	28	Warning Light (Future use)	
10▼	D4 Alt Encoder Output		29▽	OAT Sensor	GRY
11▼	C4 Alt Encoder Output		30⇨	RX1 GPS Serial Input	GRY/RED
12▼	C2 Alt Encoder Output		31▽	RX2 EIS Serial Input	GRN/BLK
13▼	C1 Alt Encoder Output		32	RX3 (Future use)	
14▼	B4 Alt Encoder Output		33	RX4 (Future use)	
15▼	B2 Alt Encoder Output		34▽	TX1 Autopilot Serial Output	BLU
16▼	B1 Alt Encoder Output		35▽	TX2 Encoder Serial Output	
17▼	A4 Alt Encoder Output		36	TX3 (Future use)	
18▼	A2 Alt Encoder Output		37	TX4 (Future use)	
19▼	A1 Alt Encoder Output				

⇨ Connected in wiring harness.
▽ Supplied as loose pinned wires.
▼ Optional wiring

Connector B Description (Remote Magnetometer)
Mating Connector: 9-pin Male D-sub (Magnetometer has 9-pin Female D-sub)

Pin	Function	Wire Color	Pin	Function	Wire Color
1◢	MAG_Y	WHT/BRN	6◢	MAG_CNTRL	WHT/BLU
2◢	MAG_Z	WHT	7	No connection	
3◢	MAG_X	WHT/GRN	8	No Connection	
4◢	MAG_PWR	WHT/RED	9	No Connection	
5◢	MAG_GND	BLK			

◢ Customer inserts pins into connector after the wires are pulled through the airframe.

Figure 5-2: *GRT-Sport Serial output array*

an external storage device. The disadvantage to this solution is the increase in cost. However, this solution saves a significant amount of development time. The GRT Sport EFIS utilizes an LCD screen to display information about the sensor readings it measures. This screen can be dimmed by turning the left knob clockwise, thus reducing power drain. Using push buttons on the front of the GRT Sport, the user can start and stop recording data and select which data to record. Information regarding all the GRT Sport EFIS's functions can be found in the GRT Sport User Manual. Although an EFIS includes unneeded functionality such as an LCD display, it fulfills the desired function of a computer system that reads and translates data from the Pitot-static tube, outside air temperature sensor, and GPS receiver and computes and stores the data as CSV files in a retrievable storage device.

EFIS Trade Study

Four EFIS systems were chosen for comparison in a trade study. Each of these units was within our price range (less than $5k), relatively compact in size and weight (less than 10 lbs), and recorded all of the needed data. The specific categories chosen to be compared are shown in Table 1 in Appendix B along with the data to be compared. Each EFIS was assigned a value from zero to ten in each of six categories as shown in Table 2 in Appendix B. A value of ten was given to the EFIS system that had the most desirable figure or feature and a zero was given to the system with the least desirable figure or feature. To determine the values for each category of an EFIS between the most and least desirable systems, we assigned to them a value based on the percentage of its range between the highest and lowest values.

Refer to Appendix B to see full trade study matrix and criteria on our EFIS selection.

B. Sensors and Pressure Measurement

To measure airspeed, altitude, and outside air temperature, our system will require measurement devices capable of gathering the data we need and operate without fault and with minimal error. By measuring these three quantities the GRT Sport EFIS will be able to calculate the aircraft's rate of climb, true airspeed, and atmospheric conditions. The following section outlines the selection of each device including the trade study on the Pitot-static tube.

Outside Air Temperature (OAT)

At higher altitudes, temperature significantly affects gas dynamics. Density, pressure and temperature all vary with increased altitude. Since velocity is related to each of these properties, failure to account for their change will result in serious error. Most air temperature sensors on the market are all the same so research was done to assure they would meet these basic requirements:

- Operate within required conditions
- Compatible with our GRT Sport EFIS
- Low cost

OAT: The air temperature sensor we chose is sold by Grand Rapid Technologies meets all of these requirements. The temperature probe will plug into our EFIS with no added complexity or required manufacturing. Since it is manufactured by GRT, it is designed to be compatible with all of their instrument systems.

Pressure Measurement

To measure airspeed and altitude, three possible velocity measurement devices were researched: hot wire anemometer, Irwin probe, and Pitot tube. All three have been implemented with success in wind tunnels and on aircraft. The chosen device must meet the three important characteristics to meet our requirements:

- Operate within required conditions
- Measure airspeed and altitude accurately
- Compatible with our GRT Sport EFIS

Pitot Tube: A Pitot tube is an effective airspeed measurement device used on most aircraft today. Depending on the design, it can perform in cold and hot temperatures and at relatively high velocities. Pitot tubes are comprised of an open tube pointed in the direction of motion and a static pressure tap. The open tube measures the ram pressure or total pressure, p_0. The static pressure tap is oriented perpendicular to the direction of motion and can be located anywhere else on the plane to measure the static pressure, p_1. The maximum velocity for our application is 300 mph,

equivalent to Mach 0.4 at sea level conditions. Most testing will not exceed Mach 0.3 (230mph); thus an incompressible flow can be assumed and Bernoulli's equation can calculate airspeed as seen in (Eq. 5-1)[3]:

$$V = \sqrt{\frac{2(p_0 - p_1)}{\rho}} \qquad \text{(Eq.5-1)}$$

However, incompressible fluid approximations become inaccurate at Mach 0.3. This indicates we are trans-compressible, where some surrounding air is compressed and some remains non-compressed. The addition of an outside air temperature sensor will allow our EFIS to account for fluid compressiblity in air and calculate velocity with more accuracy.

Since regulation and experimental aircraft use Pitot tubes, they are widely available for many different applications. The GRT Sport EFIS has built in ram and static pressure transducers that are compliant with most Pitot tubes on the market.

In comparison between a Hot Wire Anemometer and an Irwin probe, the Pitot tube's ability to measure airspeed and altitude, operate within temperature and speed ranges, and integrate with our GRT Sport EFIS fulfills our requirements for a suitable measurement device.

Pitot-tube Trade Study

With the wide variety of Pitot tubes available, all possessing the same relative limitations, we researched and compared several different models that varied in shape, material, cost, length, and any extra required manufacturing. On most aircraft, a Pitot tube is mounted on a wing or the fuselage and measures pressure difference in reference to a static port located on the aircraft. For our system, we needed the static port built into the tube to eliminate error from our own placement. Therefore, all devices in question are Pitot-static tubes.

Functional Solution: The ASSC Straight Pitot-Static tube is the best candidate for our system because it scores well in major categories and meets all requirements. The straight aluminum tube has no interference with other sensors in our system. Although it does not have the maximum length of our options, its straight design allows it to be mounted a desirable distance in front of the aircraft. With the desired shape, all the necessary manufacturing will lie outside the device. Also, it is relatively inexpensive compared to the other options.
Refer to Appendix B to see the trade study criteria and trade matrix that explores all the options for the pressure measurement device.

Pitot-tube Pivot System

In order to gather the most accurate data possible an air disturbance program was written in MATLAB to determine the most ideal location for the Pitot-static tube in front of the wing. To achieve our requirement of 1% accuracy it would have required the Pitot-static tube to be extended over 7 feet from the leading edge of the wing. However, after talking to our sponsor, the accuracy requirement was reduced to 3%. The boom extension now will be at least 2.5 feet long. In Figure 5-3 to the right, the colors indicate the severity of disturbed air. The white areas are outside the 3% tolerance requirement. The red regions are the most disturbed areas that fall within the requirement, and the dark blue regions are the regions with the

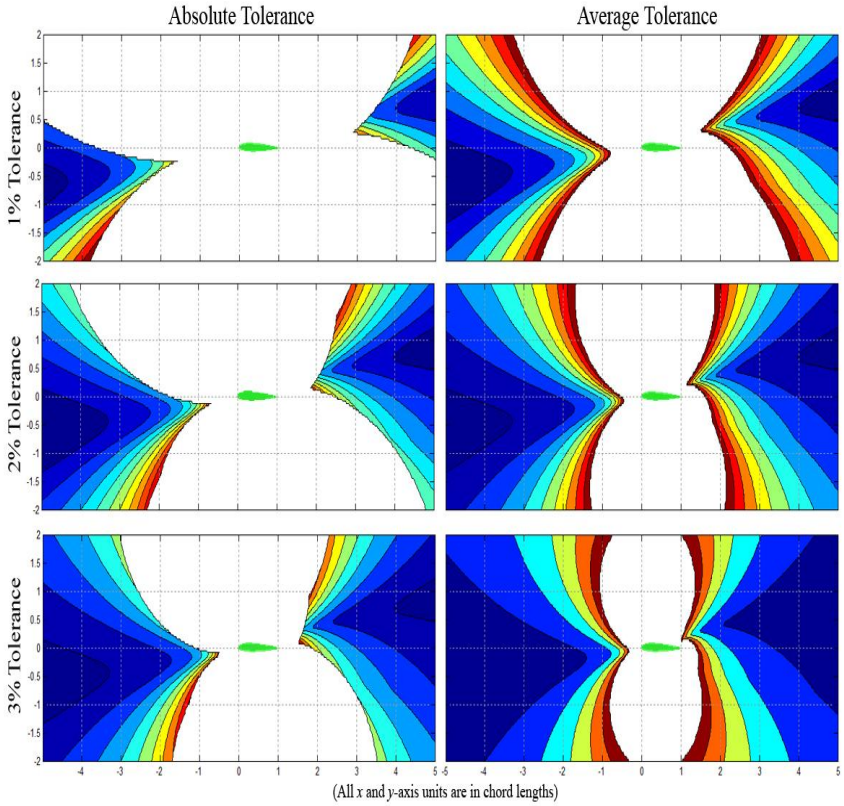

Figure 5-3: *Air disturbance analysis done in MATLAB*

least disturbed air. The analysis for this claim is seen in Appendix E.

The contour plot shows the amount of disturbed air surrounding the airfoil during all angles of attack, such that if the Pitot tube was extended into any colored region, it will always collect data within our tolerance.

The analysis accounted for wind speed, but not for wind direction. Therefore, a multi-axis pivot system (Figure 5-4) was manufactured so that the Pitot-static tube will always be pointed in the freestream. The pressure measurement system is suspended 3 feet in front of the wing off of the carbon tube. All but three components of the pressure measurement system were manufactured at Cal Poly. The three purchased components are the Pitot-static tube itself, the carbon tube, and the ball bearing at the top that allows the system to rotate from left to right. The system needs to rotate so that it is always pointed into the freestream flow because the static pressure port on the side of the Pitot-static tube has to measure pressure parallel to the flow: it cannot have any flow entering from the side. Therefore, the pressure measurement system was designed and built so that the requirement of 3% accuracy will be fulfilled.

C. Main Body and Mounting

The following section outlines the concepts and design for body and harness system. It will cover the materials chosen, concept design for the main body and the necessary CAD drawings. The mounting location decision and the mounting technique were pre-determined before building the main body so the decision between methods and locations of mounting is included.

Original Chassis and Body Design

During the construction process of this senior project, two frames for housing the components of the system were built. The design of the original chassis of our system, which holds all the components of our system including the EFIS, outside air temperature sensor, and support for the boom, was heavily influenced by two main factors. These factors were the size and shape of the EFIS, and the fact that the whole system needed to weigh less than ten pounds.

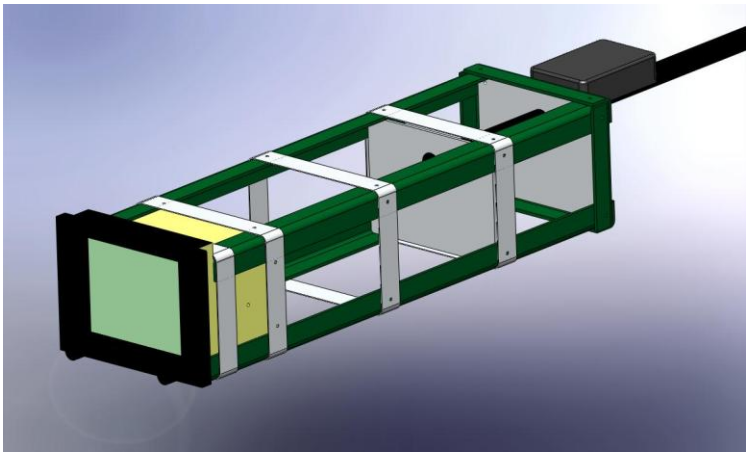

Figure 5-4: *SolidWorks CAD model of original frame, EFIS and magnetometer.*

The size and shape of the frame were purely based on the EFIS. A goal was to minimize the cross sectional area of the system; this was done by building the frame around the EFIS so that the frame and the EFIS essentially had the same cross sectional area. The length of the frame was based on the need of the EFIS's magnetometer to be at least 18 inches away from the EFIS so that the magnetometer could collect data accurately. This was a necessary requirement because, according to the EFIS instruction manual, the magnetometer needs to be at least 18 away from the EFIS and at least 12 inches away from current carrying wires.

The materials used for the construction of the frame were based on the need to reduce weight and the need to use non-ferrous materials. The frame needed to be non-ferrous because the magnetometer needs to be at least 12 inches away from ferrous materials in order for it to function properly according to the EFIS instruction manual. Based on these needs the materials chosen to make the frame were fiberglass and aluminum. Both these materials are strong, lightweight, non-ferrous, and cheap making them the ideal choices for building the frame. The frame was built with fiberglass angle that is held together with aluminum rivets. The structure also has aluminum bands wrapped around the frame for added strength and as a place for the strap to attach to the frame. The support structure for the boom is made of aluminum plates, which are mounted inside the frame using aluminum angle and aluminum rivets. Two boom collars were manufactured out of aluminum and riveted to the mounting plates so that setscrews could be used to grip the boom while it is inserted into the frame. The whole frame with the EFIS included weighs around 6.5 pounds, which meets the requirement of 10 pounds for the total weight of the system. Also, the frame is very strong and stiff enough to handle any stress it may encounter during flight. The frame took about two weeks to construct.

One concern during the construction of the frame was whether or not the fiberglass could handle the riveting process, especially when the fiberglass is being riveted to fiberglass. In order to determine whether or not the fiberglass could handle the riveting, a series of tests were conducted. The test verified that fiberglass can be riveted without any cracking or fracturing.

In addition to the frame, a fiberglass shell was constructed in order to surround the frame and reduce the drag produced during flight. The shape of the shell was based off a symmetrical airfoil in order to reduce drag as much as possible and not to create a lifting force in any direction. One downside to the fiberglass shell is that it added extra weight to the system bringing the final weight of the frame and shell to around 8 pounds, which brings the whole system weight perilously close to the maximum weight of 10 pounds. Another downside to the fiberglass shell is that it increases the cross sectional area to larger than 25 square inches.

During the first fit test, it was found that the chassis and fiberglass shell did not satisfactorily adhere to the wing. The testing revealed that the strap sagged under the weight of the system causing undesirable roll. It was determined that the system needed to be altered in order to eliminate these problems.

Chassis Redesign

Due to the previously mentioned mounting challenges with the original chassis, the frame was redesigned to allow for better attachment to the wing. During the redesign process, the team considered two options: make alterations to the current frame or rebuild an entirely different design. To determine whether an alteration of the frame was possible, the key weaknesses in the original chassis design were examined.

A. Strap-Chassis Interface

In the original chassis, the strap was positioned on top of the fiberglass frame, while aluminum braces secured the strap to the frame. When pulled tightly, it was thought that the tension in the strap would hold the chassis to the wing. This design was chosen to keep the strap from interfering with the boom. It also allows for the most surface area touching both the strap and the wing. Having more surface area touching the wing would create more friction, thus preventing the strap from slipping. However, by having the chassis below the strap, the weight of the system pulled down on the strap and caused it to sag. This created a region between the frame and the wing, which allowed the system to roll.

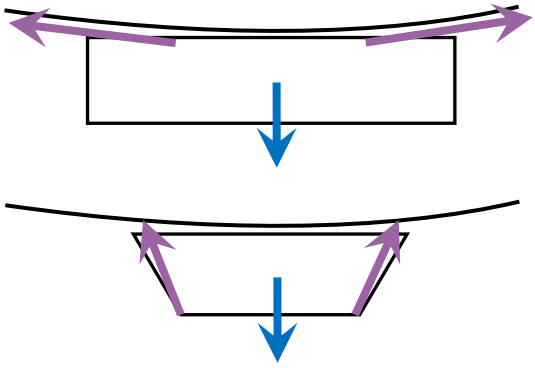

Figure 1*Tension Distribution Diagram*

The main reason for the failure of the chassis to attach to the wing is the direction of the applied forces as illustrated in Fig. 5-5. In the original design, the weight of the chassis is pulling down. To counteract this force, the tension must compensate for the weight. However, most of the force used for tensioning is being applied in the horizontal direction with only a small component in the vertical direction. Because of this, only a weak resisting force is applied to the frame to counteract the weight.

To eliminate this problem, it was proposed that the strap should run underneath the frame. Then, when tension is applied, the strap would cause the frame to pull against the wing. Figure 5-5 shows the forces acting on the bottom of the redesigned frame. It can be seen that most of the force is acting in the vertical direction, pushing the frame and the wing together. This design allows the system to take advantage of the tension in the strap and results in a more stable configuration. In order to verify this concept, several tests were made during the original attachment testing to see if the frame was more stable in the new configuration. Figure 5-6 shows one of the configurations tested. Overall, it was found that running the strap underneath the frame held it more securely to the wing.

B. Pressure Distribution

Another concern associated with the original chassis design was the lack of controlled pressure distribution between the frame and the wing. Since the aluminum brackets are not perfectly rigid, the presence of the strap causes the center to bulge upwards while the edges of the bracket sag. Because of this, only the middle section of the brackets contacts the wing. This creates an unstable configuration since only one small area of the frame holds the system in place. In the presence of a lateral force, the system can roll about the strap. The presence of the rolling motion is of concern, since it allows for oscillations that could potentially cause the mounting system to fail.

To counteract this problem, several options were considered in order control, which surfaces come into contact with the wing. Two solutions were proposed which are shown in Fig. 5-7:

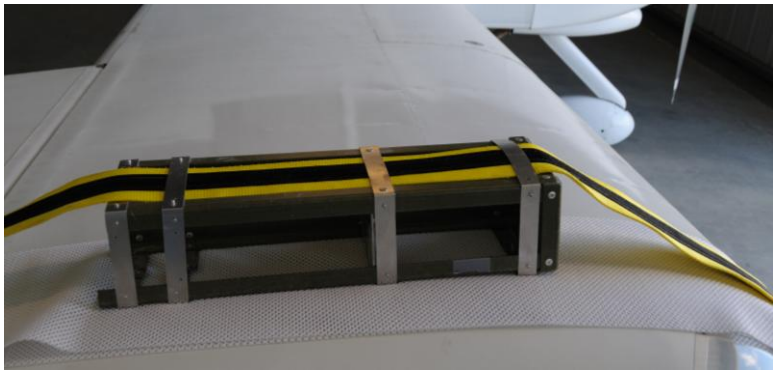

Figure 5-6: *Configuration testing*

1. *Spring Loaded Mounting Pads:*

The first solution considered involved using springs to control the pressure on each surface. When pushed against the wing, these pads would put pressure on the wing, which would hold the pads in place. They would also fill in any gaps between the surfaces, thereby preventing any possible movement and maximizing area in contact with the wing. By mounting these pads on the outside of the frame, any rolling motion could be reduced or eliminated.

One of the drawbacks associated with this design was the lack of direct user control. Since the forces in the springs and the strap must be equal and opposite, the maximum tension that could be placed in the springs is equal to the maximum tension that can be placed in the strap. Therefore, no additional tension is gained from the presence of the springs. At the same time, the lower surface of the wing is not flat which could cause some pads to bear more of the force than others. Having weaker pads creates a rolling problem, which leaves the current issue unresolved.

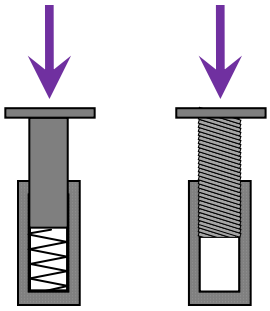

Figure 5-7: *Proposed mounting solutions.*

2. *Threaded Mounting Pads:*

An alteration made to the previous design by replacing the springs with a threaded pad. When mounted to the wing, the pads would be in their lowest position. Tension would be applied to the strap to hold the frame in place. Once the user put as much tension in the strap as he or she could supply, the pads could be raised away from the frame, effectively moving the frame away from the wing and removing any gaps between the two. This would also increase the tension in the strap. Since the pads are individually adjusted, the pressure in each can be made almost uniform.

Due to its inherent performance benefits, the second design was chosen for placement on the redesigned chassis. Four mounting pads were chosen since it would allow for maximum control while minimizing weight.

C. Drag

A major concern of the original chassis was its considerable size. The original design focused on the EFIS and other electronic components, which, at the time, were considered the most important drivers. The significant length of the chassis was caused by the mounting instructions of the magnetometer and the EFIS. The manufacturer recommended that the magnetometer be at least 18 inches from the EFIS and any current carrying wire. This resulted in a total frame length of about 22 inches. The large amount of surface area of the frame resulted in significant amounts of parasite drag. Furthermore, the box shape of the frame caused considerable wake drag. To counteract this large amount of drag, a fiberglass faring was constructed which is shown in Fig. 5-8. The fairing was designed to encompass the entire frame. The front was made to be blunt while the trailing edge was sharp to reduce any wake drag. Unfortunately, the manufacturing of the fairing took a considerable amount of time, with the fiberglass layup requiring almost 2 weeks. In addition, the fairing blocked all access to the buttons on the EFIS and an access panel needed to be made on the rear end of the fairing.

Figure 5-8: *Fiberglass fairing*

After testing the magnetometer, it was found that it could be placed significantly closer to the EFIS without any detectable difference in the data. In addition, it was decided that the new frame needed to be inherently more aerodynamic, since the amount of time to develop a new fairing was deemed unacceptable.

Much consideration was made as to whether or not to alter the old chassis or to build a new chassis. It was decided to design and build an entirely new chassis for multiple reasons. The original frame was designed to support a strap running along the top of the frame and could not support a strap along the bottom. Also, the frame needed to be cut to reduce size. Since the frame was riveted together, all of the components would need to be drilled out, which would take considerable time. The new design was also engineered to withstand a significant compression load, while most of the components in the original design are in tension.

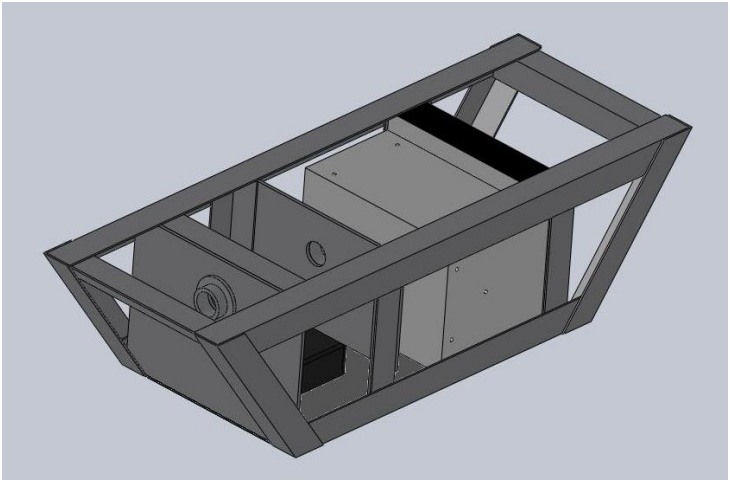

Figure 5-9. *Solid Model of Chassis Redesign*

The new frame was built out of aluminum angles instead of fiberglass in order to bear the strong compression loads caused by the strap. To reduce construction time, the frame was designed to reuse certain parts and concepts from the original frame, such as the boom support plates and the boom collars. In addition, the frame was made shorter with more aerodynamic features. The overall design of frame was made to be trapezoidal in shape instead of rectangular. The CAD model for the design is shown in Fig. 5-9. Plexiglas was used for the walls instead of fiberglass, both to reduce weight and construction time. Construction time on the first frame elapsed for 2 weeks with the fairing adding an additional 2 weeks. The redesigned frame was constructed in under one week.

Mounting Location

The team considered four options for mounting the aircraft data collection system: behind the aircraft (in a trailing cone or bomb), on the tail, on the landing gear, and on the wing of the aircraft. The optimal mounting location would allow the system to have access to the free stream without any obstructions. Also, the location should be readily accessible so the system can be easily installed and removed. Finally, the system needed to be mounted in a location that does not greatly affect the performance of the aircraft.

With much research and consideration, the tail, landing gear, and trailing systems were eliminated. Tail mounting was eliminated due to the fact that the propeller and the aircraft itself obstruct the flow before it reaches the tail. For a tail-mounted system it is difficult to get free stream going into the sensor in steady, level flight and it is even worse in a climb. The landing gear mounting option was eliminated for similar reasons; the slipstream from the propeller could cause variations in pressure, which would affect the accuracy of the data collected by the system. Trailing systems would be inaccurate due to disturbances from the aircraft. To effectively obtain accurate information a cone must be two wingspans behind the aircraft[4]. Positioning the system this far behind the aircraft causes lag in the information. This would be ineffective for calibrating instruments on the aircraft.

While the ideal location for a system is on the front of the aircraft, the presence of the propeller eliminates that option. The wing is actually the best mounting location of the system for these aircraft. This location provides the least amount of disruption to the free stream and is easily accessible from the ground. Therefore, the system will be mounted on the wing.

Mounting Technique

The mount for this system must secure the system to the wing without damaging or altering the aircraft in any way. It must be adjustable so the system can be installed on any one of Van's Aircraft. The team came up with many methods. Some options were the use straps to secure the system to the plane; a molded cuff held on by duct tape, suction cups, air bags, or Velcro; and two plates lined with padding that surround the wing and bolt to each other.

The team decided to use nylon straps to mount the system. The aircraft would not be permanently altered with this mounting method because it would simply tighten onto the wing without using bolts. The system will be secured to the wing by tightening the straps over a rubber mat that sits on the wing. The rubber mat increases friction between

the strap and the wing. Also, it can fit onto the wing of any Van's Aircraft because it can conform to the shape of any wing.

The other options were instantly eliminated due to the fact that most of them would interfere with the ailerons of the aircraft since the ailerons extend along the majority of the wingspan. The molded cuff option was eliminated because the nylon strap system is much simpler and less expensive.

The system will be attached to the nylon straps on the lower surface of the wing. The system will be housed in a container. A boom will extend out from the front of the container to hold the Pitot-static tube. The Pitot-static tube will be able to rotate freely to maintain a parallel direction to the freestream.

D. Controls Analysis

The addition of the ACDC testing device at the tip of the wing creates a yawing moment on the aircraft due to the additional drag of our testing device. To counteract an unbalanced yaw moment, the aircraft must deflect the rudder control surface to maintain straight flight. In doing so, an unbalanced roll moment is created and must be counteracted with a deflection of the aileron control surfaces to level the plane.

The following analysis is done on the Navion general aviation aircraft combined with the geometry of the RV-7, because we do not possess the necessary flight test data for the RV-7 and do not have the geometry of the Navion. The purpose of this analysis is the show the affects of our testing device for static and dynamic reactions of the aircraft during flight.

A) Static Stability

The figure to the right shows the acting forces on the aircraft, the forces and moments shown in green are the aircraft's reaction force that is equal and opposite to the forces and moments shown in red that are induced by the presence of the ACDC testing device. Our assumptions for static stability analysis are as follows,

- steady level flight
- constant speed
- no roll, pitch, or yaw rates
- constant dynamic pressure
- no side slip

The sum of the rolling moment (Eq. 5-3) and yawing moment (Eq. 5-4) are non-dimensionalized and set to zero to evaluate the control surface deflection in static conditions.

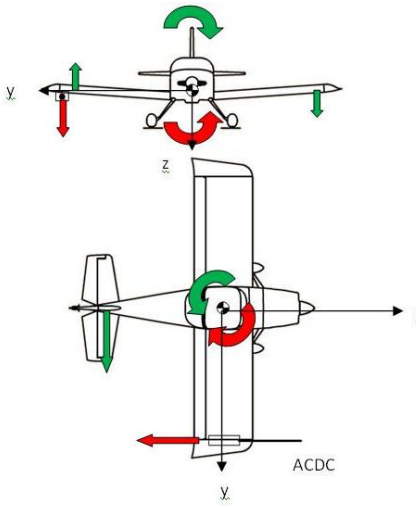

Figure 5-10: *Free Body Diagram of RV-7 with ACDC testing device. ACDC effects in red, plane reaction in green.*

Using the two equations below; rudder deflection (δ_{rudder}) and aileron deflection ($\delta_{aileron}$) are solved by plugging in the aircraft's stability derivatives, reference length, aircrafts characteristic areas, and characteristics of our testing device.

$$\frac{F_{W,ACDC}(^{b}/_{2})}{Q\bar{c}} = \left[\frac{2C_{L\alpha}\tau_{aileron}}{b}\bar{c}(y_2{}^2 - y_1{}^2)\right]\delta_{aileron} + \left[S_{tail}\frac{Z_v}{b}\tau_{rudder}C_{L\alpha W}\right]\delta_{rudder} \quad \text{(Eq. 5-3)}$$

$$\frac{C_{D,ACDC}S_{ACDC}(^{b}/_{2})}{S_{wing}\bar{c}} = \left[2KC_{L,0}C_{L,\delta aileron}\right]\delta_{aileron} + \left[V_{tail}\eta_{tail}C_{L\alpha,tail}\right]\delta_{rudder} \quad \text{(Eq. 5-4)}$$

The coefficient of drag was unknown for our testing device in this analysis, so the worst-case scenario was used: a flat plate that is perpendicular to the direction of the flow. Using a factor of safety of two, Eq. 5-3 and 5-4 were solved simultaneously to yield:

$$\delta_{rudder} = 0.865° \qquad \delta_{aileron} = 0.989°$$

Using MATLAB to perform a state space matrix analysis on the RV-7 and the RV-7 with the ACDC system we plug the values into matrices below. The values input into matrices are determined by the lateral equations of motion

and each element in the state space matrix is a function of the stability derivatives, mass, and inertial characteristics of the airplane, or in our case the airplane plus the ACDC testing device.

$$\begin{bmatrix} \dot{\Delta\beta} \\ \dot{\Delta p} \\ \dot{\Delta r} \\ \dot{\Delta\varphi} \end{bmatrix} = \begin{bmatrix} \frac{Y_\beta}{u_o} & \frac{Y_p}{u_o} & -\left(1-\frac{Y_r}{u_o}\right) & \frac{g\cos\theta}{u_o} \\ L_\beta & L_p & L_r & 0 \\ N_\beta & L_p & N_r & 0 \\ 0 & 1 & 0 & 0 \end{bmatrix} \begin{bmatrix} \Delta\beta \\ \Delta p \\ \Delta r \\ \Delta\varphi \end{bmatrix} + \begin{bmatrix} 0 & \frac{Y_{\delta r}}{u_o} \\ L_{\delta a} & L_{\delta r} \\ N_{\delta a} & N_{\delta r} \\ 0 & 0 \end{bmatrix} \begin{bmatrix} \Delta\delta_a \\ \Delta\delta_r \end{bmatrix}$$

(Eq. 5-5)

Using Eq. 5-5 in MATLAB's function *>>damp(A)* yields the three roots of our state space equation. The three roots are composed of two real roots and a pair of complex roots describing the spiral mode, roll mode, and the Dutch roll mode respectively. The addition of our ACDC should prove to have little or no affect on these modes to safely be used during flight tests. Each root or pole should lie within the left hand side of the imaginary axis in a root locus plot. The root locus plot is a powerful tool in controls analysis, it allows designers to judge the stability of the state space matrix and understand the margins of flight that the aircraft has before losing control.

B) Dynamic Stability

A pole zero plot is a plot of each root and pole of the characteristic equation. The poles and zeros for the RV-7 and RV-7 with the ACDC system attached are compared. When initially plotting the poles and zeroes of the equation for the two cases, the differences were unnoticed due to the close proximity of the roots.

Modes	RV-7	RV-7 w/ ACDC	Error
Dutch Roll	-0.378**90**±3.2783136i	-0.378**28**±3.2783149i	0.0188%
Spiral	-0.000075	-0.000049	34.48%
Roll	-4.736	-4.729	0.1393%

Table 5-1: *Eigen-values of stability matrix A. Values obtained from MATLAB >>damp(A).*

Each mode is tabulated below in Table 5-1 to examine the affect of the ACDC system on the RV-7. After integrating the ACDC into the RV-7 model, the Roll mode root remained negative, which indicates the plane will still be stable. The root only changed 0.14% from the original root of the RV-7. The calculated Dutch Roll Roots will behave in a stable damped oscillatory motion because both cases of RV-7 and RV-7 with ACDC system have real negative roots with complex pairs. The change in our Dutch Roll Roots was 0.02%. The calculated Spiral Root had a 35% change from the original. However, because the number is so small, any slight change will have a big effect on the percent change.

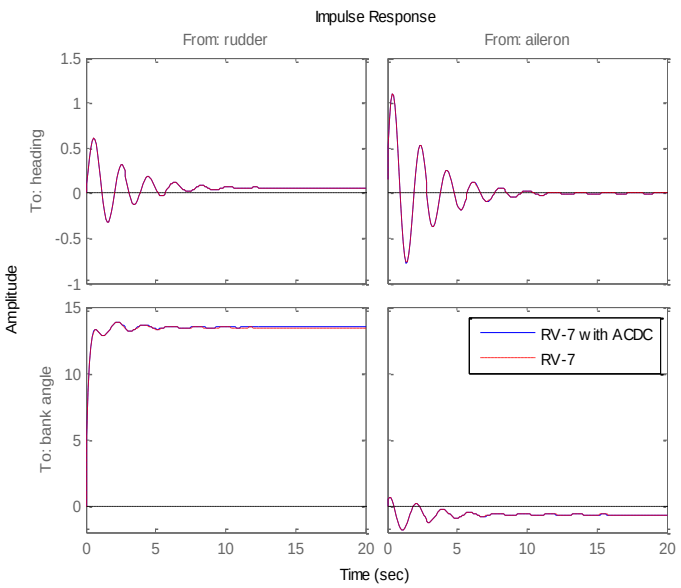

Figure 5-11: *Impulse Response of the RV-7 with ACDC system due to an impulse rudder deflection and aileron deflection. Values obtained from MATLAB >>ss(A,B,C,D)*

The only significant effect that the ACDC system has on the RV-7 is in the Spiral Mode. However, since the root is still negative, it is still stable. We can expect that this addition will require the pilot to compensate for this addition more frequently.

Using change in rudder and aileron deflection as the input and analyzing the response of the aircraft attitude in terms of bank angle (φ) and heading (β), Figure 5-11 was constructed. The response of the integrated ACDC (blue solid line) is nearly identical to the response of the RV-7 (dashed red line). This shows that there will be minimal change in response when flying with the ACDC system.

The impulse response of a rudder

deflection on the resulting heading (top left) and the roll angle (bottom left) is shown in Figure 5-11. The final value of the heading is close to zero, which indicates that the aircraft will naturally straighten itself out.

Similarly the impulse response of an aileron deflection on the resulting heading (top right) and the roll angle (bottom right) is shown in Figure 5-11. This result is in agreement with the phenomena known as adverse yaw effects to aircraft. When the response of bank angle is examined due to aileron deflection it is seen that a small spike occurs then levels itself back to nearly the original value much like the rudder affected the heading. On aircraft, an aileron deflection impulse will roll the plane slightly then, due to its geometry and design, will level itself out.

According to the graphs, the trend that the RV-7 follows for each response is closely resembled by the RV-7 with the ACDC system attached at the tip of the wing. The addition of the ACDC will not cause the plane to become unstable under normal flight conditions and changes. From static analysis, the deflection was found to be only less than one degree for each control surface (see Appendix F). The only true affect the device will induce on the aircraft is the change in Spiral mode that must be corrected by a slight rudder deflection coupled with a slight aileron deflection to maintain steady level flight.

E. EagleTree FDR Pro

While searching through previous senior project experiment's equipment, a data-recording device was found that could be a viable alternative to the more elaborate and expensive GRT-Sport EFIS. The device is a product by EagleTree Systems called the Flight Data Recorder, Pro version, or FDR PRO. The FDR PRO was unique in the sense that it was designed to be used with remote control airplanes. This meant that it was small, lightweight, and able to record very small changes in the selected parameters. It was decided that we would concurrently develop the EagleTree device along with the GRT-Sport and present it as a cheaper alternative for a flight data recording system. But before developing the FDR PRO, we had to ensure that it met all of the required specifications.

Most of the components will be mounted inside a small 5"x2.5"x2" rectangular boxed enclosure. The GPS antenna will be externally mounted in order to secure a clear line of sight with satellites. The Pitot tube will be protruding from the front of the enclosure while the switch and ports will be located in the rear as shown below in Fig. 5-12.

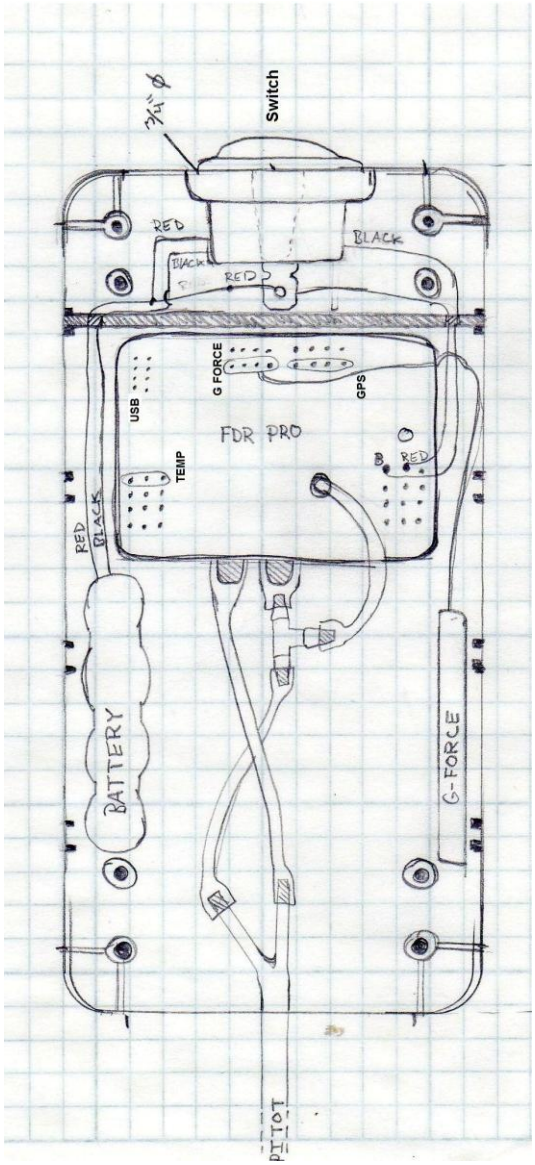

Figure 5-12: *Component Layout Sketch (5"x2" Rectangle)*

Recorder Specifications: The EagleTree flight data recorder was much smaller than the GRT-Sport EFIS, and had slightly different specifications however still within our requirements.

Airspeed: 2 MPH minimum to approximately 290 MPH maximum

Altitude: 0 to approximately 32000 feet, in approximately 1-foot increments

Operational Voltage: 4.35V to 7.0V

Weight: Recorder and Pitot tube, approximately 1 oz.

Temperature: Dual inputs, 0 degrees F to 424 degrees F

Units supported: English and Metric

Measurements: 1.97" x 1.38" x 0.67"

Record Time: Varies with sample rate, parameters being recorded, and "activeness" of the session. Anywhere from around 20 minutes to hours is attainable depending on these settings. The Pro Recorder has 4x the logging time of the other Recorders. Virtually unlimited record time is available with PC live mode recording.

Additional features needed to collect the required data:

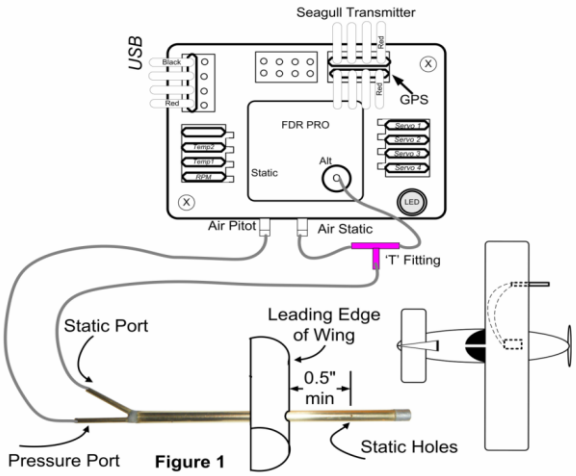

Figure 5-13: *FDR PRO Connection Diagram*

Micro Temp Sensor – Measures outside air temperature (OAT): 0 - 250 degrees max.

G-Force Expander - Measures dual axis acceleration and G-force up to +/- 38 G's

10Hz GPS Expander Module

The connection diagram for the FDR PRO is shown to the right in Fig. 5-13 The ports to connect the USB, G Force, GPS, and Temperature sensors are clearly labeled on the FDR PRO packaging. The wires from the battery connect to pins 0 and 1 of "Servo 1" counting from inward to out. This triggers the FDR PRO to begin recording and will only stop when it is full of data or the switch is turned off.

VI. Design Details

A. GRT Sport EFIS

The GRT-Sport EFIS is the flight computer that will collect and calculate all of our necessary data. It will be housed in the frame as seen in Figure ??. The block diagram to right in Figure ?? and legend below shows all the components and hardware that the Grand Rapid Technologies supplied or were integrated into the system.

- GRT-Sport
- Battery
- Power Switch
- USB port
- Pitot Tube
- Air Temperature Probe
- GPS Antenna
- Magnetometer

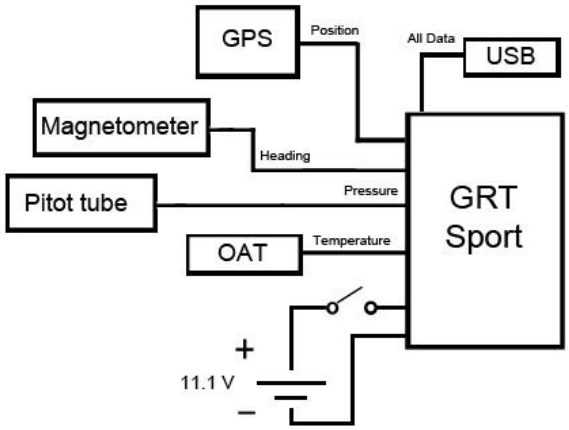

Figure 6-1: *Block Diagram of GRT-Sport EFIS*

The magnetometer is aligned with the same orientation as the GRT Sport EFIS in order to produce accurate measurements. This is because the GRT Sport EFIS uses internal accelerometers in adjusting and calculating the heading, pitch, and roll of the system. Dissimilar orientations will produce inaccurate results. 32 gauge wires connect the magnetometer and outside air temperature probe to the GRT Sport via a 37-pin dsub terminal. Connections to the magnetometer are made through a 9-pin dsub terminal.

Asymmetrical plastic snap-pin connectors and a mechanical switch make the connection between the 11.1 V 4.7 Ah rechargeable Li-Ion battery pack and the GRT Sport EFIS. Furthermore, the asymmetry of the connectors prevents the user from inverting the battery connection between either the GRT Sport EFIS or the battery re-charger. This is important because inverting the battery connection could damage the GRT Sport EFIS and cause the Li-Ion battery to explode.

A preliminary battery life test resulted in a battery operating time of 3.5 hours well exceeding the requiring 2-hour requirement. This test was conducted by powering the GRT Sport EFIS with the screen dimmed until the Li-Ion battery could no longer power the GRT Sport EFIS. Tests show that the GRT Sport EFIS is recording measurements from the Pitot-static tube, outside air temperature probe, magnetometer, and GPS system for longer than the 2-hour requirement.

B. Pressure measurement

As previously mentioned, the pressure measurement system must be at least 2.5 feet in front of the wing to meet the accuracy requirement. Therefore, the boom extends three feet in front of the system allowing for some play in the placement of the system under the wing. Also, the system must pivot in order to correct for changes in velocity direction. For this, a multi-axis pivot joint is manufactured.

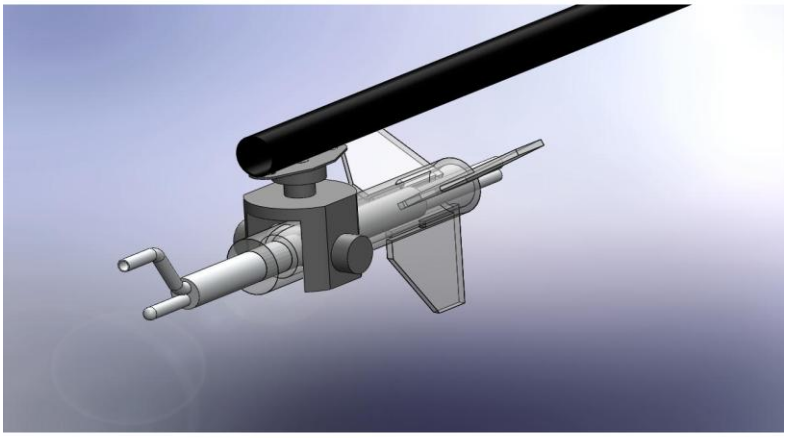

Figure 6-2: *Solidworks CAD model for multi-axis pivot joint.*

The pressure measurement system consists of a few purchased components and components that have been manufactured in one of the two Cal Poly Mechanical Engineering Machine Shops: the Senior Projects Lab (the Hangar) and Mustang '60. The purchased components are an Aircraft Spruce Pitot-static tube, a 3-foot long carbon fiber tube, and a ball bearing. The manufactured parts are a Pitot tube casing, polycarbonate fins, a clevis, and pivot pin. The fins allow the system to pivot around the pivot pin and to rotate in the ball bearing when there is a change in direction. All of the materials chosen are lightweight to fulfill the weight requirement.

C. Original Main Body

The main body is made up of the lightweight frame, strap system, and fairing. Refer to Appendix C for detailed drawings of each part.

The main body's lightweight and rigid characteristic are due to the fiberglass "L" bar used to outline around the EFIS's box shape (Figure 5-4). Referring to Figure C-1, the frames were cut to size such that they would provide the 18 inches between magnetometer and EFIS required by the Instruction Manual from Grand Rapid Technologies. Holes were drilled to attach 1/32-inch thick aluminum bands around to hold the four pieces of fiberglass stock together. The strap system was integrated by weaving the strap under the aluminum bands.

To cover the box shape of our device an aerodynamic faring was added, this will be accomplished by using a CNC machine to carve out the right shape from a SolidWorks drawing to be our negative plug. The plug will be used as a shape to lay-up fiberglass cloth and epoxy resin.

D. EagleTree FDR

The final Design will be based around a small black rectangular enclosure and the system components of the FDR PRO design will consist of:

- Recorder (FDR PRO)
- Battery
- Power Switch
- USB port
- Battery Charging Port
- Pitot Tube
- Air Temperature Probe
- GPS Antenna
- G Force Sensor

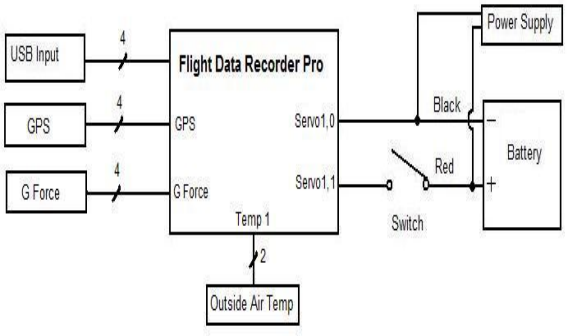

Figure 6-3: *Eagle Tree Systems Connection Block Diagram*

The system connection block diagram is shown in Figure 6-3. While the sensors have predetermined points of contact on the FDR PRO, the ports located on the back of the enclosure were added on to make the system more user friendly. The "Power Supply" input port will be used to charge the battery while the device is not in use. The switch will initiate the recording capability by allowing power to be supplied to the "Servo 1" location on the FDR PRO. The "USB Input" will allow

the user to extract the data collected and stored on the FDR PRO to a computer by way of a standard USB cable. FDR PRO version 5.54.

A few different methods have been used to test the functionality of the data recorder.

***Bench Test*:** The bench test consisted of connecting all of the components and sensors to the FDR PRO and confirming their functionality. This was done by connecting the FDR PRO to the computer via USB and checking the meters of the FDR PRO software for an input. This test confirmed that the Pitot tube did indeed record an air speed measurement when air was blown into it and even though the GPS could not receive a signal indoors, it still showed connectivity via a blinking LED on the antennae indicating no signal.

***Outdoor Test*:** The outdoor test consisted of checking the functionality of the sensors, most especially the GPS. Also tested was the length of time that the FDR PRO could record data before its internal memory was full. The system was mostly stationary except for two separate occasions when a similar route was walked around a building. The test confirmed that the GPS was functioning correctly and displayed the course traveled on the computer.

***Driving Test*:** A driving test was conducted with the sensors located on the driver's side mirror. This test was again intended to test the functionality of the sensors along with the accuracy of the GPS and Pitot tube data. The accuracy was tested by driving at a specific speed on the freeway and comparing it with the recorded GPS speed and registered air speed.

VII. Manufacturing and Procurement Plan

After the design was complete, a bill of materials was put together. The majority of the materials and system components were purchased from Grand Rapid Technologies (GRT), Aircraft Spruce & Specialty Co. (ASSC), and McMaster-Carr. Two sections of the Aircraft Data Collection System had manufactured components: the main body, and the pressure measurement system. All manufactured parts were machined and assembled in Cal Poly's Senior Project Lab Machine Shops: the Hangar and Mustang '60.

A. Body Manufacturing

As previously mentioned, the original main body is the rectangular section that houses the EFIS and supports the carbon tube to which the pressure measurement system is attached. The raw materials purchased for the main body include fiberglass angle, aluminum sheet metal, aluminum plate, and aluminum rivets. The part drawings for the main body are found in figures C-1 through C-8 in Appendix C. For the machining, the fiberglass angle was cut to length on a vertical bandsaw, the aluminum plates were cut to just larger than their specified dimensions using a plasma cutter and then sanded to their final size with a disc sander, all holes were drilled with a drill press and a hand drill, and the aluminum sheet metal was cut with a shear and bent with a sheet metal bender. The body was assembled using aluminum rivets and a rivet gun.

The redesigned chassis was manufactured with aluminum angles instead of fiberglass. Plexiglas was used for the outside panels. A laser cutter was used to manufacture these pieces. Aluminum plates were cut using a hydraulic shear to support the boom. The collars from the original chassis were reused in the new design. Most of the frame is fastened with rivets. However, some of angles are attached with nuts and bolts to allow them to be taken apart, if needed. The redesigned part drawings can be seen in Appendix ??.

B. Pressure Measurement System Manufacturing

The pressure measurement system is the other section with manufactured components. This is the mechanism that points into the freestream and collects static and ram pressure. There are three pre-manufactured components of the pressure measurement system: the Pitot-static tube, the carbon fiber boom, and the ball bearing that connects the pressure measurement system to the carbon tube. The rest of the pressure measurement system was manufactured. The raw materials bought for manufacturing include solid polycarbonate round stock for the connector, polycarbonate sheet for the fins, aluminum round stock for the clevis, and aluminum round stock for the pivoting connector. The part drawings for the pressure measurement system are figures C-9 to C-12 in Appendix C. Pressure measurement part 1 in fig. C-9, the connector, is made of polycarbonate. The polycarbonate round stock was first drilled out to specified inner diameters on a lathe so the Pitot-static tube could fit into one end and the nylon tubes could fit in the other end. Then, a quick code was written on a CNC lathe to chamfer the front end of the polycarbonate so it would be slightly more aerodynamic. After that, a hole was drilled through the side of the tube on a mill and another small hole was drilled and tapped on the mill so a setscrew can hold the Pitot-static tube in place. Finally, three small slots were milled out of the back so the fins could fit onto the connector. Pressure

measurement part 2, the clevis, shown in Fig. C-10, is made of aluminum round stock. First, part the large round stock was turned down on the lathe so it could fit into the purchased ball bearing. Then the piece was parted off to length on the lathe. Then, the large slot was milled out with a large endmill. The sides were flattened out with an endmill as well. After that, the hole was drilled through the part on the mill. Finally, all of the edges were deburred and the clevis was finished. Pressure measurement part 3, the pivoting connector, shown in Fig. C-11, was cut to length on a vertical bandsaw, the elongated hole was milled out on a mill, and then it was deburred. Pressure measurement part 4, the fins shown in fig. C-12, were cut using a laser. As for the assembly, the fins are simply pressed onto the connector, the pivoting connector is set in place using two snap rings, the Pitot-static tube is secured using a set screw, the ball bearing and clevis are attached using two set screws, and the entire pressure measurement system is connected to the carbon tube with two ¼-28 bolts.
Unfortunately, there are left over materials because some components had to be ordered in larger quantities than needed. Cost could be slightly cut if it were possible to only order necessary amounts of raw material. However if this were a production part, this would not be a problem. It would simply mean that the cost of the system would slightly decrease.

VIII. Verification and Testing Plan

There will be three separate tests performed on the Aircraft Data Collection System: a static test, a test in a vehicle, and a flight test. These tests will verify that the system meets the specified requirements.

D. Static Testing

The aircraft data collection system will be taken to an airport and the static temperature, altitude, and pressure readings will be verified against airport data. If there is a deviation, the system will be calibrated according to airport data. This test will verify that the system can accurately collect outside air temperature data, can collect data at a rate of 1 Hz or faster, is accurate to within 3%, and can be stored in Comma Separated Value (CSV) format on a removable drive. Other static tests include weighing the system to verify that it meets the 10 lb. weight requirement and measuring the system to ensure that it is within the cross sectional area requirement of 25 square inches.

E. Vehicle Testing

In the vehicle test, the system will be mounted to the roof of an automobile. The automobile will travel a route with varying altitude and speed. The speed data from the system will be verified against the speedometer of the vehicle to test for accuracy. The same route will be retraced a second time in order to test the precision of the built in GPS system. If the data lines up for both passes on the same route, it can be verified that the system is collecting accurate altitude and position readings. This test will further verify that the system can collect data at a rate of 1 Hz or faster, be accurate to within 3%, and can be stored on a removable drive in CSV format. It will also verify that the system can collect true and indicated airspeed, pressure altitude, outside air temperature, latitude and longitude data with the GPS, and gravitational acceleration readings for pitch and roll. The gravitational acceleration for yaw cannot safely be tested in an automobile, so that will come with the aircraft test.

F. Aircraft Testing

Once the static and vehicle tests are complete and yield adequate results, the system will move to the aircraft-testing phase. The aircraft tests will take place in San Luis Obispo, California, on an RV-7, a Vans Aircraft plane. Aircraft testing will begin with a timed installation of the system in order to ensure that it will meet the physical requirements of taking no longer than 30 minutes to install and installation without permanently altering the aircraft. After that test is complete, the aircraft will fly a certain path with the system attached to the wing. Data from the aircraft's instruments will be recorded during the flight and once the plane has landed, the data from the aircraft's instruments will be compared to the data from the Aircraft Data Collection System. This test will verify that the system meets the data requirements which are collecting data at a rate of 1 Hz or faster, accuracy to within 3%, and data storage on a removable drive in CSV format. It will also verify the collection requirements of collecting true and indicated airspeed, ground speed, pressure altitude, outside air temperature, longitude and latitude location data, and gravitational acceleration readings for pitch, yaw, and roll. The durability requirements are more difficult to test because they cover very extreme situations such as a temperature range of -40°F to 120°F, accelerations up to 10Gs, an altitude range from -500ft. to 18,000ft., and speeds up to 300mph. The aircraft on which the aircraft test will be performed is a Van's Aircraft RV-7. Even with a 200hp engine, the RV-7's top speed is 217mph, so the 300mph requirement cannot be fully verified on this aircraft. Since the test is taking place in San Luis Obispo, California, the

lower altitude range of -500ft. cannot be tested because there is nowhere in the area with that low of an altitude. However, the RV-7 has a flight ceiling of approximately 25,000ft so the upper altitude range of 18,000ft can be tested. As for the 10G gravitational acceleration requirement, the test pilot will pull as many Gs as he feels comfortable pulling and, whether it is 10Gs or not, that will be the extent of the gravitational acceleration test. Once the static, vehicle, and aircraft tests are complete, the system requirements will be verified as completely as possible be with the available resources.

D. Eagle Tree Testing & Verification

The GPS and Pitot sensors attached to the Eagle Tree Systems Flight Data Recorder seem to be in good working condition and collect reasonable data that has yet to be verified pending more in depth testing analysis. The G Force attachment does not produce readable data and is thus unable to get past the calibration phase. The data that is generated by the G Force attachment appears to jump sporadically between the two extremes for negative and positive G force while laying down on a flat surface and not moving, where it should be reading zero. The G Force was deemed dysfunctional and sent back to the manufacturer who confirmed the analysis that the attachment was not working correctly. The manufacturer then tested and sent a new G Force attachment for use with the project but when the new G Force was attached, the data was still inconsistent. This lead to the conclusion that the problem was most likely in the Data Recorder itself as we do not know the history of the device or what other projects in which it has been used. At this point further production of the design was stopped in order to focus all of the team's efforts towards the main EFIS based data recorder.

If further investigation into the functionality of the unit is desired some useful suggestions and procedure advice are provided below.

1) The connector that connects the large ¼" pitot tube from the carbon fiber boom to the smaller 1/16" air tubes for the Eagle Tree are not designed to be reducers and were just quickly thrown together for fitting and very basic testing purposes. A proper ¼" to 1/16" air line convertor will be needed.
2) A new Flight Data Recorder can be purchased from the Eagle Tree Systems website. http://www.eagletreesystems.com/
3) The instruction for use and the software to interface with the Eagle Tree Unit is available on the Eagle Tree Website under "Support" and then "Download Latest Software." The most updated software should be compatible. http://www.eagletreesystems.com/Support/apps.htm
4) Once calibrated, the G Force meter placement could use more support to properly secure it.

IX. Verification and Testing Procedure

A. Vehicle Testing

The system has been through three automobile tests. The first test verified that the system collected data. However, two complications were found during this test. Corrections were made and the second test verified that the system performed flawlessly. The third test was performed solely for calibration of the system's true airspeed data.

For the first test, the system was strapped to the roof of an automobile. The pressure measurement system was placed in front of the windshield so it could collect undisturbed flow data. Straps were used to secure the system to the roof of the vehicle. The automobile then drove a planned route at varying speeds ranging from 0mph to 65mph. During this test, however, the pressure measurement system began vigorously oscillating. The test was prematurely aborted and the system was taken back to the machine shop for a thorough examination. It was found that the pressure measurement system was not fastened securely enough to the boom. An aluminum insert was designed and manufactured in order to more securely fasten the multi-axis pivot device to the carbon fiber tube. Upon extracting the data, it was found that the data was stored in a ".LOG" proprietary file format. Therefore, the data had to be converted into a format that is compatible with Microsoft Excel as stated in the requirements. A program called GRTDECODE[5] was found that converted the data into xml format, which is compatible with Excel.

Once the problems were fixed, the second car test was performed. This car test was very similar to the first because the system was strapped to the same vehicle in the same manner: with the pressure measurement system in front of the windshield. This car test verified that the pressure measurement insert allowed the pivoting system to securely mount to the tube. Because the system was secure mounted, there was a lot less oscillation of the pressure

measurement system during the second test. Also, it was verified that the data could be plotted in Excel once it was converted. The second test was very successful: it verified that our system verified all of its requirements so far.

Before collecting data with the GRT Sport EFIS, it was important to perform several calibrations. Three calibrations that were made to the EFIS included a magnetometer calibration, a true airspeed calibration, and an altimeter calibration. All three calibration procedures were performed according to the GRT Sport EFIS User Manual. The magnetometer was calibrated by placing the EFIS and magnetometer inside the chassis and set in alignment with each other. The EFIS was rotated 360 degrees in 1 minute taking measurements as part of the self-calibration procedure.

To calibrate the EFIS true airspeed calibrations, the EFIS required taking measurements while at speed on a constant heading for 30 seconds and then measurements on the opposite heading for 30 seconds. Since the EFIS needed to be operated for this self-calibration procedure, the entire system was strapped to the hood of a truck. The EFIS was then calibrated by driving up and down a straight road at approximately 40 mph. After calibration, the true airspeed was roughly the same as the vehicle's speedometer confirming that readings were as accurate as could be determined without comparing to other airspeed sensors.

An anomaly in magnetometer readings appeared during this test. The heading, according to the EFIS display, constantly rotated counter clockwise. This led us to believe there was interference with the magnetometer. Some possible causes for this could have been that the wires connecting the EFIS to the battery pack ran underneath part of the magnetometer. Additionally, the interference could have been due to a misalignment of the magnetometer with the EFIS. Having the system operating on the hood of a truck also could have lead the vehicle's engine to cause interference with the magnetometer. After repositioning the wires away from the magnetometer and aligning and securely fastening the magnetometer to the chassis, this issue was no longer observed.

The final calibration procedure involved calibrating the altimeter, which should be calibrated before each flight for highest accuracy. The altimeter was calibrating using the known elevation at the site of calibration and the barometric pressure obtained typically from an airport tower. For details in calibrating the GRT Sport EFIS, see the GRT Sport EFIS User Manual. The User Manual can be found on the documents page of Grand Rapids Technologies website:

http://www.grtavionics.com

B. Fit Testing

When the frame was completed, a fit test was performed to determine whether the frame would strap securely to the wing. The test showed that the frame would be unable to securely strap to the wing. The main problem that was seen during the strap test was that, no matter how much the strap was tightened, the frame would still droop underneath the wing. Another problem the test showed was that the tension force from the strap was acting along the whole surface of the frame when it would be better for the force from the strap to be concentrated on a smaller area. After this first strap test it was determined that a new frame would need to be designed and built if our system was going to be securely attached to the wing.

After the new frame was constructed, another fit test was performed in order to determine if the new frame fixed the problems encountered during the first fit test. The second fit showed that the new frame design was a drastic improvement over the old frame. The new frame, with its adjustable pads that increase the tension force on the strap and concentrate the force from the strap, allowed the new frame to securely attach to the wing. The new frame did not wobble in any direction and proved that the frame would not detach from the aircraft during flight. In addition to the adjustable pads, the general shape of the design was much more aerodynamic than the rectangular cube of the old design. Therefore, an aerodynamic shell would not be needed in order to perform a flight test. There was one problem that occurred during the second fit test, which was a slight structural weakness in the frame. The flat aluminum strip that runs under the EFIS controls bent under the tension force from the strap. This problem was fixed by replacing the weaker strip with a thicker strip of aluminum.

C. Aircraft Testing

The testing of our device on the RV-7 was done in three stages, a dry run test, data collection test, and maximum limit test. For each run we established that the testing device gathered the correct data and did what

Figure 9-1: *Aircraft testing of system.*

it was expected to do. With the help of Kurt Colvin, who assisted in building of the RV-7 for Cal Poly, six flight tests were performed.

The dry run was performed, and for this trial we replaced the GRT-Sport EFIS with a dummy weight so the plane felt the same characteristics of the testing device, but the expensive electronics were not at risk. The system was attached to the wing and timed for its total installation time, which had to be less than 30 minutes. The installation was recorded and documented to be approximately 14 minutes, fulfilling the requirement. Once the system was securely strapped to the aircraft, Dr. Colvin performed a taxi along the side of the runway to assure that simple vibration of the wing and aircraft did not cause the strap of the system to slip off. Small strips of tape were placed along the edge of the strap to indicate whether the strap shifted or sheared during the flight. A take off was performed and the aircraft followed the traffic pattern. Then, the tape was checked to verify that the strap had remained in its initial position.

The GRT-Sport EFIS was installed once the system successfully completed the dummy flight test. The computer was turned on and allowed to align itself. A more rigorous flight test was performed following a specified flight path. In this flight plan, the aircraft was to take off and climb to an altitude of 6000 feet then perform banked turn maneuvers and descents in order to test and verify all sensors. Data was collected for speed, GPS, altitude, and attitude during the test. The data was retrieved from the EFIS once the RV-7 returned to the hangar. The data was removed on a USB flash drive and plotted against the RV-7's flight log. Once it was verified that the collected data was accurate, the flight test was repeated with different maneuvers to accumulate as much data as possible for comparison.

Performing a system limit test required the aircraft to climb to an altitude then accelerate downward to gain as much speed as possible. In this test a max speed of approximately 190mph was attained. At this speed the system still functioned properly and remained stationary on the wing. During this test, a verification of the stability on the aircraft was assessed. The pilot indicated that, without compensation in the rudder, the plane would yaw and veer to the right as expected. Dr. Colvin claimed to add approximately 5 lbs of force to correct for the additional yawing moment. To verify our controls analysis, the rudder was marked in increments of 1, 3, 5, 7, and 14 degrees of deflection and, while in the air, it was observed than not even 1 degree of rudder deflection was needed. Aileron deflection was not verified since the ailerons were constantly being deflected to maintain steady level flight.

X. Data Analysis

After flight testing was conducted, the data was analyzed to verify its accuracy. In addition to the data collected by the system, data was also collected on the RV-7's onboard computer. The two sets of data were overlaid and the average absolute difference was calculated. The onboard computer calculated pressure altitude, indicated airspeed, true airspeed, outside air temperature, and angle of attack. Of this data only the pressure altitude and indicated airspeed were compared. It was found that the temperature sensor on the RV-7 seemed to be faultily calibrated, since the outside air temperature data was inconsistent with the temperature data known that day. Because of this, the true airspeed data was not used since it is calculated using the temperature readings. Also the angle of attack data seemed to be corrupted, since the readings were erratic and contained impossible values.

Figure 10-1 shows a comparison of the altitude and airspeed data read by the RV-7 and the system. The onboard computer is shown in blue while the designed system is shown in magenta. It can be seen that for both sets of data, the trends are virtually identical. The pressure altitude data almost perfectly overlays the data collected from the RV-

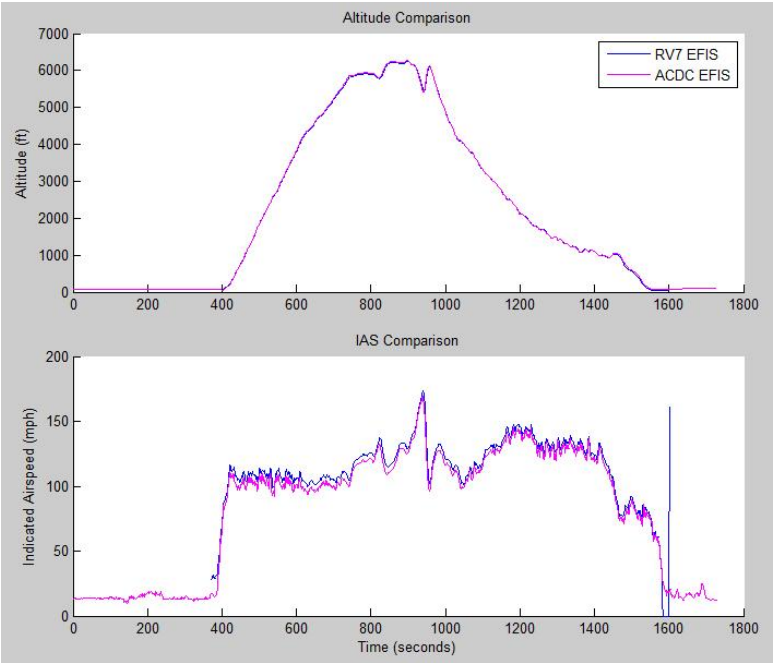

Figure 10-1: *Comparison of ACDC system to RV-7 onboard computer.*

7. The average difference between the two is 0.697%. While the indicated airspeed data follows a nearly identical trend, it can be seen that the actual values collected by our system are shifted down slightly. As can be seen in the figure, the average absolute difference is much higher. Between takeoff and landing, the average difference is 3.8%. There are several possible factors that could cause this difference. A faulty calibration could be the cause of the error, either in the RV-7 or in our system. Another factor could be the location of the pressure collecting sensors. The pressure sensors on the RV-7 are located on the left wing and along the body between the wing and the tail. Along these areas, the freestream air is slightly disturbed by the aircraft. On our system, the sensors extend out on a boom 3 ft in front of the wing (See Appendix E). This results in cleaner freestream air and more accurate data.

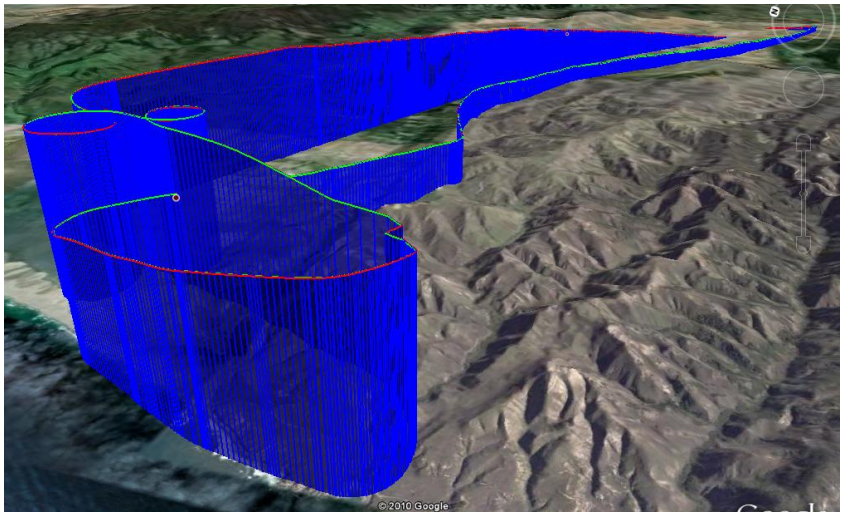

Figure 10-2: *GPS data from system in Google Earth*

In addition to the pressure data collected by the Pitot-static system and the temperature data, GPS data was recorded from the GPS receiver in a strap pocket on top of the wing. Data from the previously analyzed flight test was imported into Google Earth and plotted in Fig. 10-2. It can be seen that the system accurate locates its position and shows a take-off from the San Luis Obispo County Regional Airport. The airplane follows the pre-planned flight plan which included two 360° turns and a simultaneous descent and speed test.

Appendix A

[1]EFunda, Inc. "Hot-Wire Anemometers." *Introduction to Hot-Wire Anemometers*. Web. 8 Nov. 2009 http://www.efunda.com/designstandards/sensors/hot_wires/hot_wires_intro.cfm

[2]Tom Lawson, FREng., *Building Aerodynamics*, pp. 230-233. Published by: Imperial College Press, © 2001.

[3]John D. Anderson Jr., *Fundamentals of Aerodynamics* Fourth Edition, pp. 210-219. Published by: McGraw-Hill, © 2007.

[4]Gracey, William, *Measurement of Aircraft Speed and Altitude*, pp. 124-125. Published by: John Wiley & Sons, © 1980.

[5]Morgan, Carl. "RV7A - ZK-VII - GRTDecode - GRT LOG File Decoding Utility." *RV7A - ZK-VII - Welcome to the Construction Log for ZK-VII*. Carl Morgan, 24 Mar. 2010. Web. 09 June 2010. <http://www.rvproject.gen.nz/grt/>.

Appendix B

A. EFIS Trade Study Criteria and Decision Matrix

The EFIS was evaluated according to the criteria below. Each of the six categories was assigned a weight based on importance.

Cost: The cost of the EFIS systems included the purchase of options that were being considered in the other categories. These options included items such as the addition of Altitude and Heading Reference System (AHRS) sensors or an integrated GPS.

Weight/Volume: The EFIS systems were assigned values for their weight and volume separately then the two categories were combined into one. We also decided to make the volume hold more precedence than the weight so we decided to count the value for the volume twice, add it to the value for the weight and divide that number by three. (*Weight/Volume* = [(Weight + Volume + Volume)/3]
Also, for the volume, the longest dimension of the EFIS was considered to be negligible as the design of the product provided much greater length than required by any system. So for the "*Volume"* only the area of the two lowest dimensions was used for comparison.

Power Drawn: This value was calculated by the General Formula using the ratings for current.

Data Storage: These values were assigned based on a judgmental basis. The top score was given to the GRT Sport because it used a portable USB drive for data storage, which was more compatible with computers than the SD card used by AF-3400 and Enigma. While the Dynon was able to stream its output, it did not have a direct data storage capability.

GPS: The EFIS received a ten if the GPS was built into the system and a zero if it was not. The AF-3400 received a 2 because it did not have the GPS integrated into it, but it did have an option for an external GPS unit. The Dynon provided a connection for a GPS system but did not provide any GPS unit.

Data Range: The data range category represents if the EFIS can collect data up to the 300 MPH requirement. The four systems had varying minimum speed limits but the values were thought to be negligible because they were all less than 50 MPH (the perceived speed required for flight).

EFIS Criteria	**GRT Sport**	**Dynon D10A**	**AF-3400**	**Enigma**
Cost	$3.2k	$2.2K	$4.3k	$3.5k
Power Supply	Battery	Battery	battery	Battery
Weight	3.5 lbs	1 lb 15 oz	3.6 lbs	2lbs 15oz
Volume	7.1x5.25x4.75(cu in)	4.1x3.4x6.8 (cu in)	6.3x5.55x5.5(cu in)	8.35x5.5x5 (cu in)
Data Storage	USB flash Drive	Internal Storage, serial output	SD card	SD card
Data Types Required	yes	yes	yes	yes
GPS	Integrated	external unit w/antenna	external unit w/antenna	Integrated
Collection Rate (1 Hz)	yes (15 per second)	Yes	yes (5Hz)	Yes
Data Range (>300mph)	300+ mph	300+ mph	up to 280 MPH	300+ mph
Built-in Transducer	yes	yes	yes	yes
Required Current	1A@12V	10-30V (1.5A@12V)	10-16V @ 2A	12V@0.8A

Table 1: *Table of criteria and EFIS characteristics*

		GRT Sport		**Dynon D10A**		**AF-3400**		**Enigma**	
Category	**Weight**	**Value**	**Score**	**Value**	**Score**	**Value**	**Score**	**Value**	**Score**
Cost($)	0.28	5.2	1.456	10	2.8	0	0	3.8	1.064
Weight / Vol	0.05	2.5	0.125	10	0.5	0	0	2.5	0.125
Power Drawn	0.07	8.3	0.581	4.2	0.294	0	0	10	0.7
Data Storage	0.3	10	3	0	0	9	2.7	9	2.7
GPS	0.2	10	2	0	0	2	0.4	10	2
Data Range	0.1	10	1	10	1	9.3	0.93	10	1
Total	1		**8.162**		**4.594**		**4.03**		**7.589**

Table 2: *Trade Study Matrix for EFIS*

B. Pitot-tube Trade Study Criteria and Decision Matrix

The Pitot-tube was first compared to other pressure measurement devices such as a Hot Wire Anemometer and an Irwin Probe, however, it was concluded that a Pitot-Static tube was the most viable choice. Trade evaluated according to the criteria below. Each of the six categories was assigned a weight based on importance.

Hot wire anemometer: A hot wire anemometer is a highly accurate airspeed measurement device. It consists of a very fine heated wire to calculate the flow velocity by measuring a change in temperature. Resistivity in a wire is proportional to the surrounding temperature and the type of metal. Two popular choices of metal are platinum and tungsten and, based on the change in electrical resistance, the flow velocity can be calculated. Airspeed can be calculated in (Eq. 5-1) [1].

$$\left\{\left(\frac{I^2 R_{Ref}\left[1+\alpha\left(T_w-T_{Ref}\right]\right)}{A_w\left(T_w-T_f\right)}-\alpha\right\}_{\left]\frac{1}{c}\right)} \qquad \text{(Eq.5-1)}$$

Note: *Recall variable values in Nomenclature section pp.1.*

Although it can accurately measure airspeed, the hot wire anemometer has no way of independently measuring altitude so a static hole would need to be installed as well.

The hot wire anemometer is not a practical choice for our data collection system. It is expensive, fragile, and difficult to maintain. Even a small particle could damage the wire at high speeds. Integrating a hot wire anemometer into aircraft would require complex calibrations contrary to our requirement of a simple installation. Because of its drawbacks, we decided not to choose the hot wire anemometer.

Irwin probe: Also known as the Irwin wind sensor, the Irwin probe was designed by Peter Irwin Ph.D., an expert in wind tunnel testing of pedestrian level winds. The instrument measures velocity by having a static cavity on the surface that has specific depth, *H*, and diameter, *D*. Then a small tube in the center of the cavity stands a specific height above the surface, *h*, with inner and outer diameters of d_1 and *d* respectively. The standard configuration[2] is as shown:

$$h / d = 1.0$$
$$H / d = 3.1$$
$$d_1 / d = 0.72$$
$$D / d = 1.56$$

A flow velocity could be calculated by the relationship between the static pressure and the pressure measured above the surface. The static cavity would measure a pressure to indicate our altitude along with airspeed calculation.

The Irwin probe was implemented as a tool for measuring pedestrian level winds for buildings and structures built at sea level. Revolutionary for its application, but not suited for high speed measurements, the Irwin Probe would introduce tremendous error through manufacturing, calibration, and maintenance if it was integrated into our data collection system. Even though it has the ability to calculate airspeed and altitude, it is not compatible with our GRT Sport EFIS. With the complexity and lack of expertise with this design, the Irwin Probe fails to be an accurate device for aircraft data measurement.

Cost: Cost and budget are important in any project. Project managers usually want to minimize costs in order to maximize profit or to leave a bigger cap in expenses. Decisions should not be made solely based on cost because other factors and criterion may be compromised.

Mounting/Integration: Pitot-static tubes are manufactured in two different shapes: L-shaped and straight. Straight Pitot-static tubes clamp in line with the leading edge of the airfoil, while L-shaped Pitot-Static tubes are mounted to the bottom surface of the airfoil wing. In our collection system, in-line mounting would be preferred over bottom surface mounting. In-line mounting would also better fit our physical requirements.

Length: Pitot-static tubes need to be present in undisturbed airflow in order to collect accurate data. We will be mounting the Pitot-static tube onto a boom to reach the freestream more easily. Longer Pitot-static tubes are more desirable because a long boom is not required, thus decreasing costs and work time.

Material: Because our aircraft data collection system will include magnetometers (integrated in the EFIS and GPS), ferrous metals should be avoided, since they could disrupt our GPS. Many Pitot-Static tubes are made of stainless steel, which is ferrous. The system should include a Pitot-static tube that is composed of nonferrous material, such as aluminum.

Required Manufacturability: A pre-built Pitot-static tube would save time and money. We considered the option to build our own Pitot-static tube because we can then customize our system for optimal performance. However, this process could potentially be time consuming and expensive.

PitotTube Critieria	Build Our Own	ASSC Straight	ASSC L-Shaped	Dwyer 160	APEX Type S
Cost	$35	$20.85	$25.85	$49.75	$120
Mounting and Integration	In-line Leading Edge	In-line Leading Edge	Mount to surface	Mount to surface	In-line Leading Edge
Length	Any length	14” long	10” long	8 – 5/8” long	24” long
Material	Aluminum	Aluminum	Stainless steel	Stainless steel	Stainless steel
Required Manufacturing	Build it yourself	None	None	None	None

Table 3: *Table of criteria and Pitot-Tube characteristics*

		Build Our Own		ASSC Straight		ASSC L-Shaped		Dwyer 160		APEX Type S	
Category	**Weight**	**Value**	**Score**	**Value**	**Score**	**Value**	**Score**	**Value**	**Score**	**Value**	**Score**
Cost	0.2	8.57	1.714	10	2	9.5	1.9	7.09	1.418	0	0
Mounting/Integration	0.35	7	2.45	7	2.45	3	1.05	3	1.05	7	2.45
Length	0.1	10	1	3.82	0.382	0.89	0.089	0	0	10	1
Material	0.15	10	1.5	10	1.5	0	0	0	0	0	0
Required Manufactur.	0.2	0	0	10	2	10	2	10	2	10	2
Total	**1**		**6.664**		**8.332**		**5.039**		**4.468**		**5.45**

Table 4: *Trade Study Matrix for Pitot-Static Tube*

Appendix C

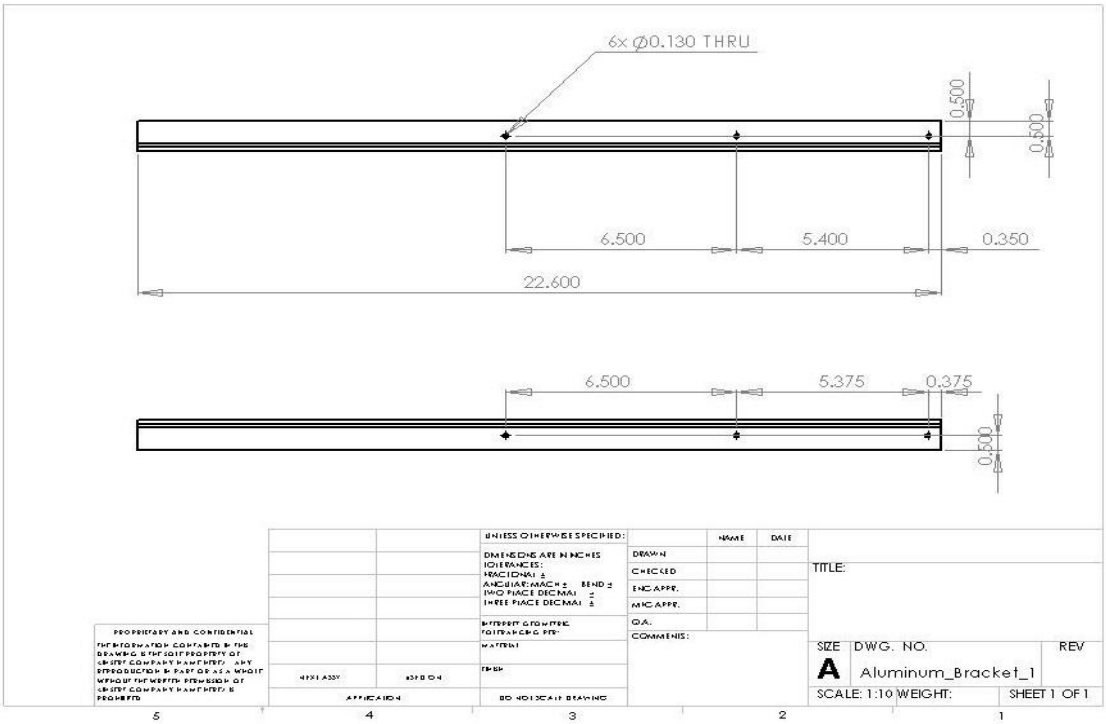

Figure C-1. Fiberglass Angle 1 (Original Frame)

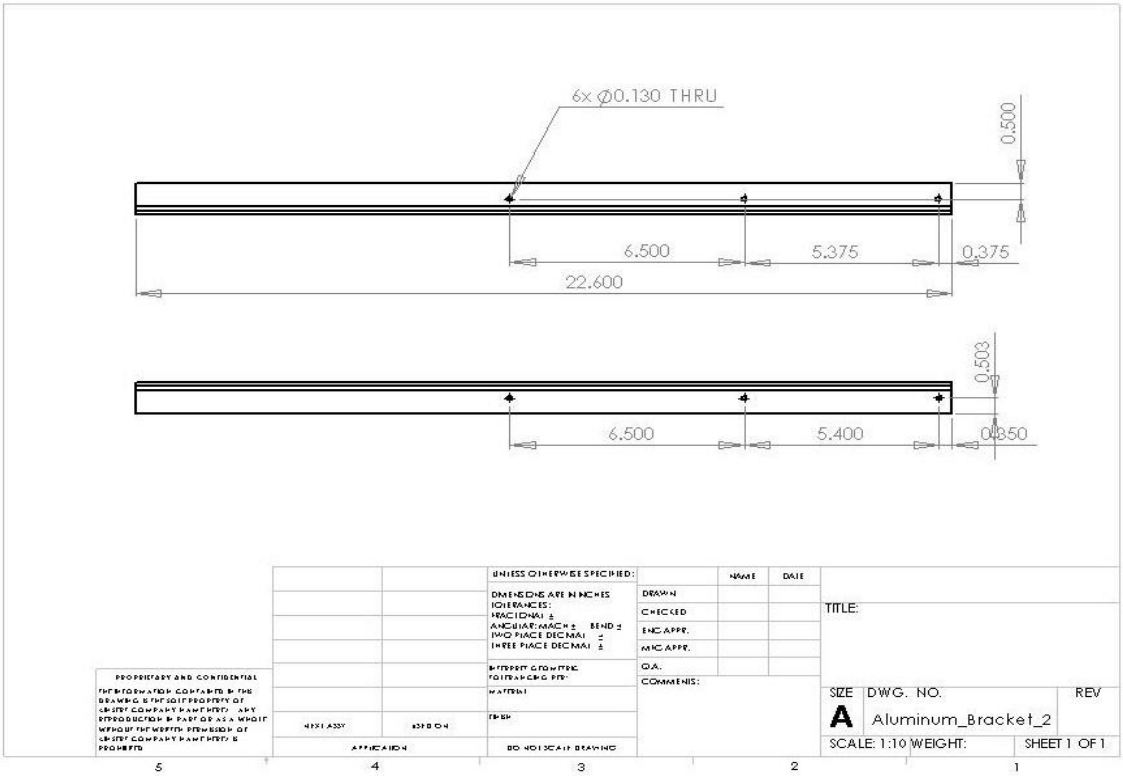

Figure C-2. Fiberglass Angle 2 (Original Frame)

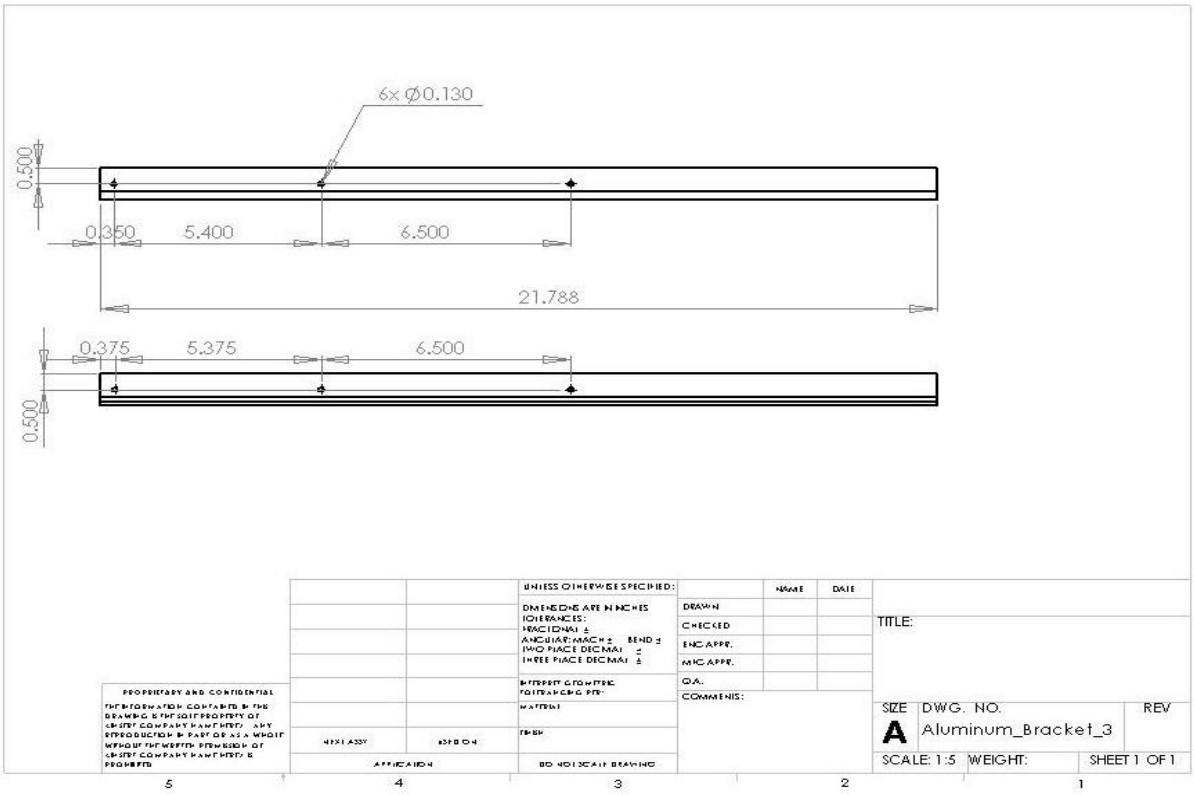

Figure C-3. Fiberglass Angle 3 (Original Frame)

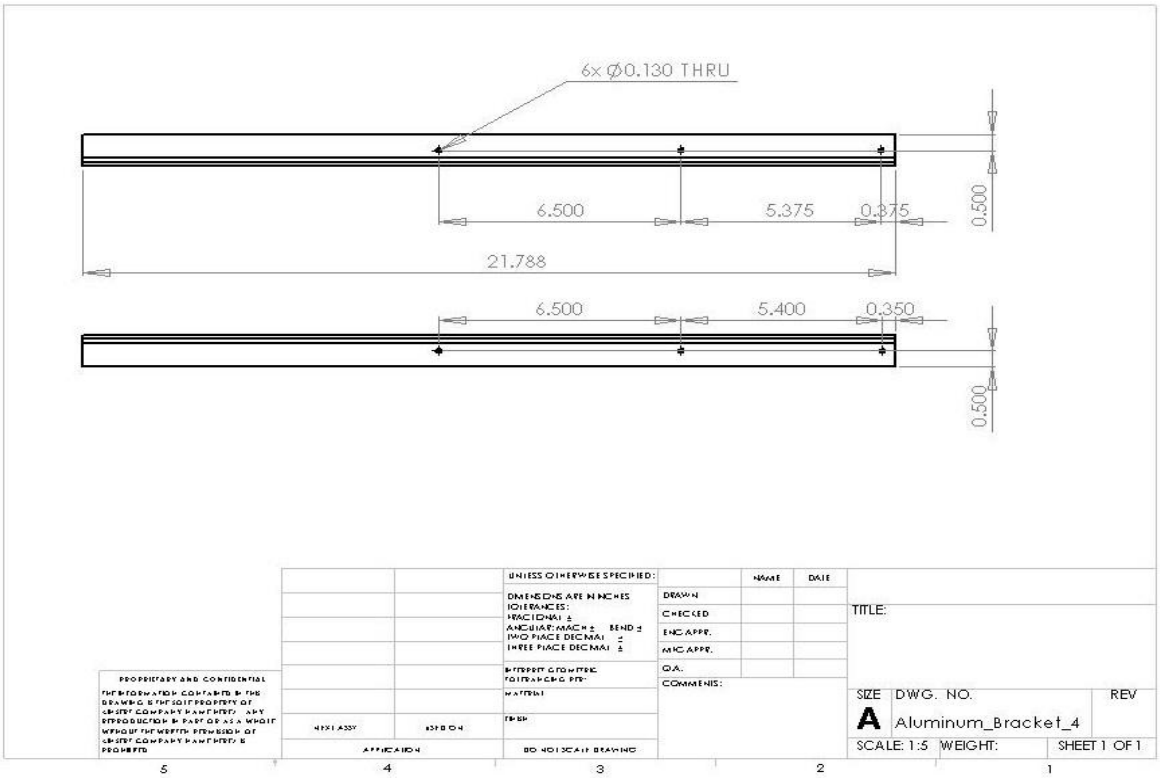

Figure C-4. Fiberglass Angle 4 (Original Frame)

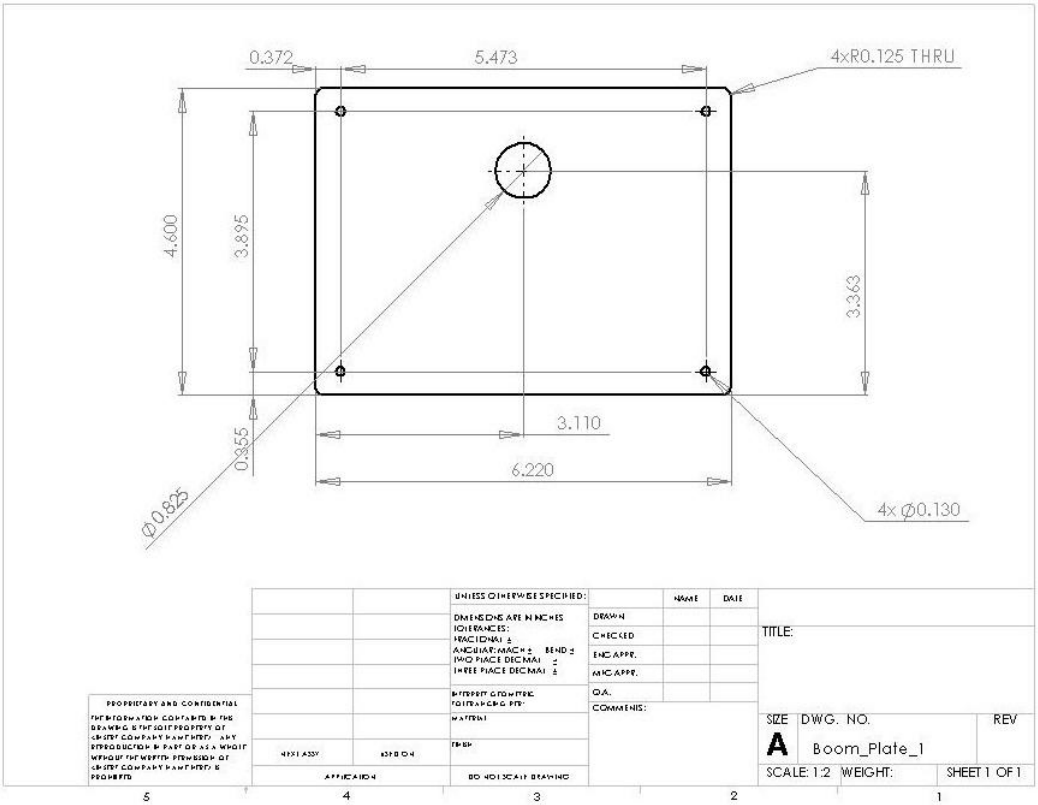

Figure C-5. Aluminum Plate 1 (Original Frame)

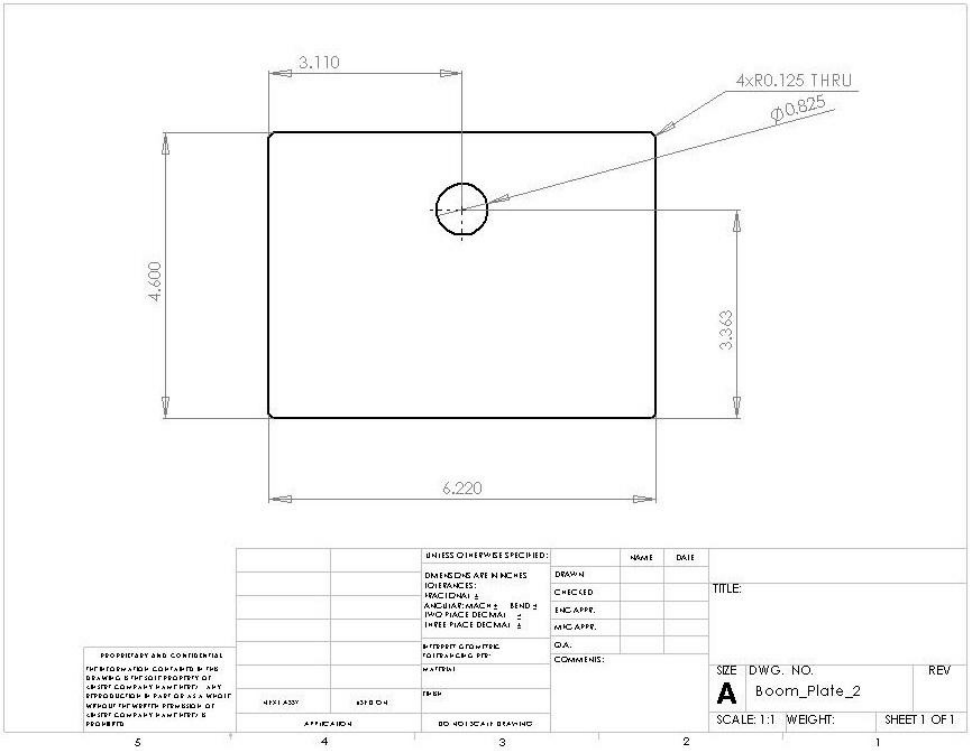

Figure C-6. Aluminum Plate 2 (Original Frame)

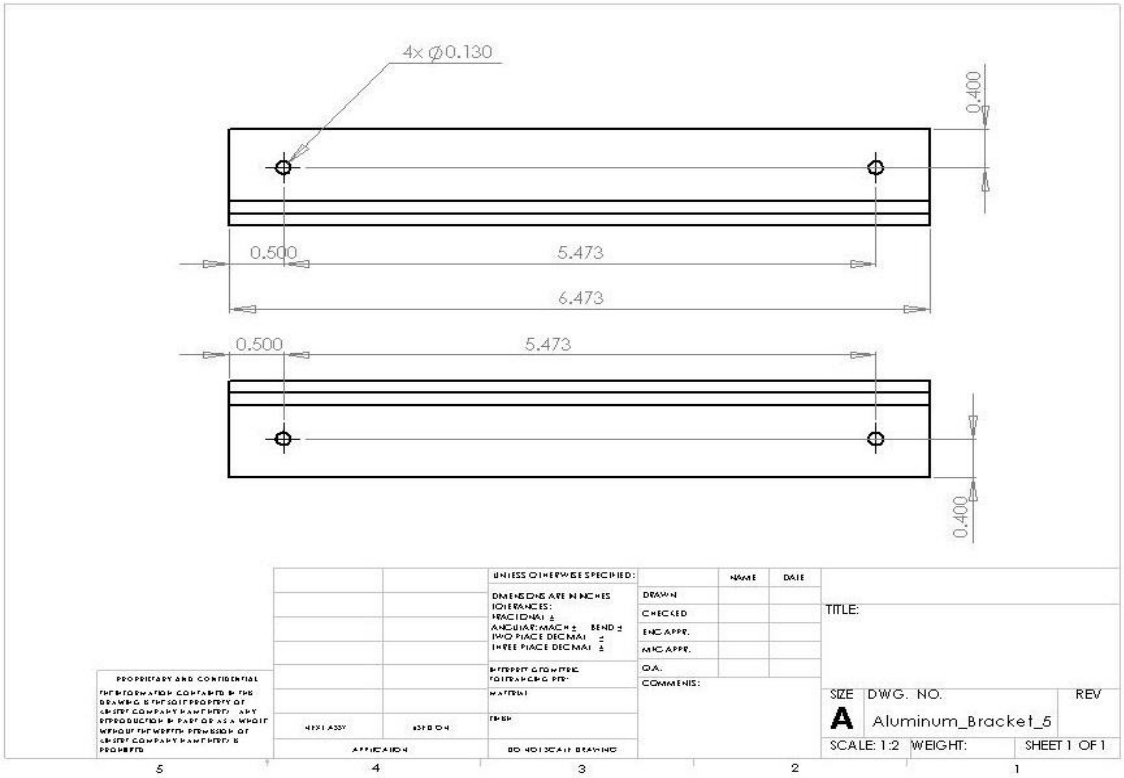

Figure C-7. Fiberglass Brackets (Original Frame)

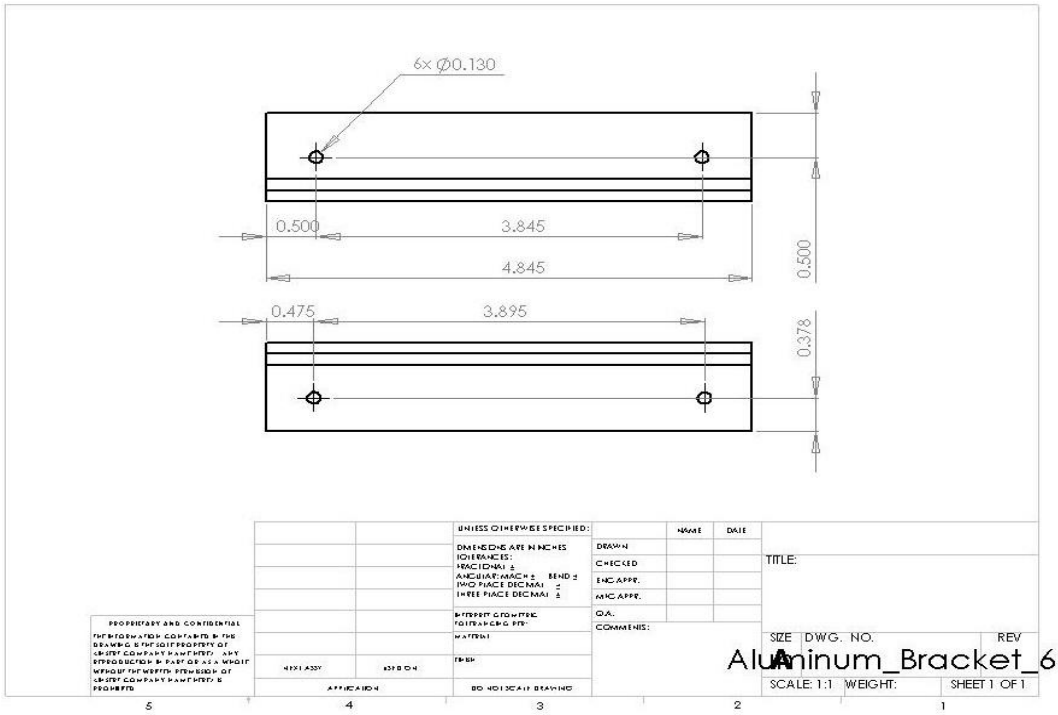

Figure C-8. Fiberglass Brackets (Original Frame)

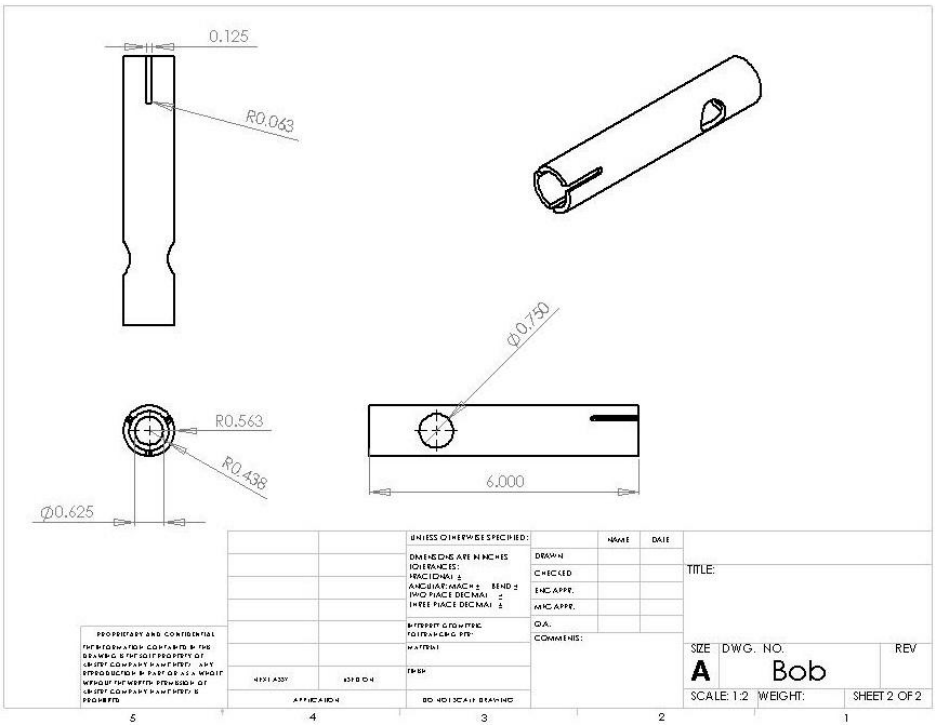

Figure C-9. Pressure Measurement Part 1.

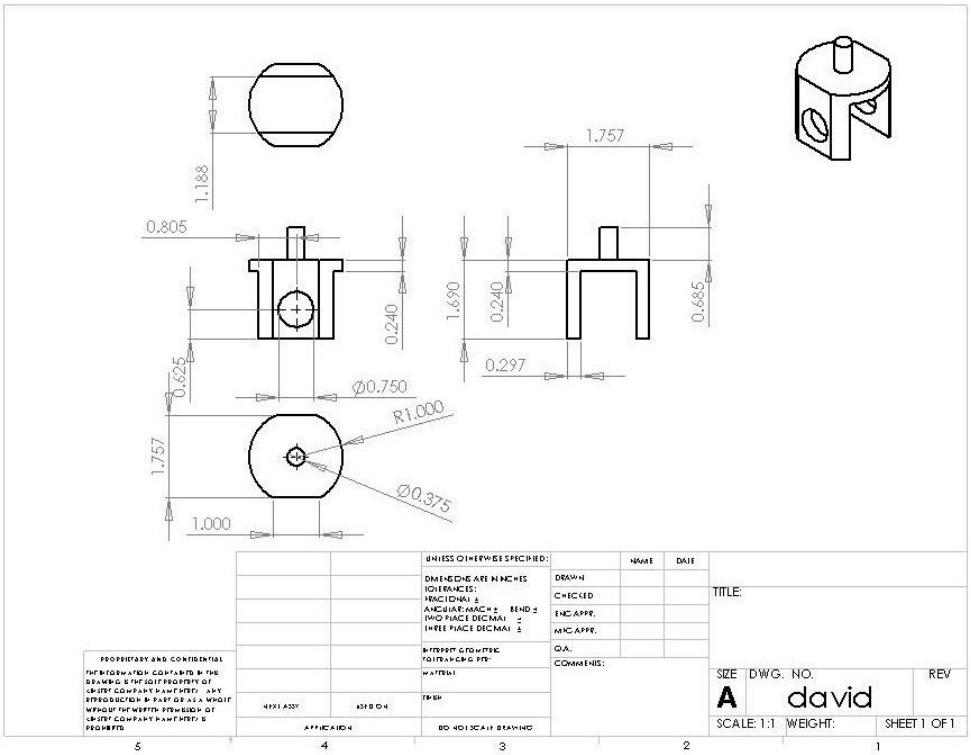

Figure C-10. Pressure Measurement Part 2.

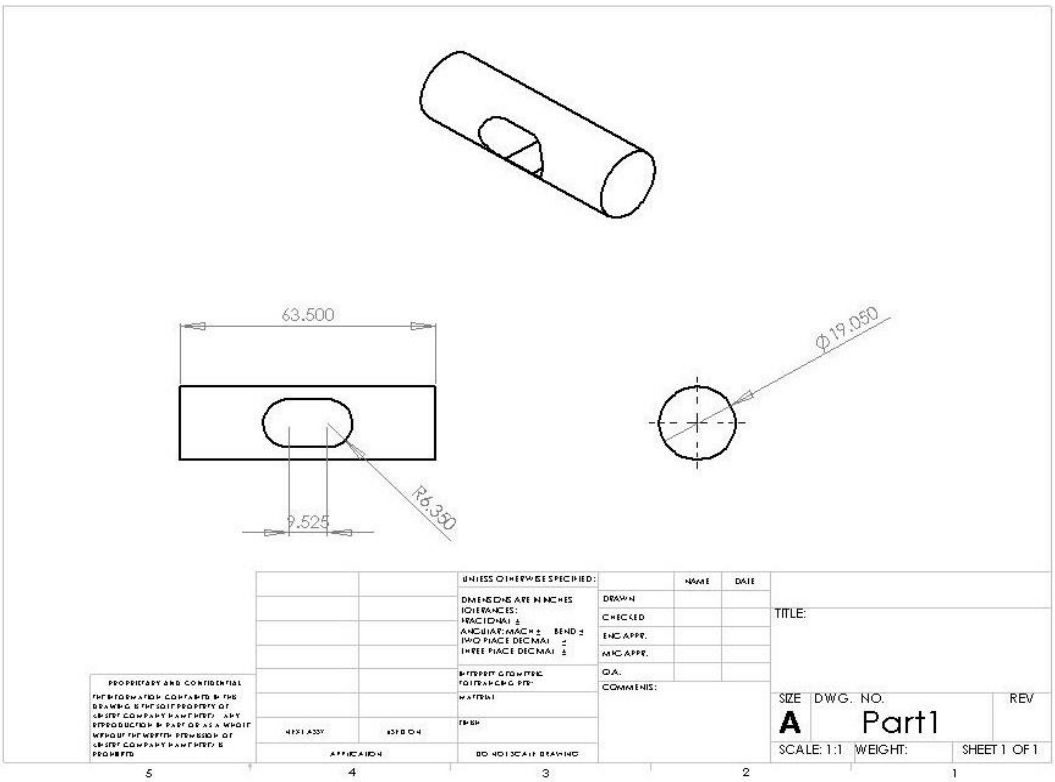

Figure C-11. Pressure Measurement Part 3.

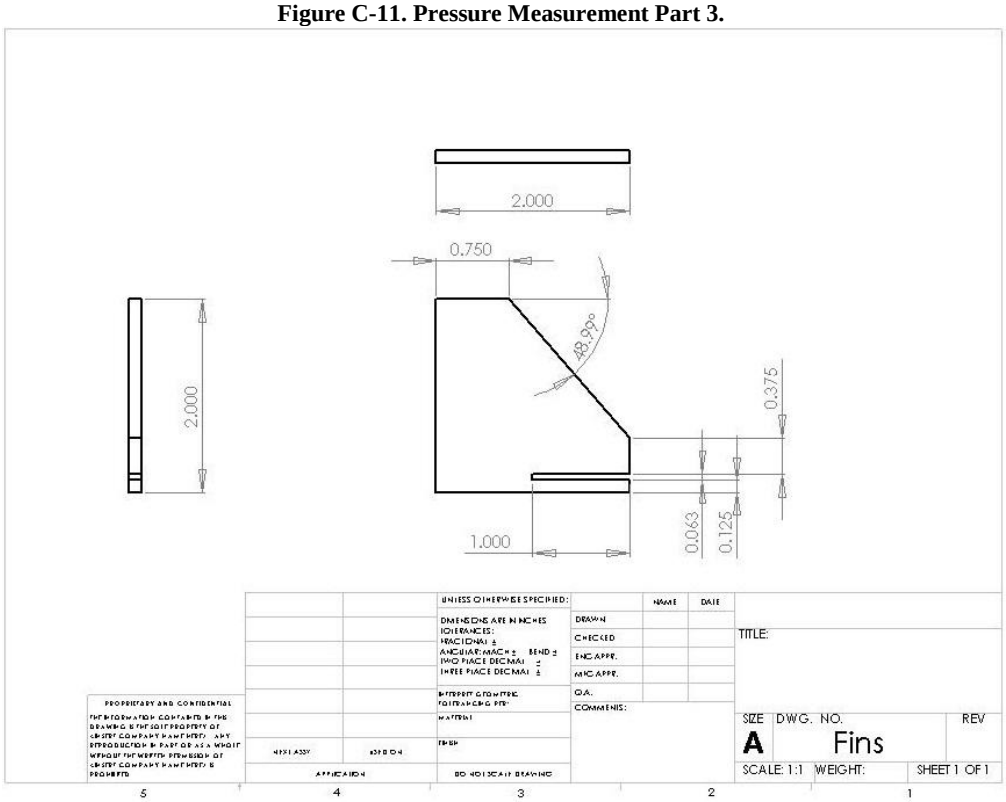

Figure C-12. Pressure Measurement Part 4.

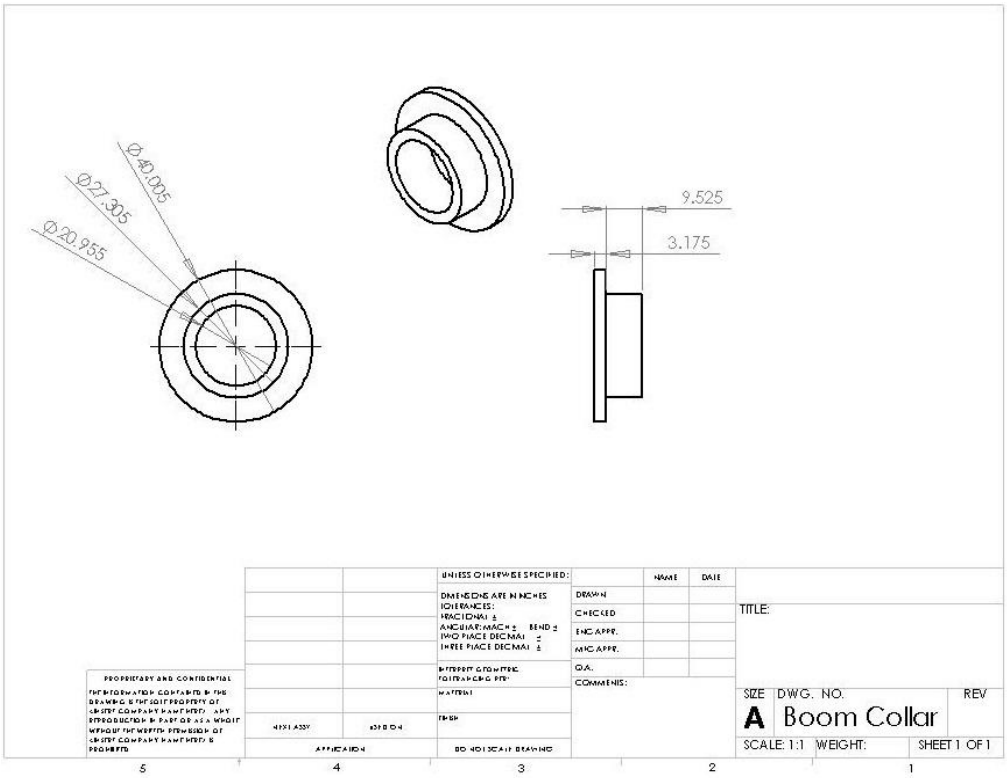

Figure C-13. Boom

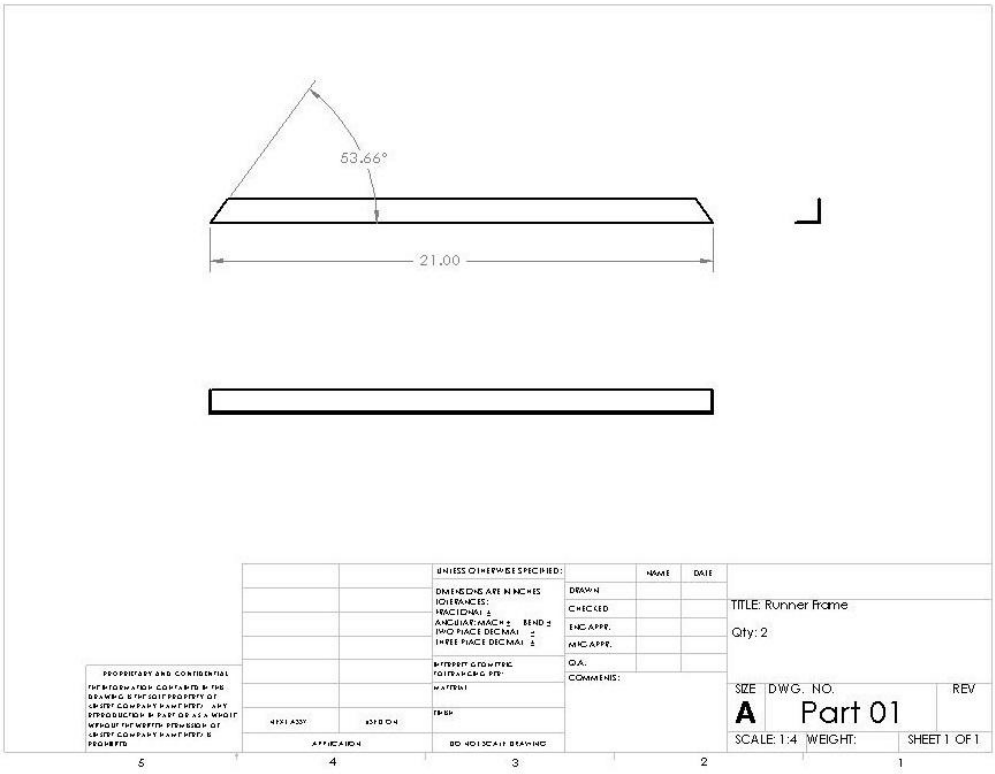

Figure C-14. Aluminum Angle 1 (New Frame)

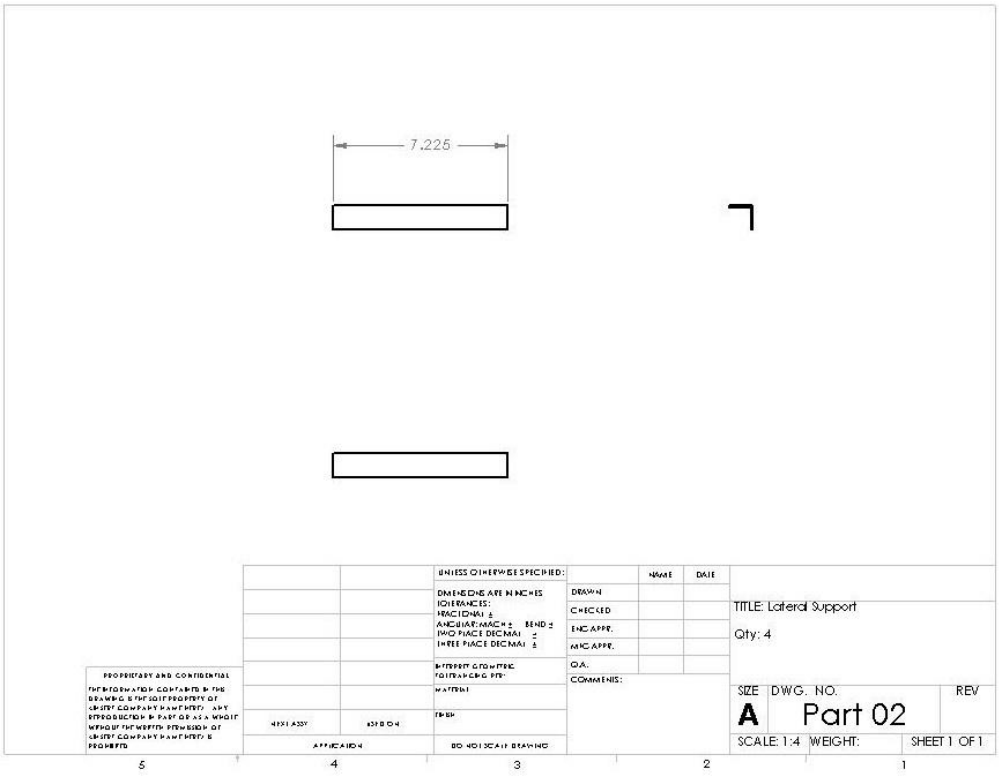

Figure C-15. Aluminum Angle 2 (New Frame)

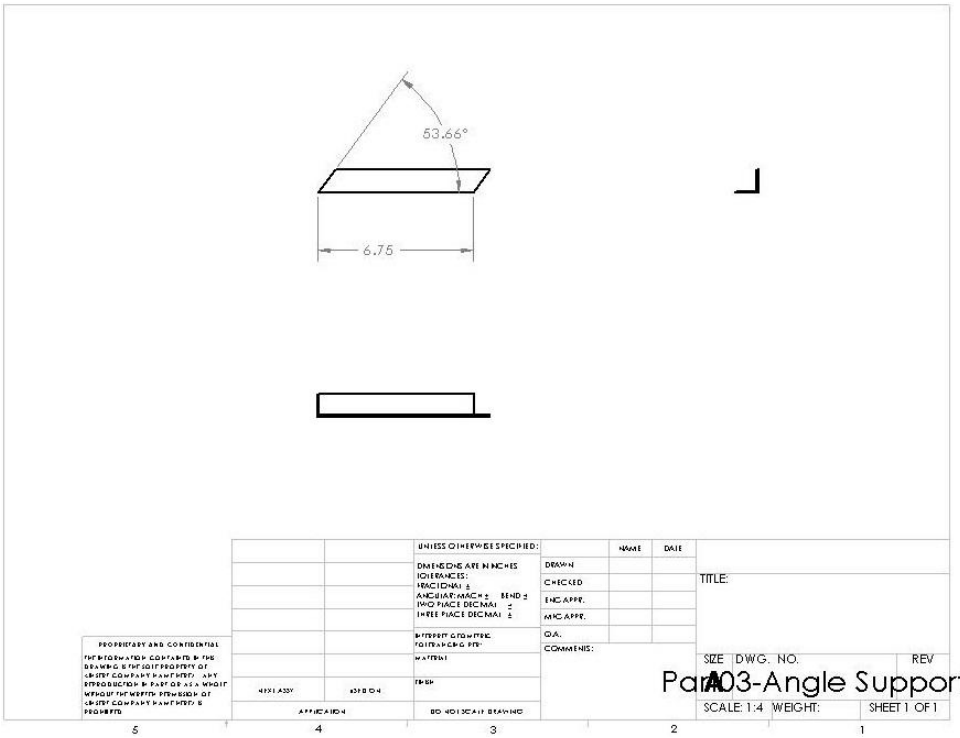

Figure C-16. Aluminum Angle 3 (New Frame)

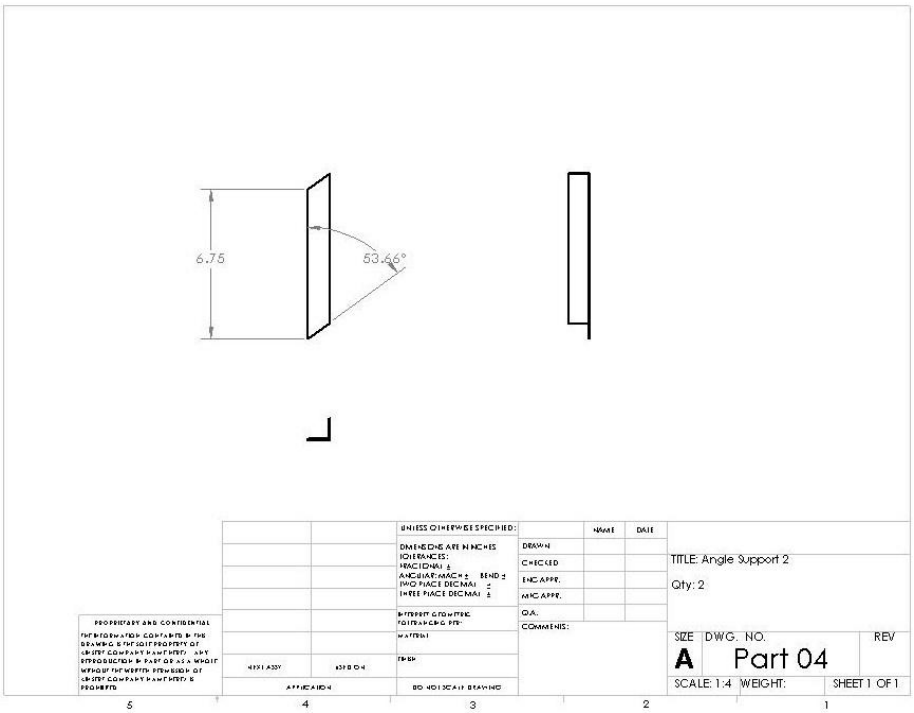

Figure C-17. Aluminum Angle 4 (New Frame)

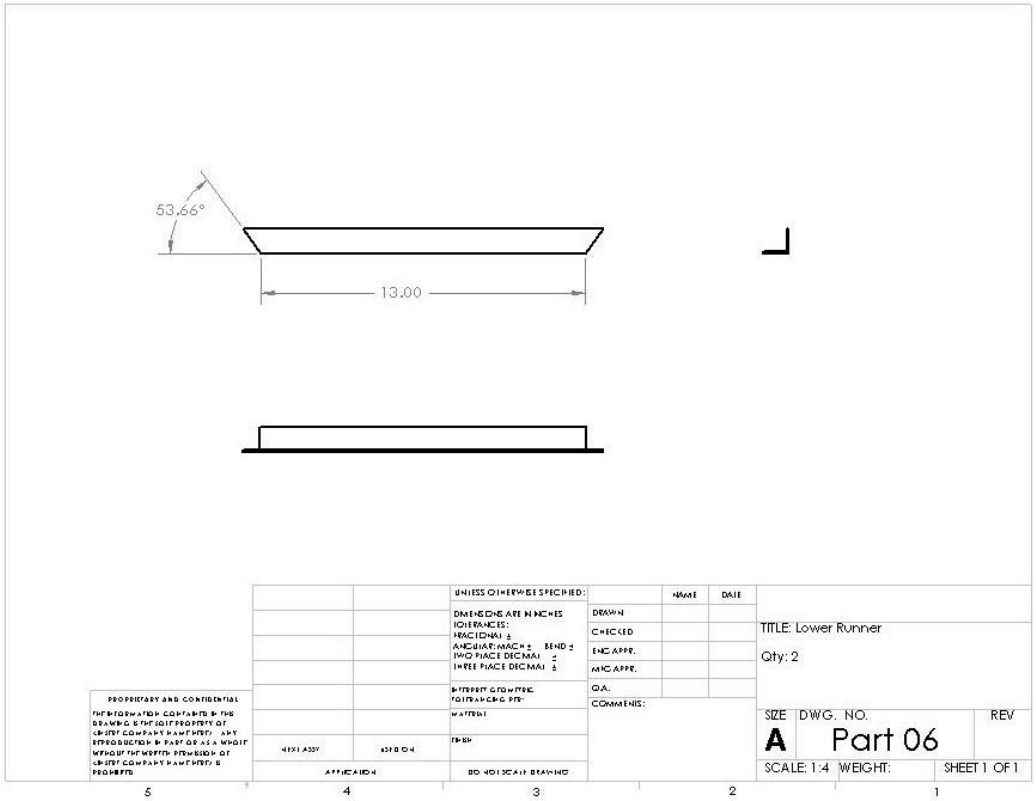

Figure C-18. Aluminum Angle 5 (New Frame)

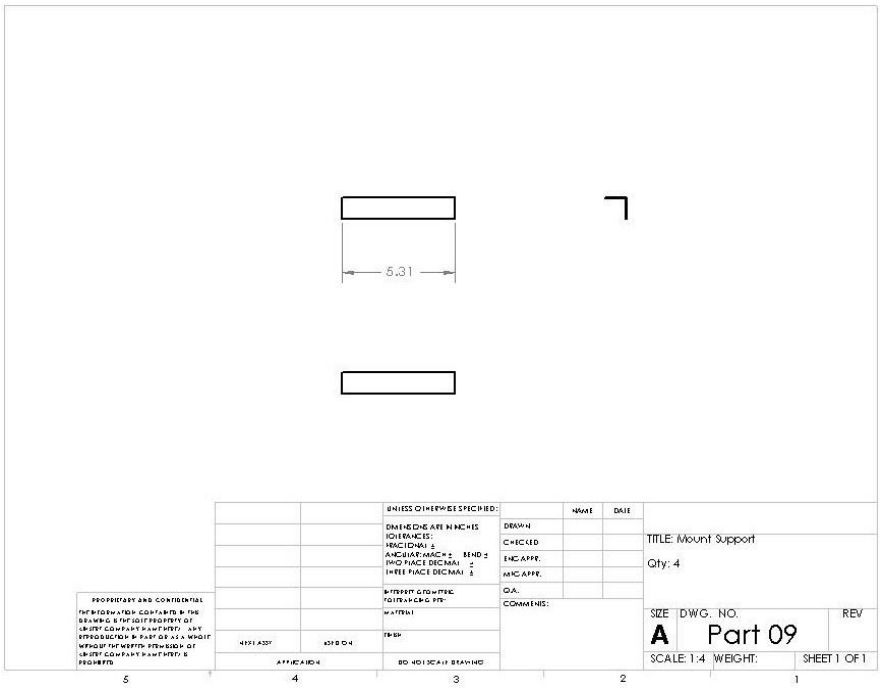

Figure C-19. Aluminum Angle 6 (New Frame)

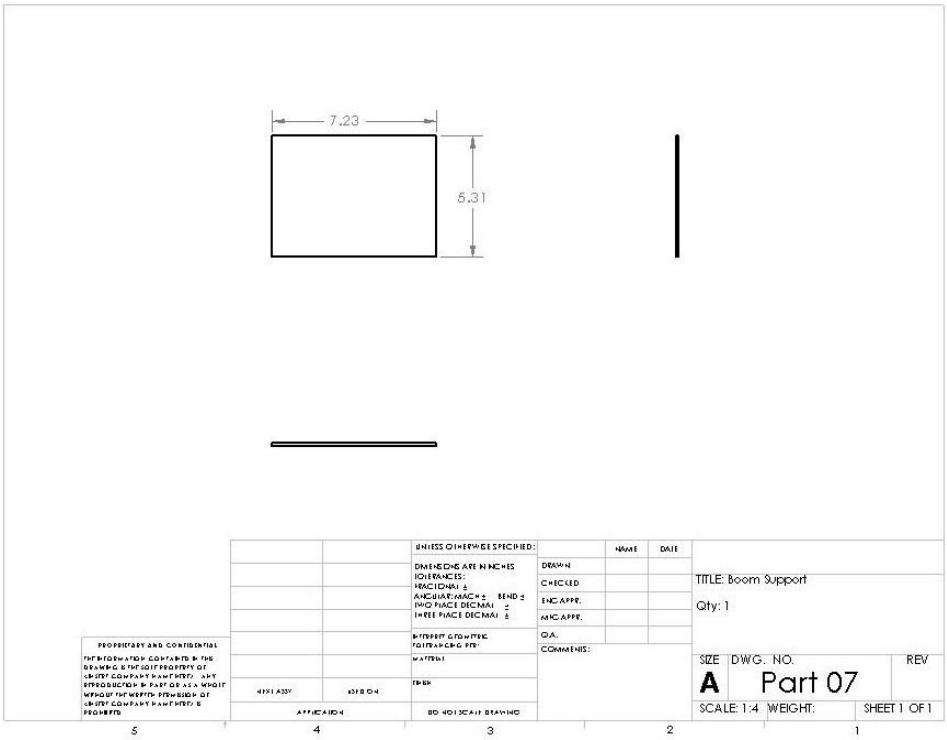

Figure C-20. Aluminum Mounting Plate 1 (New Frame)

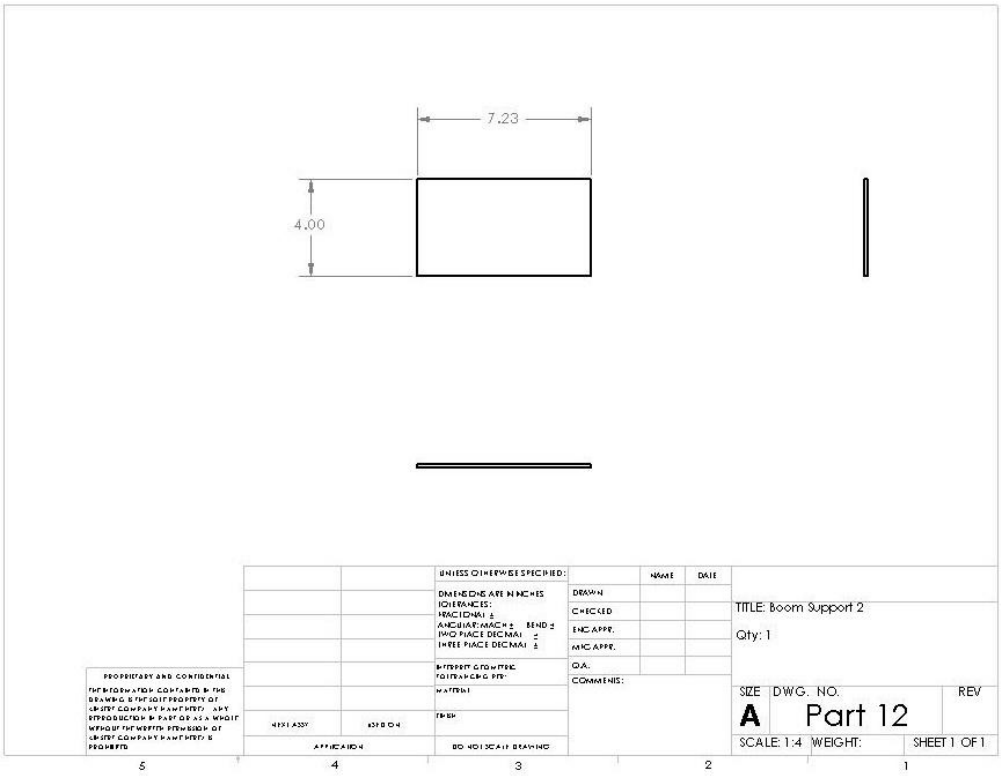

Figure C-20. Aluminum Mounting Plate 2 (New Frame)

Appendix D

Grand Rapids Technologies, Inc.
3133 Madison Ave.
Wyoming, MI 49548-1211
(616) 245-7700

Aircraft Spruce and Specialty
225 Airport Circle
Corona, CA 92880
800-861-3192

McMaster-Carr
200 Aurora Industrial Pkwy.
Aurora, OH 44202-8087
(330) 995-5500

BatterySpace.com/ AA Portable Power Corp.
860 South 19th street, Unit #A
Richmond, CA 94804
Phone: 510-525-2328

Eagle Tree Systems
4957 Lakemont Blvd SE
Bellevue, WA 98006
425-614-0450

Radio Shack
300 RadioShack Circle
Fort Worth, TX 76102-1964
Phone: (817) 415-3700

Carbon Fiber Tubing Shop
Ultra Carbon Fiber
Eagle Mountain, UT 84005
Phone: 801-471-4150

Appendix E

Effect of Flow Disturbance on Data Accuracy

Nomenclature

L	=	length of line vortex
U_X	=	velocity in x-direction at point P
U_Y	=	velocity in y-direction at point P
γ	=	vortex strength at endpoint of line vortex
η_P	=	perpendicular distance from line vortex to point P
ξ_P	=	parallel distance from endpoint of line vortex to point P

I. Airfoil Flow Analysis

The following section outlines the analysis of the flow around a NACA 23013.5 airfoil. The original requirements state that all data must be accurate to within 1%. In order to achieve this accuracy, the amount location of disturbances caused by the airfoil needs to be understood. This analysis attempts to determine the feasibility of this requirement and locate the optimal location for placement of critical sensors. *Note: Due to the large natures of the plots, all figures have been moved to the end of this section.*

II. Method of Analysis

Several Methods of analyzing the velocity potential around the airfoil were considered. Based on the experience of the team, a panel method algorithm was used for the initial analysis. For implementation of a panel code, the airfoil is divided into a series of flat panels, as shown in Fig. 1. Each panel along the airfoil is assumed to be a line vortex. The strength of the line vortex varies linearly along the length of the panel. By determining the vortex strengths at the intersections of the panels, gamma_n, the line vortices along the airfoil are fully defined.

The induced velocity at any point in two-dimensional space, P, from panel n can be modeled by the following equations.

$$U_x = \gamma_n C[G\cos(\theta) - J\sin(\theta)] + \gamma_{n+1} C[H\cos(\theta) - K\sin(\theta)]$$
$$U_y = \gamma_n C[G\sin(\theta) + J\cos(\theta)] + \gamma_{n+1} C[H\sin(\theta) + K\cos(\theta)]$$

where,

$$G = 2L\beta - \eta_P R - 2\xi_P \beta$$
$$H = \eta_P R + 2\xi_P \beta$$
$$J = LR - \xi_P R + 2\eta_P \beta - 2L$$
$$K = 2L - 2\eta_P \beta + \xi_P R$$
$$R = \ln\left(\frac{{\eta_P}^2 + (\xi_P - L)^2}{{\eta_P}^2 + {\xi_P}^2}\right)$$
$$\beta = \tan^{-1}\left(\frac{\xi_P}{\eta_P}\right) - \tan^{-1}\left(\frac{\xi_P - L}{\eta_P}\right)$$
$$C = \frac{1}{4\pi L}$$

The total velocity at any point, P, can be obtained by summing the contributions of each line vortex:

$$U_x = \sum_{i=1}^{n-1} \gamma_i C[G\cos(\theta) - J\sin(\theta)] + \gamma_{i+1} C[H\cos(\theta) - K\sin(\theta)]$$
$$U_y = \sum_{i=1}^{n-1} \gamma_i C[G\sin(\theta) + J\cos(\theta)] + \gamma_{i+1} C[H\sin(\theta) + K\cos(\theta)]$$

In order to accurately model an airfoil, a condition is stated such that the sum of the velocities due to the vortices and free-stream is perpendicular to each panel. This condition is stated mathematically through the following system of equations:

$$U_{1,1} \cdot n_1 + U_{1,2} \cdot n_1 + \cdots + U_{1,j} \cdot n_1 = -U_\infty \cdot n_1$$
$$U_{2,1} \cdot n_2 + U_{2,2} \cdot n_2 + \cdots + U_{2,j} \cdot n_2 = -U_\infty \cdot n_2$$
$$\vdots$$
$$U_{k,1} \cdot n_k + U_{k,2} \cdot n_k + \cdots + U_{k,j} \cdot n_k = -U_\infty \cdot n_k$$

where Uk,j represents the velocity in the center of the kth panel by the vortex located at panel j and nk represents the normal vector on the kth panel. Finally the Kutta-condition is applied to the system by requiring the both the vortex strength and the velocity of the flow at the trailing edge to equal zero.

Finally, by solving the system of equations in terms of vortex strengths, gamma, a line vortex model of the airfoil is fully obtained and the velocity at any point can be calculated. For the simulation described in later sections, five thousand panels were used to create a model for the NACA 23013.5 with each panel being approximately .025inches long. This large number of panels ensures a high degree of accuracy. A variety of angles of attack were tested ranging from -9degrees to 14degrees. This range was determined by analyzing the stall characteristics of the airfoil and represents the predicted operating range of the aircraft.

III. Results and Analysis

After the vortex strengths and flow velocities were calculated, the results were plotted in a MATLAB GUI. Figure 2 represents a sampling of the streamlines at several angles of attack. As mentioned earlier, the goal of this analysis is to determine the most undisturbed air around the airfoil. For the initial analysis, the speed at each data point around the airfoil was calculated. The percent difference from the free-stream velocity was then calculated. Since our current design allows the pitot tube to automatically correct its direction into the flow, only the difference in speed of the flow was considered, not the change in direction. If this difference was found to be greater than one percent, the data point was eliminated from the analysis. Figure 3 represents disturbance profiles for varying angles of attack. The red sections represent the greatest disturbances, whereas the blue areas represent the least disturbance.

A total disturbance profile was created, which combined the disturbance profiles of each angle of attack. If any point was eliminated in any of the individual disturbance profiles, it was automatically eliminated in the total disturbance profile. The percent differences were then averaged. Figure 4 represents the total disturbance profile. After analyzing the total disturbance profile, the closest location within our tolerances was located 1.3 chord lengths in front of our airfoil. Since the chord length for our airfoil is about 5 feet, the tip of our pitot tube would need to extend at least 6.5 feet in front of our airfoil. Due to concerns of portability and weight, a 6.5 foot boom seems to be an impractical solution to our problem

IV. Tolerance Analysis

More plots were created to determine amount of error generated by moving our sensor closer to the airfoil. The error tolerance was relaxed and the tolerances were generated in two different ways, represented in Fig. 5:

- Absolute Tolerance: Absolute tolerance is generated by calculating the disturbances for each angle of attack. If the absolute value of the disturbance is outside of the tolerance, then the point is eliminated from the total disturbance plot. All the remaining points are averaged.
- Average Tolerance: Average tolerance is calculated by averaging the absolute value of the disturbances and eliminating all points whose average falls outside the tolerance. Average tolerance does not guarantee that the data will be within our accuracy ratings for the extreme angles of attack, but will be within tolerance for most angles of attack.

Figure 5 displays acceptable regions for multiple tolerance levels from 1% to 3%. Once again, the red areas represent the most disturbed portions of the air, while the blue areas are least disturbed.

V. Conclusion

Based on the analysis above, a increase in the accuracy tolerance was recommended to the project sponsor. A new tolerance of 3% was agreed upon. Therefore, the original requirement has been altered to state, “All data shall be accurate to within 3%.”

VI. Figures

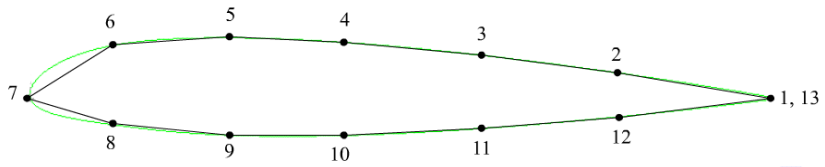

Figure 1. Panel representation of airfoil. *For the method described above, the airfoil was divided into a series of panels. In the actual code, about 5000 panels were used.*

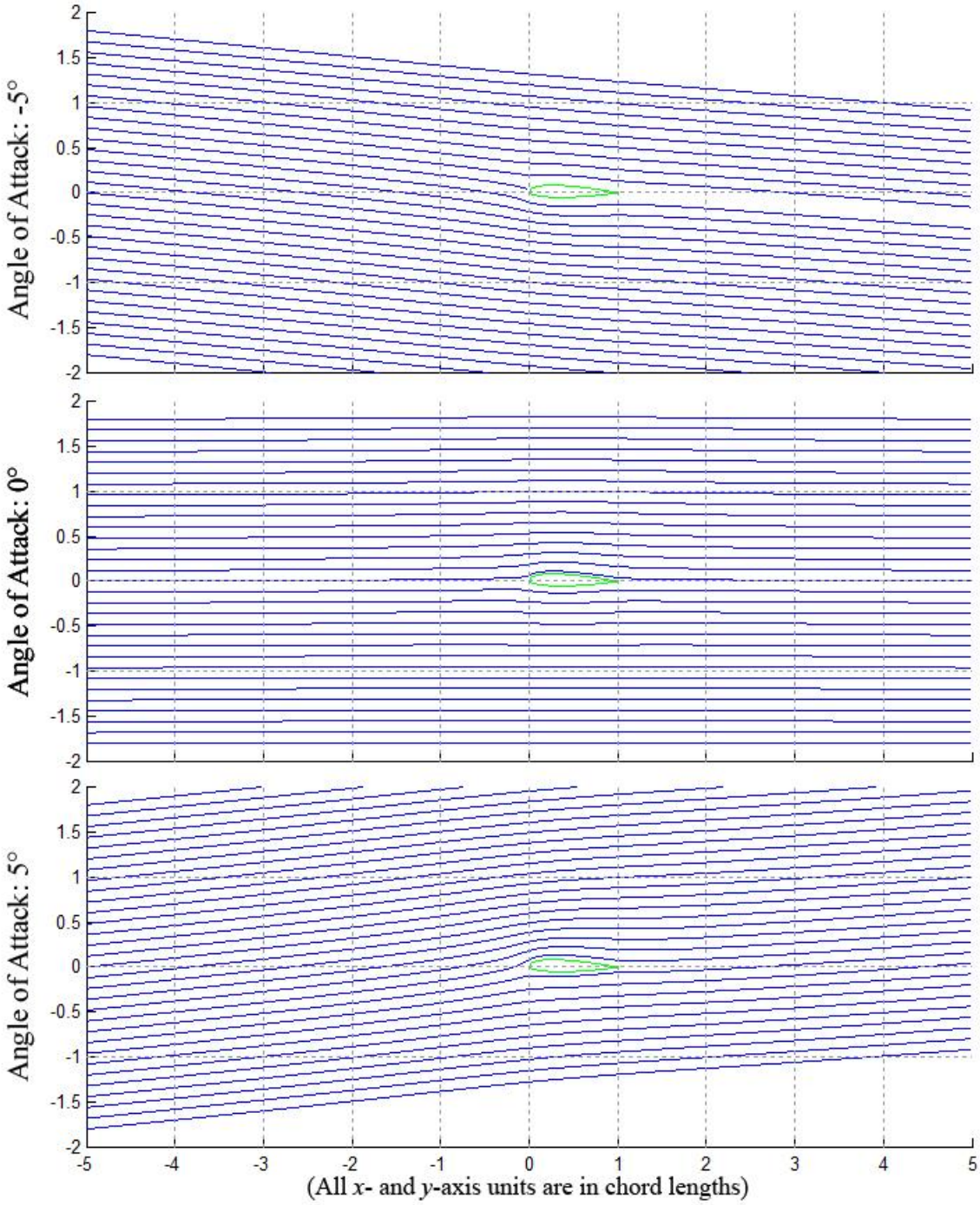

Figure 2. Streamlines at varying angles of attack. *Streamlines created using the panel method code. Results here were used to better understand the disturbance profiles.*

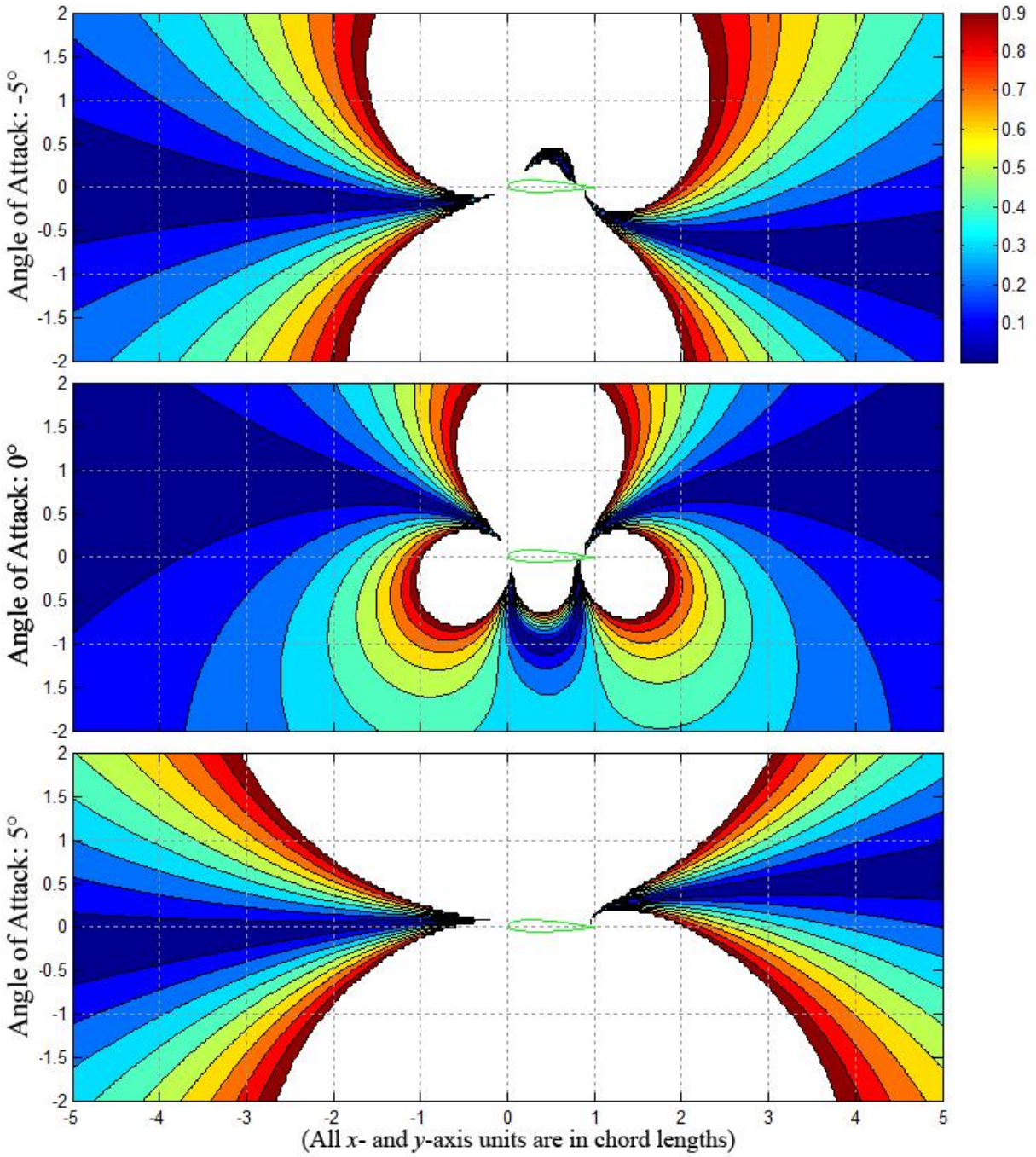

Figure 3. Disturbance profiles for varying angles of attack. *Graphical representation of the change in speed of the flow. Red areas represent the greatest disturbance. Color-bar scale is in percent difference.*

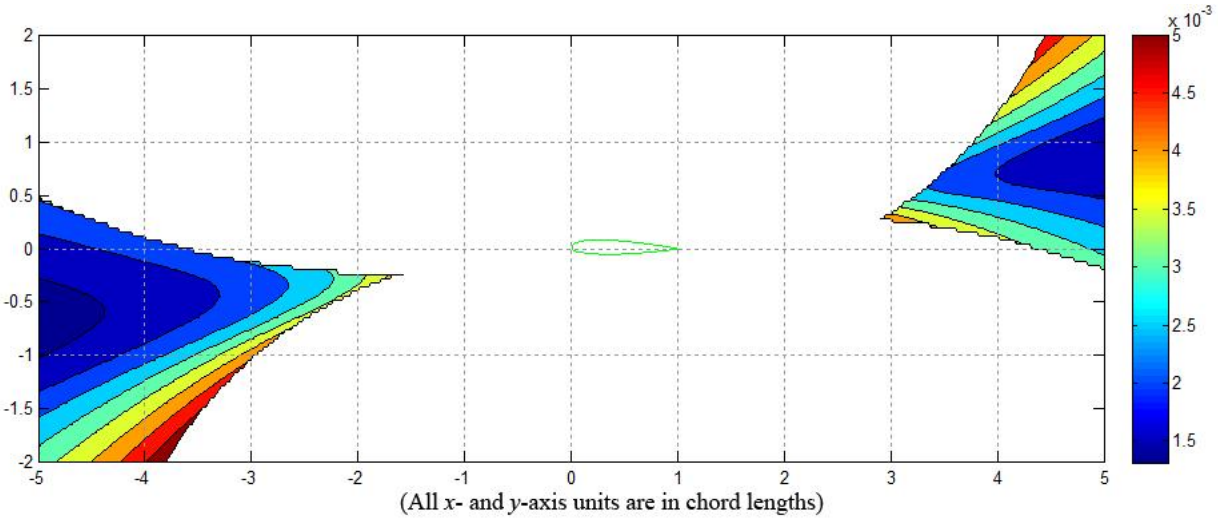

Figure 4. Total disturbance profile. *Conglomeration of disturbance profiles for entire range of angles of attack. Color-bar scale is percent difference/100.*

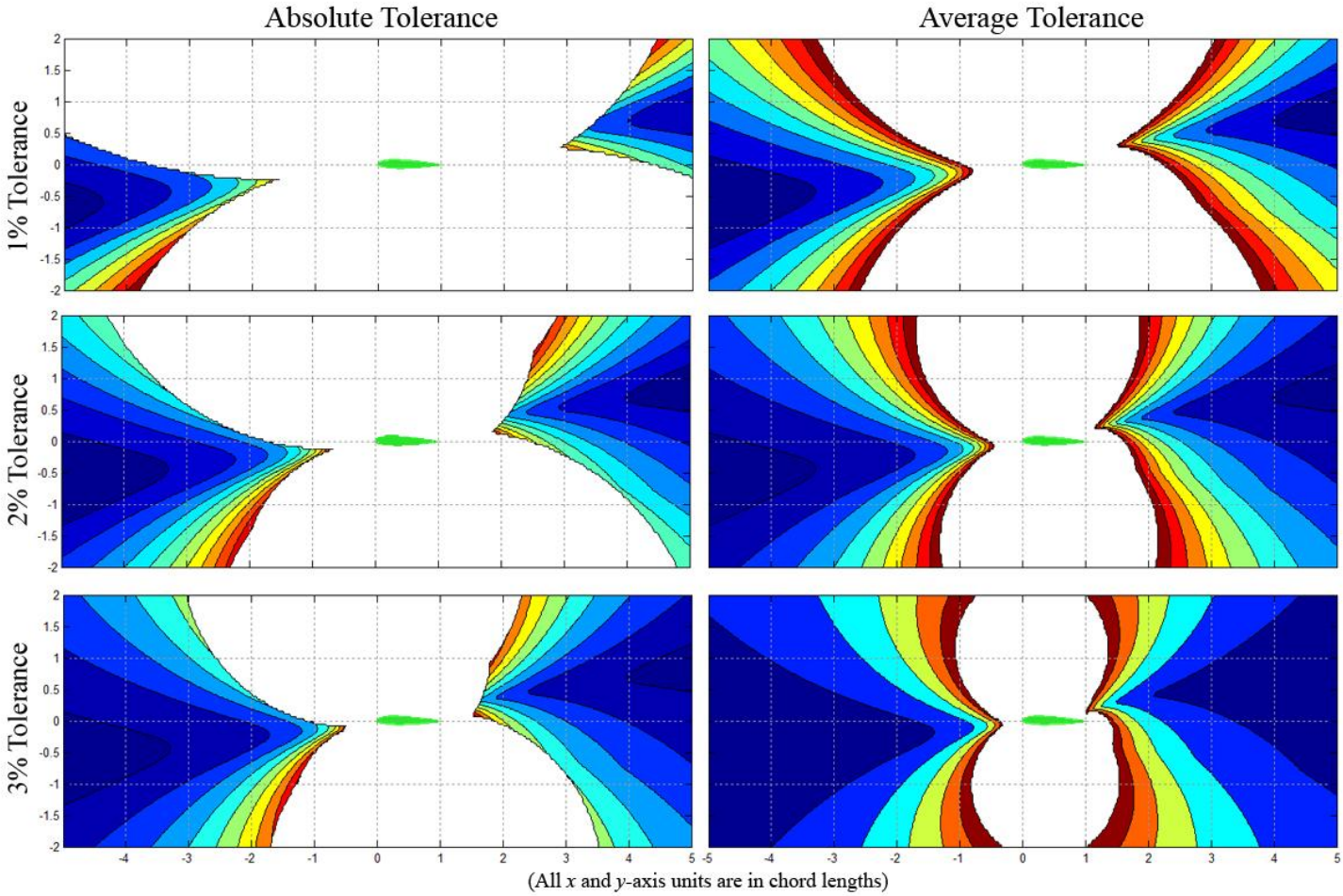

Figure 5. Total disturbance profiles for varying tolerances. *Red areas represent the greatest disturbance*

Appendix F

RV-7 Lateral Stability Analysis

Nick Riccobono[1], Albert Liu[1]
California Polytechnic State University, San Luis Obispo, CA, 93401

This paper discusses the lateral stability of an RV-7 with and without the aircraft data collection system built from the Cal Poly ACDC team. The aircraft data collection system or ACDC was designed to strap to the tip of the right wing and collect accurate pressure data to be used to calibrate newly built experimental aircraft's instruments. A control surface deflection analysis was performed to show than the existence of the excess drag at the tip of the wing will not cause instability in the plane and only require minimal rudder and aileron deflection to compensate. The rudder and aileron deflection were calculated under static stability conditions with a factor of safety of two and found to be less than one degree.

Nomenclature

Symbol		Meaning	Units
L	=	Roll moment	$ft * lbf$
N	=	Yaw moment	$ft * lbf$
F_W	=	Force due to weight	lbf
F_D	=	Force due to drag	lbf
Δp	=	Roll rate	rad/s
Δq	=	Pitch rate	rad/s
Δr	=	Yaw rate	rad/s
Q	=	Dynamic pressure	lbf/ft^2
c	=	chord	ft
S	=	Area	ft^2
b	=	Wing span	ft
l	=	Characteristic length	ft
C_L	=	Coefficient of lift	$-$
V	=	Velocity	ft/s
K	=	Aileron empirical factor	$-$
g	=	Gravitational constant	ft/s^2
Y	=	Side force	lbf
u_o	=	Freestream velocity	ft/s
τ	=	Flap effectiveness	$-$
δ	=	Control surface deflection	rad
θ	=	Pitch angle	rad
η	=	Dynamic pressure ratio	$-$
ρ	=	Density	$slugs/ft^3$
$\Delta\beta$	=	Yaw angle rate	rad/s
$\Delta\varphi$	=	Roll angle rate	rad/s

I. Introduction

The addition of the ACDC testing device at the tip of the wing creates a yawing moment on the aircraft due to the additional drag our testing device possess. To counteract an unbalanced yaw moment, the aircraft must deflect the rudder control surface to maintain a straight flight. In doing so, an unbalanced roll moment is created and must be counteracted with a deflection of the aileron control surfaces to level the plane out.

Lateral stability control is a crucial design aspect in general aviation aircraft, because the plane must be designed such that it can handle extreme disturbances, such as cross wind landings: where the wind direction is perpendicular to the runway during landing or adverse yaw: where the plane will tend to yaw during banked turns. The rudder and aileron control surfaces are located at the vertical tail and at the trailing edge near the wing tips respectively, these two control surfaces are a coupled system which allows the plane to flight straight and level when small disturbances affect the aircraft.

The following analysis is done on the Navion general aviation aircraft combined with the geometry of the RV-7, because we do not possess the necessary flight test data for the RV-7 and do not have the geometry of the Navion; this data refers to mostly control derivatives of the aircraft, in which numerical values are assigned to the differential equations that describe the motion of the aircraft and its responses to small disturbances. The purpose of this analysis is the show the affects of our testing device for static and dynamic reactions of the aircraft during flight.

II. Analysis and Procedure

To analyze if the ACDC system truly effects the RV-7 during flight, both static and dynamic stability must be met. Static conditions is the case where at some arbitrary time the sum of forces and moments are equal to zero. In our case we are concerned with rolling and yawing moments being set to zero. For dynamic stability the later equations of motion are used which consist of side force, rolling moment, and yawing moment. Figure 1 shows the RV-7 with the ACDC system attached to the right wing, shown are the force and moment vectors that are acting on the plane during steady level flight.

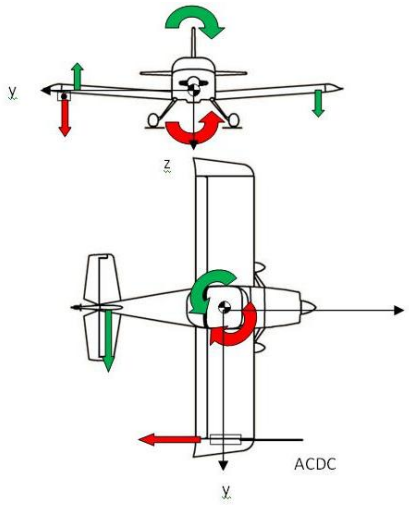

Figure 1: Free Body Diagram of RV-7 with ACDC testing device. ***ACDC effects in red, plane reaction in green.***

A) Static Conditions

The figure to the right shows the acting forces on the aircraft, the forces and moments shown in green are the aircraft's reaction force that is equal and opposite to the forces and moments shown in red that are induced by the presence of the ACDC testing device. Our assumptions for static stability analysis are as follows,

- steady level flight
- constant speed
- no roll, pitch, or yaw rates
- constant dynamic pressure
- no side slip

The sum of the rolling moment (Eq. 1) and yawing moment (Eq. 2) are set to zero to evaluate the control surface deflection in static conditions.

$$\sum L = -F_{W,ACDC}\, x \left({}^{b}/_{2}\right) + F_{aileron}\, x \left({}^{b}/_{2} - {}^{l_{aileron}}/_{2}\right) = 0 \qquad \text{(Eq. 1)}$$

$$\sum N = -F_{D,ACDC}\, x \left({}^{b}/_{2}\right) + F_{rudder}\, x \left(l_{ac,tail}\right) = 0 \qquad \text{(Eq. 2)}$$

Where b is the wing span, l is the characteristic length to the control surfaces, and F is the force due to drag, weight of our testing device, rudder deflection, and aileron deflection. Since the actual forces generated by the surfaces are unknown, the equations are non-dimensionalized by the dynamic pressure, reference length, and reference areas to yield,

$$\frac{F_{W,ACDC}\left({}^{b}/_{2}\right)}{Q\bar{c}} = \left[\frac{2C_{L\alpha}\tau_{aileron}}{b}\bar{c}\left(y_2{}^2 - y_1{}^2\right)\right]\delta_{aileron} + \left[S_{tail}\frac{Z_v}{b}\tau_{rudder}C_{L\alpha W}\right]\delta_{rudder} \qquad \text{(Eq. 3)}$$

$$\frac{C_{D,ACDC}S_{ACDC}(^{\rho}/_{2})}{S_{wing}\bar{c}} = [2KC_{L,0}C_{L,\delta aileron}]\delta_{aileron} + [V_{tail}\eta_{tail}C_{L\alpha,tail}]\delta_{rudder} \quad \text{(Eq. 4)}$$

The two equations above can solve the two unknowns: rudder deflection (δ_{rudder}) and aileron deflection ($\delta_{aileron}$) by plugging in the aircraft's stability derivatives, reference length, aircrafts characteristic areas, and characteristics of our testing device. *V*, *y*, and *Z* are the wing volume ratio, distance to each edge of the aileron, and the distance to the finite tail center of pressure, respectively. Factors like *K*, aileron empirical factor and τ, flap effectiveness factor, are found in Flight Stability and Automatic Control by Robert Nelson [1]. The coefficient of drag was unknown for this analysis, so the worst case scenario was used: a flat plate that is perpendicular to the direction of the flow. The control derivatives were supplied by Nelson [1] and values found from XFOIL airfoil analysis program.

B) Dynamic Conditions

The later equations of motion that describe the aircraft's attitude consist of the side force, rolling moment, and yawing moment equation as seen below.

$$\left(\frac{d}{dt} - Y_v\right)\Delta v + Y_p\Delta p - (u_o - Y_r)\Delta r + g\cos\theta\Delta\varphi = Y_{\delta r}\Delta\delta_r \quad \text{(Eq. 5)}$$

$$-L_v\Delta v + \left(\frac{d}{dt} - L_p\right)\Delta p - \left(\frac{I_{xz}}{I_{xx}}\frac{d}{dt} + L_r\right)\Delta r = L_{\delta r}\Delta\delta_r + L_{\delta a}\Delta\delta_a \quad \text{(Eq. 6)}$$

$$-N_v\Delta v + \left(\frac{I_{xz}}{I_{xx}}\frac{d}{dt} + N_p\right)\Delta p + \left(\frac{d}{dt} - N_r\right)\Delta r = N_{\delta r}\Delta\delta_r + N_{\delta a}\Delta\delta_a \quad \text{(Eq. 7)}$$

The equations are the sum of forces and moments equal to zero to represent the aircraft in steady un-accelerated flight in all directions. The left hand side of the equations can be rearranged into a state space matrix *A*, and the right hand side is represented by matrix *B*. The purpose of a state space matrix is to be able represent a time rate of change of the planes current state that is coupled by equations 5, 6, and 7. The characteristic equation has three roots composed of two real roots and a pair of complex roots. Each root describes the airplanes response to small disturbances or a pilot command input like aileron and/or rudder deflection. The following equation is the final form of the state space equation.

$$\dot{x} = Ax + Bu \quad \text{(Eq. 8)}$$

It sometimes is more convenient to use the sideslip angle $\Delta\beta$ instead of side velocity Δv. Using small angle approximations

$$\Delta\beta \cong tan^{-1}\frac{\Delta v}{u_o} \cong \frac{\Delta v}{u_o} \quad \text{(Eq. 9)}$$

and plugging in this relationship into equations 5, 6, and 7 then arranging terms to be in matrix form, where

$$A = \begin{bmatrix} \frac{Y_\beta}{u_o} & \frac{Y_v}{u_o} & -\left(1 - \frac{Y_r}{u_o}\right) & \frac{g\cos\theta}{u_o} \\ L_\beta & L_p & L_r & 0 \\ N_\beta & L_p & N_r & 0 \\ 0 & 1 & 0 & 0 \end{bmatrix} \quad \text{(Eq. 10)}$$

Then matrix *B* is the input coefficient matrix along with the variable matrix *x* and input matrix *u* are denoted as,

$$B = \begin{bmatrix} 0 & \frac{Y_{\delta r}}{u_o} \\ L_{\delta a} & L_{\delta r} \\ N_{\delta a} & N_{\delta r} \\ 0 & 0 \end{bmatrix} \quad \text{(Eq. 11)}$$

$$x = \begin{bmatrix} \Delta\beta \\ \Delta p \\ \Delta r \\ \Delta\varphi \end{bmatrix} \qquad u = \begin{bmatrix} \Delta\delta_a \\ \Delta\delta_r \end{bmatrix} \qquad \text{(Eq. 12, 13)}$$

Plugging in equations 10, 11, 12, and 13 into equation 8 yields the final form of the state space equation to represent the aircrafts lateral motion.

$$\begin{bmatrix} \dot{\Delta\beta} \\ \dot{\Delta p} \\ \dot{\Delta r} \\ \dot{\Delta\varphi} \end{bmatrix} = \begin{bmatrix} \frac{Y_\beta}{u_o} & \frac{Y_p}{u_o} & -\left(1 - \frac{Y_r}{u_o}\right) & \frac{g\cos\theta}{u_o} \\ L_\beta & L_p & L_r & 0 \\ N_\beta & L_p & N_r & 0 \\ 0 & 1 & 0 & 0 \end{bmatrix} \begin{bmatrix} \Delta\beta \\ \Delta p \\ \Delta r \\ \Delta\varphi \end{bmatrix} + \begin{bmatrix} 0 & \frac{Y_{\delta r}}{u_o} \\ L_{\delta a} & L_{\delta r} \\ N_{\delta a} & N_{\delta r} \\ 0 & 0 \end{bmatrix} \begin{bmatrix} \Delta\delta_a \\ \Delta\delta_r \end{bmatrix} \qquad \text{(Eq. 14)}$$

Each element in the state space matrix is a function of the stability derivatives, mass, and inertial characteristics of the airplane, or in our case the airplane plus the ACDC testing device. A characteristic equation is found by taking the Eigen-values of matrix *A* which yields,

$$\lambda^4 + 5.486\lambda^3 + 14.469\lambda^2 + 51.51\lambda + 2.545E - 3 = 0 \qquad \text{(Eq. 15)}$$

Where this forth order polynomial represents matrix *A* which defines the RV-7 with the ACDC testing device. Eq. 15 has three roots; two real numbers and a complex pair, which should all be negative to prove the aircraft is stable with our testing device.

C) Lateral motion modes

The three roots composed of two real roots and a pair of complex roots describing the spiral mode, roll mode, and the Dutch roll mode respectively. The addition of our ACDC should prove to have little or no affect on these modes to safely be used during flight tests. Each root or pole should lie within the left hand side of the imaginary axis in a root locus plot, as seen in Figure 2. The root locus plot is a powerful tool in controls analysis, it allows designers to judge the stability of the state space matrix and understand the margins of flight that the aircraft has before losing control.

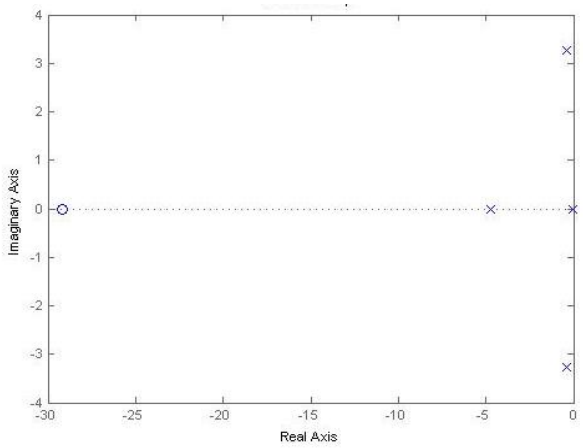

Figure 2: Pole Zero Map of RV-7 and RV-7 with ACDC. ***Figure from MATLAB >>pzplot.***

The spiral mode is a slowly convergent or divergent motion that is a very small negative real root and is analogous to an automobile with a slight misalignment, where the driver must constantly be correcting to continue driving straight. This mode should have such a small influence on the aircraft that if the pilot were to let go of the rudder pedals the aircraft would slowly turn and "spiral" in a turn with a very large radius. When dealing with spiral motion, like the automobile driver, the pilot corrects for this involuntarily when flying due to wind gusts and atmospheric conditions.

The roll mode is a highly convergent motion, or a large real negative root that is dependent on the wing and vertical tail size. Since the vertical tail of an aircraft has pressure force acting above the center of gravity there will be a tendency to roll the plane without correction. It is essential that this mode dampen as quickly as possible because the pilot should not be worrying about the plane rolling out of control if he was to let go of the stick for a short time.

The Dutch roll mode, represented by the complex pair root, is a combination of the aircraft's tendency to yaw and roll at the same time to resemble a "swaying motion". This motion was named after it reminded someone of the weaving motion of a Dutch ice skater. This mode is lightly dampened oscillatory motion that has a relatively low frequency, such that the pilot corrects this similarly to the spiral mode.

III. Computational Steps

After gather all the control derivatives available, aircraft geometry, and ACDC geometry, the rest of the stability derivatives and characteristic lengths were approximated by XFOIL and physically measuring the RV-7.

In XFOIL, a drag polar was constructed for the NACA 23013.5 and the NACA 0009 for the RV-7 main wing and vertical tail respectively. The lift curve slope for each airfoil was generated in Microsoft Excel with the data from XFOIL as seen in Figure 2. Since XFOIL is a sectional wing (2-D wing) analysis, the following equation is a finite wing (3-D wing) approximation from Nelson [1],

$$C_{L\alpha,3D} = \frac{C_{L\alpha,2D}}{1+\frac{C_{L\alpha,2D}}{\pi AR}} \qquad \text{(Eq. 16)}$$

This equation can be used for both the main wing and vertical tail wing, where the *AR* is the aspect ratio of finite wing surface.

Inputting Eq. 14 into MATLAB, the function *>>damp(A)*, will yield the Eigen-values, damping ratio, and natural frequency for each mode of lateral motion for both the RV-7 and the RV-7 with the ACDC testing device.

To gather terms like *K and* τ, a plot digitizer program, from the University of Alabama was used to interpolate values from charts found in Nelson [1]. Figures 3 is a curve that relates ratio between control surface and lifting surface to find the flap effectiveness. Figure 4 is a relationship between *K* and the ratio between aileron location and semi span, or the length of one wing.

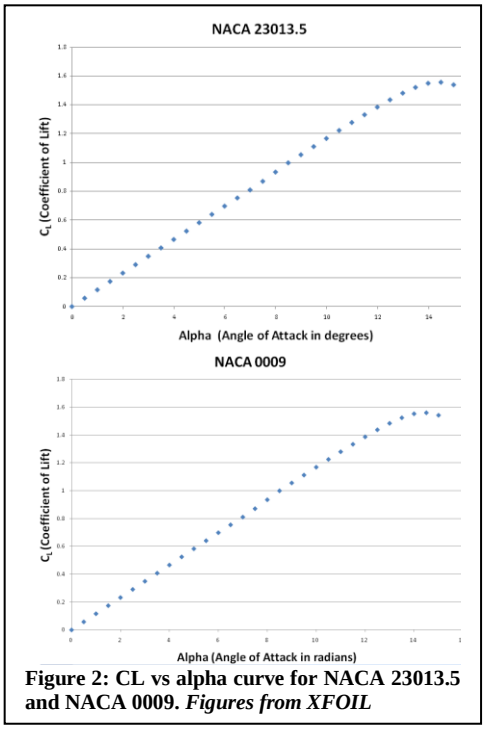

Figure 2: CL vs alpha curve for NACA 23013.5 and NACA 0009. *Figures from XFOIL*

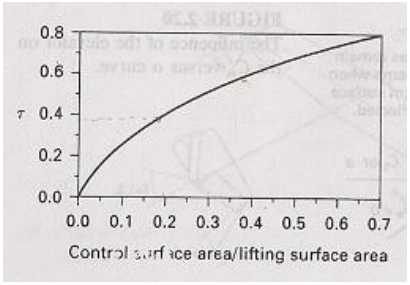

Figure 3: Flap effectiveness graph with respect to control surface area to lifting surface area ratio.

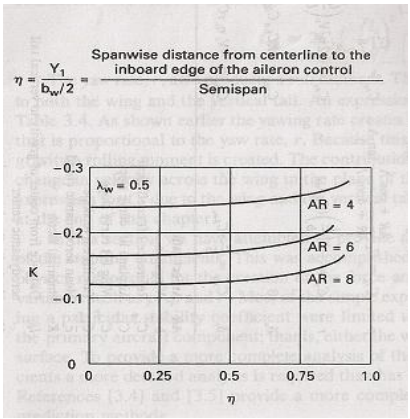

Figure 4: Empirical factor for aileron effects with respect to aileron location and semi-span ratio.

IV. Results and Verification

Using Eq. 14 in MATLAB's function >>*damp(A)* yields the three roots of our characteristic equation. Figure 3 is a pole zero plot of each root and pole of the characteristic equation found for the RV-7 and RV-7 with the ACDC system attached. When initially plotting the poles and zeroes of the equation for the two cases the differences were unnoticed due to the location of the roots (Figure 2). Figure 5 shows the zoomed in locations of the RV-7 and the RV-7 with ACDC system.

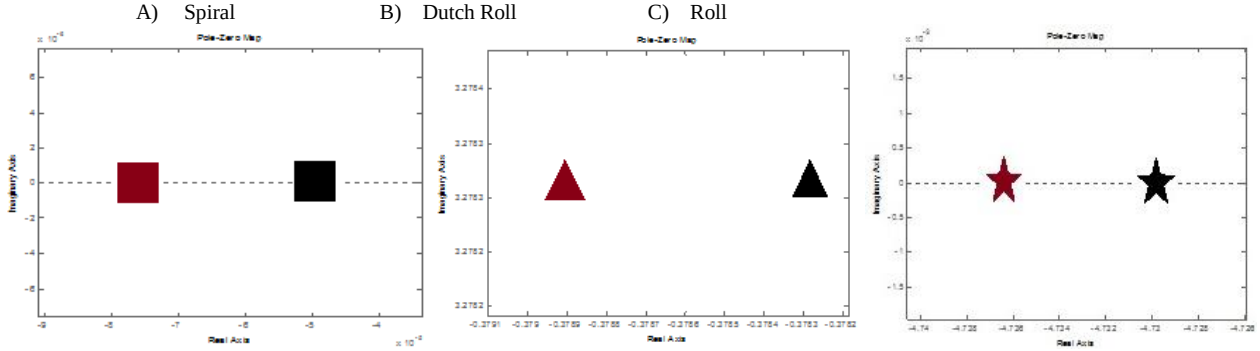

Figure 5: Zoomed in pole zero plot locations of each mode root. Figure obtained from MATLAB >>pzplot.

Each mode is tabulated below in Table 1 to see the affect of the ACDC system on the RV-7. After integrating the ACDC into the RV-7, the Roll mode root remained negative which indicates the plane will still be stable and only changed 0.14% from the original root of the RV-7. Our calculated Dutch Roll Roots will behavior in a stable damped oscillatory motion because both cases of RV-7 and RV-7 with ACDC system have real negative root with complex pair. The change in our Dutch Roll Roots was 0.02%.The calculated Spiral Root had a 35% change from the original, however, because the number is so small, any slight change will have a big effect on the percent change.

The only significant effect that the ACDC system has on the RV-7 is the Spiral mode, since the root is still negative, it is still considered stable. We can expect that this addition will require the pilot to compensate for this addition more frequently.

Modes	RV-7	RV-7 w/ ACDC	Error
Dutch Roll	-0.378**90**±3.2783136i	-0.378**28**±3.2783149i	0.0188%
Spiral	-0.0000**75**	-0.0000**49**	34.48%
Roll	-4.7**36**	-4.7**29**	0.1393%

We were able to use the system of equations of lateral motion to find the impulse response of the system. Using change in rudder and aileron deflection as the input and analyzing the response of the aircraft attitude in terms of bank angle (φ) and heading (β). Referring to Figure 4 the response of the integrated ACDC (blue solid line) is almost exact with the response of the RV-7 (dashed red line). This shows that there will be minimal change in response when flying with our ACDC system.

The impulse response of a rudder deflection on the resulting heading (top left) and the roll angle (bottom left) is shown in Figure 4. The resulting heading will spike up and then oscillate to a dampened final value when the rudder is deflection with an impulse command. The final value of the heading is close to zero which indicates that the aircraft will natural straighten itself out. The affect of the rudder deflection on the bank angle will result in a rise to a final value then settle at a much larger magnitude, this is due to fact that the plane is not designed to balance itself with only rudder deflection.

Similarly the impulse response of an aileron deflection on the resulting heading (top right) and the roll angle (bottom right) is shown in Figure 4. The resulting heading spikes to a very large value and then dampens to its original value due to the design of the aircraft, which indicates that aileron deflection has influence however it is not the primary control to heading. This result is in agreement with the phenomena known as adverse yaw effects to aircrafts. When the response of bank angle is examined due to aileron deflection it is seen that a small spike occurs and then levels itself back to nearly the original value much like the rudder affected the heading. On aircrafts an aileron deflection impulse will roll the plane slightly, and then due to its geometry and design will level itself out.

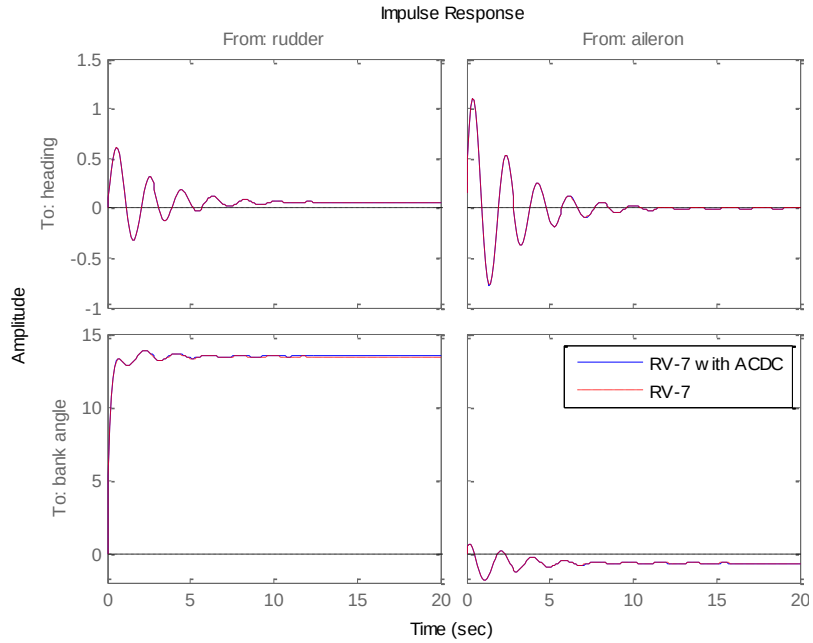

Figure 4: Impulse Response of the RV-7 with ACDC system due to an impulse rudder deflection and aileron deflection. Values obtained from MATLAB >>*ss(A,B,C,D)*

V. Conclusion

According to the graphs, the trend that the RV-7 follows for each response is closely resembled by the RV-7 with the ACDC system attached at the tip of the wing. The addition of the ACDC is concluded that it will not cause the plane to become unstable under normal flight conditions and changes. From static analysis, the deflection was found to be only less than one degree for each control surface (see appendix A). The only true affect our device will induce on the aircraft is the change in Spiral mode that must be corrected by a slight rudder deflection coupled with a slight aileron deflection to maintain steady level flight.

References

[1] Flight Stability and Automatic Control 2nd edition, Robert C. Nelson-Department of Aerospace and Mechanic Engineering University of Norte Dame.
ISBN-13: 978-0-07-066110-3
Tata McGraw-Hill, ©1998

[2] Fluid Mechanics 9th edition, Clayton T. Crowe, Donald F. Elger, Barbara C. Williams, John A. Roberson.
ISBN-13: 978-0-470-25977-1
Wiley, www.wiley.com/college/crowe

[3] MATLAB R2008b
The Mathworks, Inc. ©1984-2010

[4] XFOIL 6.9, Mark Drela- MIT Aero & Astro
Harold Youngren, Aerocraft, Inc.

[5] Plot Digitizer,
Department of Physics
University of South Alabama
Mobile, AL 36688

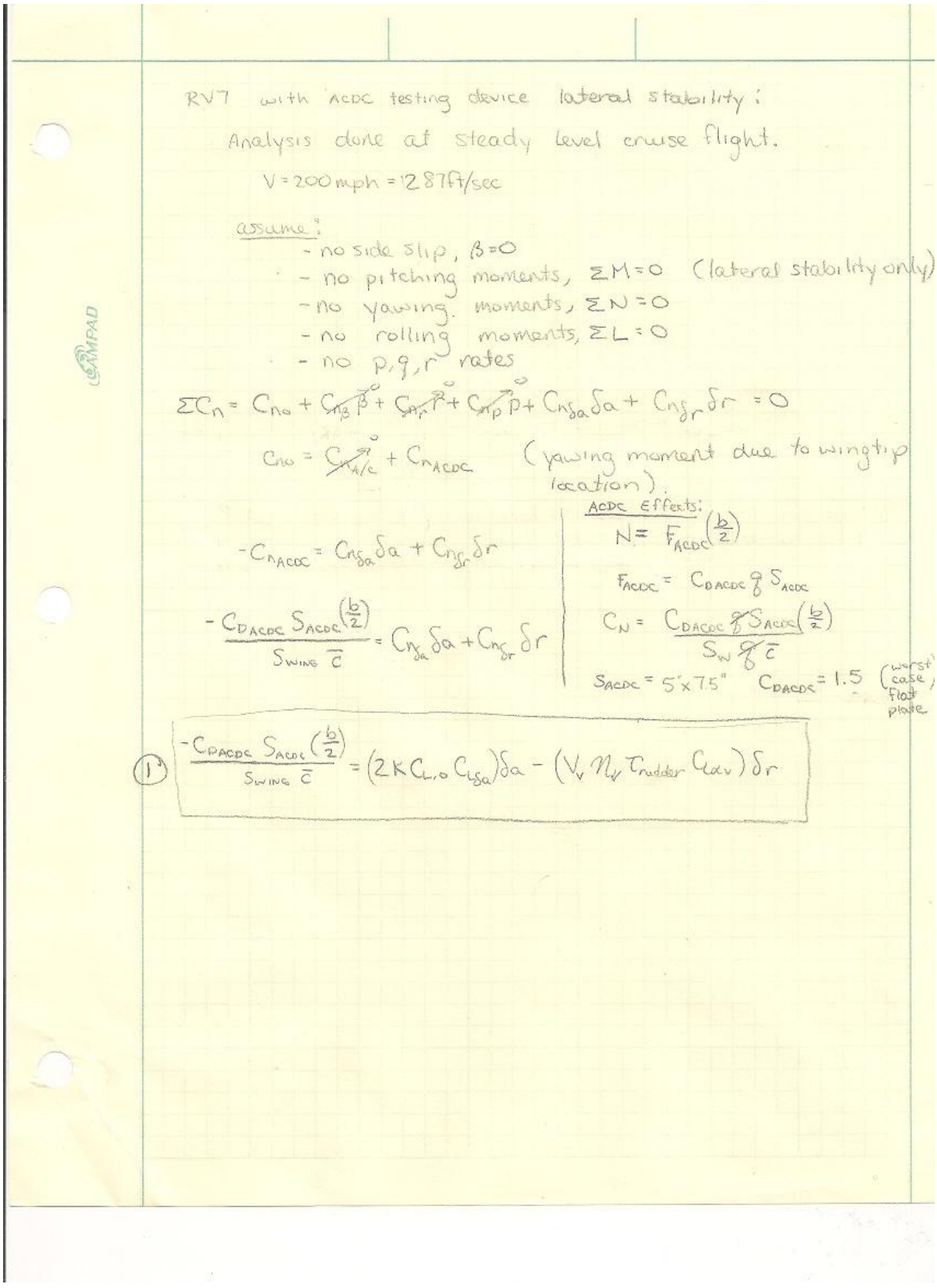

RV7 with ACDC testing device lateral stability:

Analysis done at steady level cruise flight.

$V = 200\,mph = 287\,ft/sec$

assume:

- no side slip, $\beta = 0$
- no pitching moments, $\Sigma M = 0$ (lateral stability only)
- no yawing moments, $\Sigma N = 0$
- no rolling moments, $\Sigma L = 0$
- no p, q, r rates

$$\Sigma C_n = C_{n_0} + C_{n_\beta}\beta + C_{n_r}r + C_{n_p}p + C_{n_{\delta a}}\delta a + C_{n_{\delta r}}\delta r = 0$$

$$C_{n_0} = C_{n_{a/c}} + C_{n_{ACDC}}$$ (yawing moment due to wingtip location).

ACDC Effects:

$$N = F_{ACDC}\left(\frac{b}{2}\right)$$

$$F_{ACDC} = C_{D_{ACDC}}\, q\, S_{ACDC}$$

$$C_N = \frac{C_{D_{ACDC}}\, q\, S_{ACDC}\left(\frac{b}{2}\right)}{S_W\, q\, \bar{c}}$$

$S_{ACDC} = 5' \times 7.5''$ $C_{D_{ACDC}} = 1.5$ (worst case flat plate)

$$-C_{n_{ACDC}} = C_{n_{\delta a}}\delta a + C_{n_{\delta r}}\delta r$$

$$-\frac{C_{D_{ACDC}}\, S_{ACDC}\left(\frac{b}{2}\right)}{S_{WING}\,\bar{c}} = C_{n_{\delta a}}\delta a + C_{n_{\delta r}}\delta r$$

(1) $$\frac{-C_{D_{ACDC}}\, S_{ACDC}\left(\frac{b}{2}\right)}{S_{WING}\,\bar{c}} = (2K C_{L,0} C_{l_{\delta a}})\delta a - (V_v \eta_v \tau_{rudder} C_{l\alpha v})\delta r$$

Appendix G

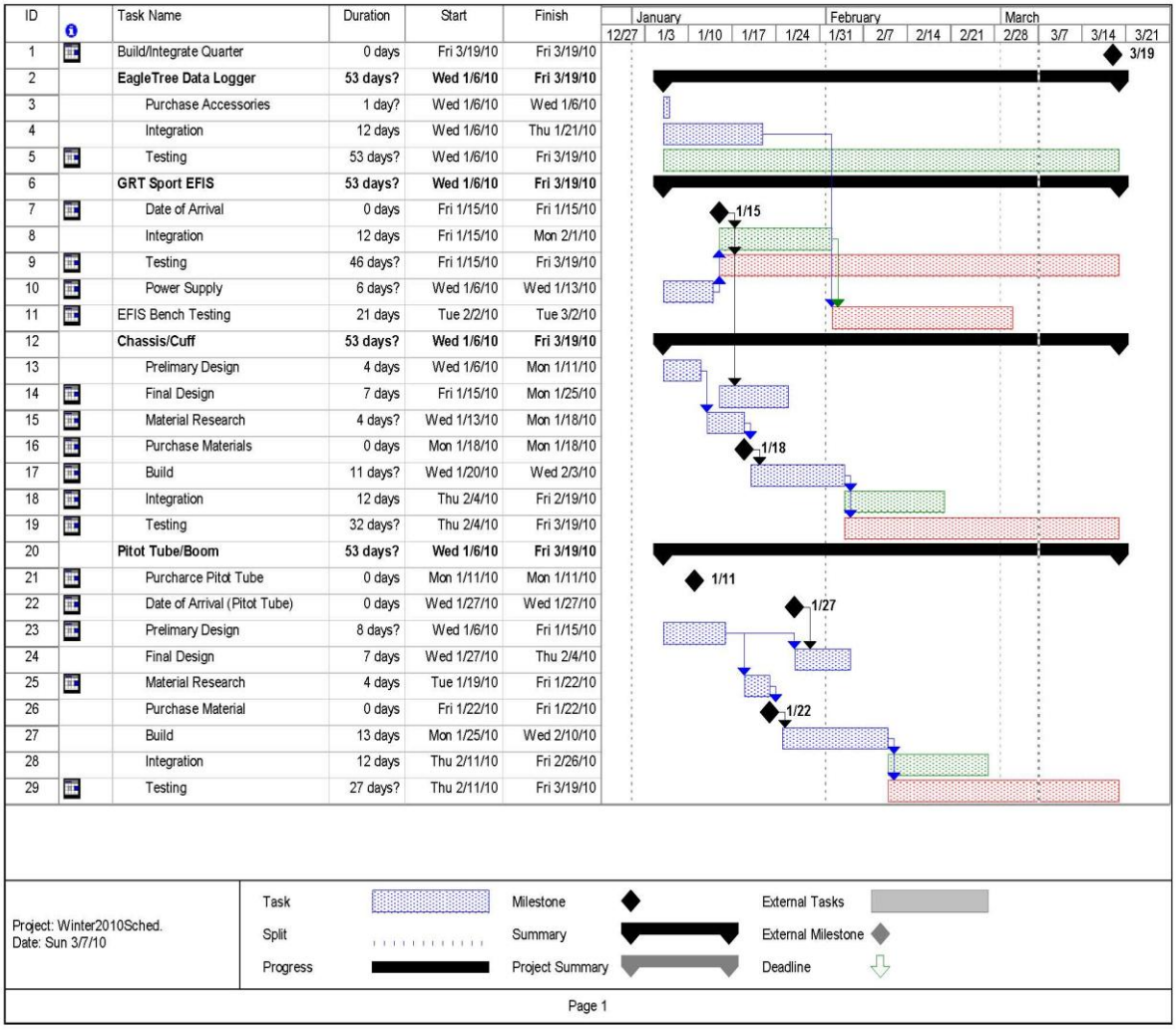

ID	Task Name	Duration	Start	Finish
1	Build/Integrate Quarter	0 days	Fri 3/19/10	Fri 3/19/10
2	**EagleTree Data Logger**	**53 days?**	**Wed 1/6/10**	**Fri 3/19/10**
3	Purchase Accessories	1 day?	Wed 1/6/10	Wed 1/6/10
4	Integration	12 days	Wed 1/6/10	Thu 1/21/10
5	Testing	53 days?	Wed 1/6/10	Fri 3/19/10
6	**GRT Sport EFIS**	**53 days?**	**Wed 1/6/10**	**Fri 3/19/10**
7	Date of Arrival	0 days	Fri 1/15/10	Fri 1/15/10
8	Integration	12 days	Fri 1/15/10	Mon 2/1/10
9	Testing	46 days?	Fri 1/15/10	Fri 3/19/10
10	Power Supply	6 days?	Wed 1/6/10	Wed 1/13/10
11	EFIS Bench Testing	21 days	Tue 2/2/10	Tue 3/2/10
12	**Chassis/Cuff**	**53 days?**	**Wed 1/6/10**	**Fri 3/19/10**
13	Prelimary Design	4 days	Wed 1/6/10	Mon 1/11/10
14	Final Design	7 days	Fri 1/15/10	Mon 1/25/10
15	Material Research	4 days?	Wed 1/13/10	Mon 1/18/10
16	Purchase Materials	0 days	Mon 1/18/10	Mon 1/18/10
17	Build	11 days?	Wed 1/20/10	Wed 2/3/10
18	Integration	12 days	Thu 2/4/10	Fri 2/19/10
19	Testing	32 days?	Thu 2/4/10	Fri 3/19/10
20	**Pitot Tube/Boom**	**53 days?**	**Wed 1/6/10**	**Fri 3/19/10**
21	Purcharce Pitot Tube	0 days	Mon 1/11/10	Mon 1/11/10
22	Date of Arrival (Pitot Tube)	0 days	Wed 1/27/10	Wed 1/27/10
23	Prelimary Design	8 days?	Wed 1/6/10	Fri 1/15/10
24	Final Design	7 days	Wed 1/27/10	Thu 2/4/10
25	Material Research	4 days	Tue 1/19/10	Fri 1/22/10
26	Purchase Material	0 days	Fri 1/22/10	Fri 1/22/10
27	Build	13 days	Mon 1/25/10	Wed 2/10/10
28	Integration	12 days	Thu 2/11/10	Fri 2/26/10
29	Testing	27 days?	Thu 2/11/10	Fri 3/19/10

Appendix I

Body				
Type	**Quantity**	**Name**	**Unit Price**	**Total cost**
B	1	3M Glass Bubbles 1lb	7.95	7.95
B	***3***	***Standard E-Glass Fiberglass***	***5.95***	***17.85***
B	***1***	***Steel Flange Mounted Ball Bearing [3/8"D x 2+1/2"L]***	***20.17***	***20.17***
B	***1***	***Aluminum 6061 Sheet [.032" x 6" x 48"]***	***16.88***	***16.88***
B	***1***	***Polycarbonate Rod [1+1/8"D x 1'L]***	***11.2***	***11.2***
B	***1***	***Aluminum 6061 Precision-Ground rod [3/4"D x 1'L]***	***9.53***	***9.53***

B	***1***	***Aluminum 6061 Rod [2"D x 1'L]***	***14.8***	***14.8***
B	***1***	***Polycarbonate Sheet [1/16" x 12" x 12"]***	***3.84***	***3.84***
B	***2***	***Structural Fiberglass Angle [(1" x 1")L-shape x 5']***	***9.65***	***19.3***
B	***1***	***Aluminum Blind Rivets [1/8"D x .188"-.250"T] (250)***	***9.42***	***9.42***
B	***1***	***Aluminum 6061 Sheet [.125" x 12" x 12"]***	***26.29***	***26.29***
B	***1***	***Carbon Fiber Tube***	***66.41***	***66.41***
		Total Body Cost:	223.64	

Table I-1: Body Costs

Big System				
Type	**Quantity**	**Name**	**Unit Price**	**Total cost**
E	**1**	**GRT Sport EFIS**	2800	2800
E	**1**	**GPS Option**	400	400
E	1	EFIS SPORT Cable	0	0
E	1	Memory Stick	0	0
E	**1**	**Unheated Straight Pitot**	**20.85**	**20.85**
E	1	Urethane Foam ["1/2 x24"x48"]	9	9
E	25	Extra-Flex Nylon 11 Tubes [.232" ID, 5/16" OD] per 1'	0.56	14
		Big System Cost:	3243.85	

Table I-2: Big System Costs

Small System				
Type	**Quantity**	**Name**	**Unit Price**	**Total Cost**
S	**1**	**Micro Temp Sensor**	**$9.99**	**$9.99**
S	**1**	**Pitot-Static Tube Kit**	**$9.99**	**$9.99**
S	**1**	**Dual Exis G-Force Expander - 38G**	**$79.99**	**$79.99**
S	**1**	**GPS Expander V4 (10Hz GPS)**	**$79.99**	**$79.99**
S	**1**	**USB Flight Data Recorder Pro**	**$299.99**	**$299.99**
S	**10**	**USB Connector Ports**	**$0.50**	**$5.00**
S	**1**	**Project Box [5"x2.5"x2"]**	**$3.69**	**$3.69**
S	**1**	**A/C Round Rocker Spst.**	**$3.99**	**$3.99**
S	**1**	**Detector Plug**	**$3.29**	**$3.29**
S	**1**	**2.5MM Power Jack**	**$3.29**	**$3.29**
	1	**Spring 2010 costs**	$23	**$23.00**
		Small System Cost:	522.21	

Table I-3: Small System Costs

Other				
Type	**Quantity**	**Name**	**Unit Price**	**Total cost**
O	1	OAT Probe	0	0
O	5	3M Sandpaper 180	1.37	6.85
O	5	3M Sandpaper 100	1.21	6.05
O	5	Sandpaper 36	1.16	5.8
O	2	3M Spreader Assorment	4.25	8.5
O	5	3M Sandpaper 220	0.86	4.3
O	1	Surface Tape Darcon Smooth [1"]	2.95	2.95
O	10	Brush [1"]	0.38	3.8
O	10	Brush [2"]	0.49	4.9
O	1	Mixing Cups [12oz] (60)	13.75	13.75
O	1	Mixing Cups [3oz] (100)	4.95	4.95
O	1	Mixing Sticks (500)	10.75	10.75
O	1	West System 300 Ratio Pumps	10.95	10.95
O	1	Grooved Aluminum Lam Roller [1"x3"]	8.5	8.5
O	3	Lightweight Industrial Cloth [1.45oz]	5.25	15.75
O	10	3M Particle Respirator	0.54	5.4
O	1	Disposable Latex Gloves (100)	10.85	10.85
O	1	Gorilla Superbond Polyurethane Glue [4oz]	8.28	8.28
O	1	West System Epoxy Kit A-1 Fast	39	39
O	1	MRX Silicone Spray, Mold Release	10.5	10.5
		Other Cost:	181.83	

Table I-4: Other Costs

Big System		
	EFIS	$3,243.85
	Old Frame	$223.64
	New Frame	$80.00
	Other	$181.83
	Total	$3,729.32
Small System		
	System	$522.21
	Body	$223.64
	Other	$181.83
	Total	$927.68

Overall Cost	$4,171.53	
	GRT EFIS	$3,243.85
	Eagle Tree	$522.21
	Old Frame	$223.64
	New Fram	$80.00
	Other	$80.00
		$4,149.70

Table I-5: Total Costs